International Journal of Plasticity 76 (2016) 244–284

Contents lists available at ScienceDirect

International Journal of Plasticity

journal homepage: www.elsevier.com/locate/ijplas

Review

A review of constitutive models and modeling techniques for shape memory alloys

Cheikh Cisse [a], Wael Zaki [a, *], Tarak Ben Zineb [a, b, c]

[a] Khalifa University of Science, Technology, and Research, P.O. Box 127788, Abu Dhabi, United Arab Emirates
[b] Université de Lorraine, LEMTA, UMR 7563, Vandoeuvre-lès-Nancy F-54500, France
[c] CNRS, LEMTA, UMR 7563, Vandoeuvre-lès-Nancy F-54500, France

ARTICLE INFO

Article history:
Received 18 April 2015
Received in revised form 30 July 2015
Available online 28 August 2015

Keywords:
Shape memory alloys
A. Twinning
A. Phase transformation
B. Constitutive behavior

ABSTRACT

Constitutive models for shape memory alloys have seen significant development in the last decades. They have evolved from uniaxial, mostly empirical, relations to full-fledged mathematical descriptions accounting for many of the effects observed in these materials with an ever-higher degree of detail. The models available today are constructed using various approaches ranging from micromechanics with or without scale transition, to statistical physics and particle dynamics, to methods of classical plasticity, to energy approaches coupled with thermodynamic and conservation principles. They have finally matured to the extent where they can be utilized in reasonably accurate numerical analysis of potentially complex shape memory alloy devices subjected to non-trivial thermomechanical loading. This paper aims at providing an up-to-date review of key constitutive models for shape memory alloys, with an attempt to track their evolution from their inception to their most recent versions. The models are categorized in terms of the approach they use in describing the behavior of shape memory alloys.

1. Introduction

Shape memory alloys (SMAs) are a family of smart materials capable of sustaining large inelastic strains that can be recovered by heating or unloading, depending on prior loading history. The origin of this unusual behavior is the ability of SMAs to undergo a first-order solid–solid diffusionless and reversible phase change called martensitic transformation (MT) (Olson and Cohen, 1982). The transformation occurs at the lattice scale between a parent phase called austenite (A), stable at high temperature and low stress, and a product phase called martensite (M), metastable at low temperature and high stress. Of these two phases, austenite has the higher crystallography symmetry. Depending on the applied thermomechanical loading, different martensite variants may develop, characterized by their orientation with respect to the interface with austenite called "habit plane". Early crystallographic theories for MT are attributed to Wechsler et al. (1953) and Bowles and Mackenzie (1954). During cooling, the transformation of austenite to martensite begins at a characteristic "martensite start" temperature M_s and concludes at a lower "martensite finish" temperature M_f. If the material is then heated, the reverse transformation to austenite starts at the "austenite start" temperature A_s and concludes at the "austenite finish" temperature A_f. These transformation temperatures can be measured using different techniques including Differential Scanning

* Corresponding author.
E-mail addresses: cheikh.cisse@kustar.ac.ae (C. Cisse), wael.zaki@kustar.ac.ae (W. Zaki), tarak.ben-zineb@univ-lorraine.fr (T. Ben Zineb).

http://dx.doi.org/10.1016/j.ijplas.2015.08.006
0749-6419/

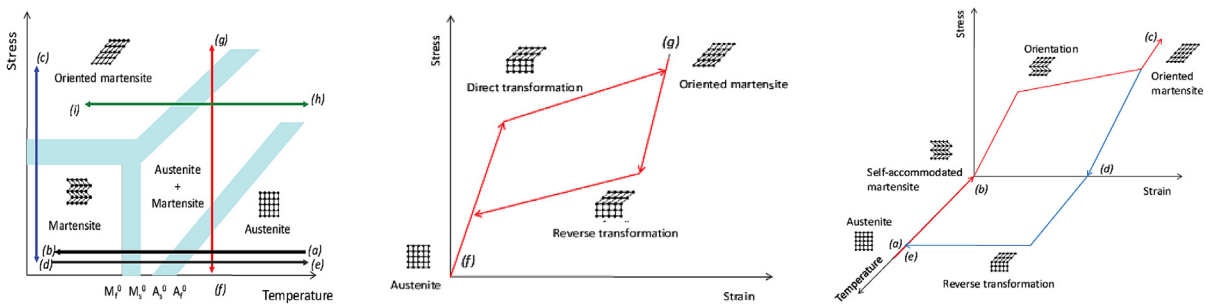

(a) schematic phase diagram for a SMA. (b) pseudoelastic behavior. (c) One-way shape memory effect.

Fig. 1. Illustration of a typical phase diagram and key behaviors for SMAs (Morin, 2011).

Calorimetry (DSC) (Shaw and Kyriakides, 1995). In the absence of stress, the phase transformation temperatures are denoted M_f^0, M_s^0, A_s^0 and A_f^0. Fig. 1(a) shows a schematic phase diagram that illustrates the dependence of phase transformation stress on temperature.

The martensitic transformation is at the origin of the two main effects observed in SMAs, namely the shape memory effect (SME) and pseudoelasticity (PE).

1.1. Pseudoelasticity

If austenite is loaded along path $(f) \rightarrow (g)$ in Fig. 1(a), it transforms to detwinned martensite with potentially large inelastic strains (Brinson, 1993; Brinson and Lammering, 1993; Leclercq and Lexcellent, 1996). The reverse transformation takes place during unloading $(g) \rightarrow (f)$ allowing the recovery of inelastic strain (Wayman and Bhadeshia, 1983). The stress–strain curve of a pseudoelastic thin walled CuAlBe cylinder subjected to uniaxial loading is shown in Fig. 2(a), where the simulation results by Gu et al. (2015) and the experimental work of Bouvet et al. (2004) are reported. Additional results are shown in Fig. 2(b) based on the work of Panico and Brinson (2007), Arghavani et al. (2010b) and Gu et al. (2015), and the experimental results of Sittner et al. (1995).

1.2. The one-way shape memory effect

The one-way shape memory effect (OWSME) was first observed in a Gold–Cadmium alloy by Chang and Read (1951) and in NiTi by Buehler et al. (1963). Later, Sato et al. (1982) discovered the OWSME in Fe690Mn30Si1 (wt.%) Fe-based alloy leading

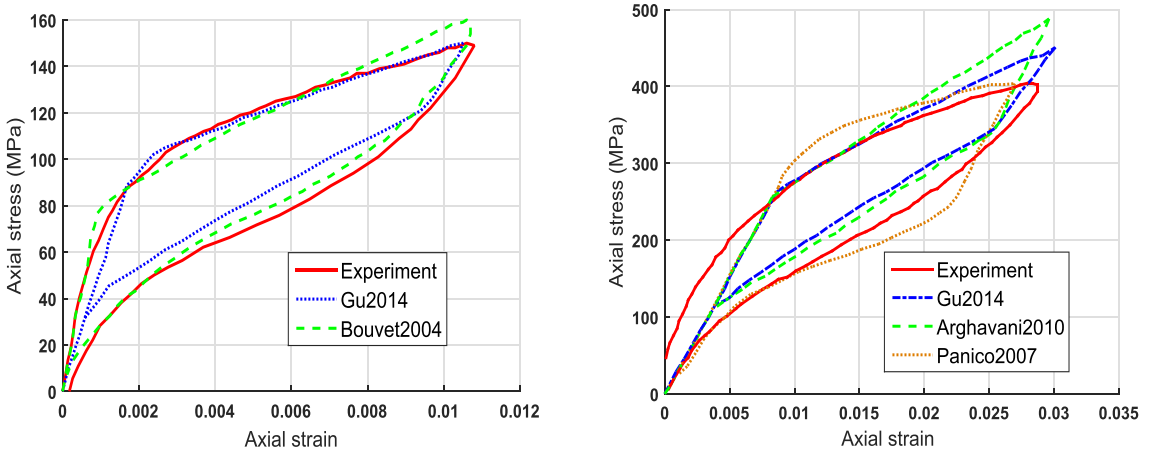

(a) pseudoealstic stress-strain behavior of CuAlBe. (b) pseudoealstic stress-strain behavior of CuAlZnMn.

Fig. 2. Stress–strain behavior of pseuoelastic SMAs (Gu et al., 2015).

to the development of Fe64Mn30Si6 (wt%) SMA with perfect shape memory by Murakami et al. (1986). The OWSME manifests itself under appropriate thermomechanical loading like the one illustrated by the sequence $(a) \rightarrow (b) \rightarrow (c) \rightarrow (d) \rightarrow (e)$ in Fig. 1(a). When austenite is cooled below M_s^0 in the absence of stress ($(a) \rightarrow (b)$), the forward transformation produces twinned or self-accommodating martensite M_T, which in NiTi and Cu-based SMAs consists of 24 randomly oriented variants (Hane and Shield, 1999a; James and Hane, 2000). If this M_T is then subjected to stress, the variants are detwinned ($(b) \rightarrow (c)$). Contrary to self-accommodation, the orientation of twinned martensite induces macroscopic orientation strain that is inelastic. Upon unloading, the oriented martensite M_σ remains stable as does the orientation strain ($(c) \rightarrow (d)$). Heating above A_f, however, allows for reverse transformation and the recovery of the inelastic strain ($(d) \rightarrow (e)$). The OWSME is emblematic of the behavior of SMAs and is therefore accounted for by most SMA models. Fig. 3(a) shows the simulated stress–strain curve following path $(b) \rightarrow (c) \rightarrow (d)$ by Zaki and Moumni (2007a) which was validated against the experimental data of Shaw and Kyriakides (1995).

1.3. The two-way shape memory effect

Unlike the OWSME, the two-way shape memory effect (TWSME) is not an intrinsic behavior in SMAs but is rather acquired. Early work on the TWSME is due to Perkins (1974), Miyazaki et al. (1981), Liu and McCormick (1990), Rogueda et al. (1991) and Stalmans et al. (1992). The TWSME can generally be induced by cyclic loading at $T < M_f^0$ or $T > A_f^0$, referred to as "training" (Schroeder and Wayman, 1977; Cingolani et al., 1995; Pons et al., 1999), or by deformation of stress-induced martensite at $T > M_s^0$ (Delaey et al., 1974) or the creation of precipitates in the material (Oshima and Naya, 1978; Amengual et al., 1995; Guilemany and Fernández, 1995). The physical mechanism responsible for the development of TWSME in trained SMAs was explained by Perkins and Sponholz (1984), Contardo (1988), Tadaki et al. (1988), Lovey et al. (1995) and De Araujo (1999) as follows: Unrecovered strain at the end of each loading cycle accumulates during training until saturation. The resulting permanent dislocations, defects and the residual stress stabilize a fraction of the martensite plates which are then identically recreated during subsequent transformations, thus producing macroscopic strain. This allows a trained SMA to switch configurations between stable austenite and oriented martensite phases by heating or cooling without requiring any mechanical load. If the orientation of martensite during cooling ($(h) \rightarrow (i)$ in Fig. 1(a)) is facilitated by external stress, the process is called assisted two-way shape memory effect (ATWSME) or superthermal effect (see Fig. 3(b)) and favors the nucleation of oriented martensite variants (Kim, 2004, 2005). Numerical models for TWSME were proposed, among others, by Rogueda et al. (1991), Hebda and White (1995), Bo and Lagoudas (1999), Lexcellent et al. (2000), Auricchio et al. (2003) and Zaki and Moumni (2007a).

The most commonly used SMAs to-date are NiTi-based also called Nitinol, as well as Cu-based and Fe-based alloys. Nitinol and single crystal Cu-based SMAs are capable of the highest inelastic strain recovery (up to 10%) due to their thermo-elastic phase change (Otsuka and Wayman, 1999; Johnson, 2013; Bel Haj Khalifa et al., 2013). In addition, Nitinol is biocompatible (Buehler and Cross, 1969; Shabalovskaya, 1996; Es-Souni et al., 2005; Bansiddhi et al., 2008), whereas Cu-based SMAs are brittle and thus more delicate to use in applications (Casciati et al., 2007; Ueland and Schuh, 2012). Compared to NiTi, Cu-based SMAs

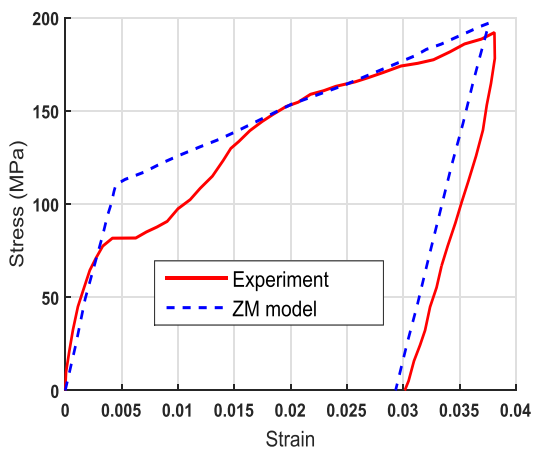

(a) OWSME stress-strain curve at T=-10 °C. Simulation by Zaki and Moumni (2007a) vs. experimental data by Shaw and Kyriakides (1995).

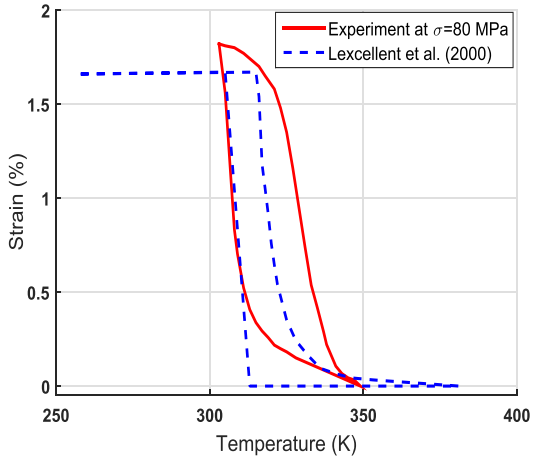

(b) TWSME strain-temperature curve by (Lexcellent et al., 2000).

Fig. 3. One-way and two-way shape memory behaviors in a SMA.

exhibit less dependence on temperature (Sutou et al., 2009; Niitsu et al., 2011), loading rate (Araya et al., 2008; Araki et al., 2012), and grain size (Sutou et al., 2013) as well as lower pseudoelasticity (Araki et al., 2011). On the other hand, Fe-based SMAs show very large hysteresis and ductility but lower shape recovery (about 4%). However, this low SME can be improved by training (Federzoni et al., 1993; Zhao, 1999), precipitation (Rong et al., 1995; Wen et al., 2008) or by a suitable combination of aging, pre-straining and shape memory training (Lin et al., 2014). In Fe-SMAs, the non-thermoelastic transformation is crystallographically non-reversible. In addition to the SME and PE, SMAs display other properties such as the rubber-like effect that results from aging of martensite and allows reversible twinning and detwinning of martensite variants.

Over the last four decades, the complex behavior of shape memory alloys has motivated intense theoretical and experimental research. In particular, significant effort was dedicated to developing models that would help understand the physical mechanisms underlying the martensitic transformation in SMAs and facilitate the design and fabrication of SMA devices. The objective of this paper is to provide an up-to-date review of key constitutive models for SMAs, including a classification of these models in terms of modeling scale and mathematical structure and a discussion of their strengths and weaknesses. An effort is made to use a uniform notation in reporting the various mathematical relations and, where feasible, to replot numerical simulation results from surveyed publications for improved clarity. A section is dedicated to showing how the basic constitutive relations for one class of models can reduce to a single mathematical formulation under certain loading cases, which allows for direct comparison of their parameters. The paper follows a comparable work by Patoor et al. (2006) and Lagoudas et al. (2006), which is now becoming dated. In Patoor et al. (2006), the authors reviewed the kinematics of the martensitic transformation with a discussion of micromechanical modeling for single crystal SMAs while Lagoudas et al. (2006) focused on micromechanical and phenomenological models of polycrystalline SMAs. A more recent and detailed review can be found in the book of Lexcellent (2013).

2. Microscopic thermodynamic models

Models in this category are those intended to describe microstructural features in SMA behavior such as phase nucleation, interface motion, martensite twin growth, and so on, at the lattice or grain-crystal levels. They are mostly developed based on the Ginzburg–Landau theory or using molecular dynamics.

2.1. Microscopic models based on the Ginzburg–Landau theory

The constitutive equations in these models are derived from a polynomial energy expression, usually written in terms of observable variables such as strain and temperature. The polynomial potential models of Falk (1980, 1983) are recognized as the earliest constitutive models for SMAs, later followed by Ball and James (1989), Barsch and Krumhansl (1988) and Abeyaratne and Knowles (1990). In his work, Falk (1980) used a Landau-Devonshire-like free energy based on similarity of the electromagnetic curves of ferromagnetic materials with the uniaxial stress–strain response of SMAs. Phase transition was assumed to occur at unstable equilibria where the slope of the stress–strain curve is negative. Three years later, the author modeled the martensite transformation based on the static Ginzburg–Landau (GL) theory within the framework of continuum thermodynamics. The structure of the static domain walls for austenite and martensite was determined from equilibrium conditions. A discrete spectrum of domain structures was obtained in finite crystals whereas four types of domain walls were found in unbounded crystals. To avoid the unphysical minima that appear in 3D simulations of GL models, Levitas and Preston (2002a,b) and Levitas et al. (2003) used an order parameter that averages out the variables used to describe the atomic lattice vibrations. Wang and Melnik (2007) and Dhote et al. (2014) also used the GL theory to develop mesoscale phase field models for martensite transformation in SMA nanowires. Mahapatra and Melnik (2006) proposed a consistent GL potential that minimizes the number of parameters for Simulation of 3D single crystal NiAl samples using finite element method (FEM), with no need to track the austenite–martensite and variant–variant interfaces. Wang and Khachaturyan (1997) and Jin et al. (2001) used time-dependent Ginzburg–Landau (TDGL) kinetic equations to develop phase field models for the martensitic transformation. Later, Idesman et al. (2008), Cho et al. (2012), and Zhong and Zhu (2014) used FEM to solve the kinetic equations in their multivariant 3D TDGL-based models. In the same line of thought, She et al. (2013) showed the particular influence of the inertial and surface energies on the martensite transformation in NiAl, with focus on nuclei growth and generation of invariant habit planes. Fig. 4 shows the MT at the nanoscale at $t = 3 \times 10^{-12}$ s, $t = 4 \times 10^{-12}$ s and $t = 5 \times 10^{-12}$ s under surface stress free condition ($\sigma_n = \tau_n = 0$ MPa) for which case the phase transition is completed at $t = 11 \times 10^{-12}$ s. The presence of a compressive surface stress at the boundaries of the 50 nm × 50 nm NiTi plate was found to increase the total nucleation time ($t = 13 \times 10^{-12}$ s), while tensile surface stress tend to decrease the completion time ($t = 10 \times 10^{-10}$ s). The use of these models for structural simulations remains impractical to-date, mainly because of their computational cost and inconvenient modeling scale.

2.2. Microscopic models based on molecular dynamics

Molecular dynamics is a branch of theoretical physics started in the late 1950s to simulate systems of atoms and molecules (Alder and Wainwright, 1959; Rahman, 1964). Molecular dynamics models (MDM) use Newton's equations to describe the motion of each particle in a system consisting of a finite number of particles. The motion of the ith particle is governed by

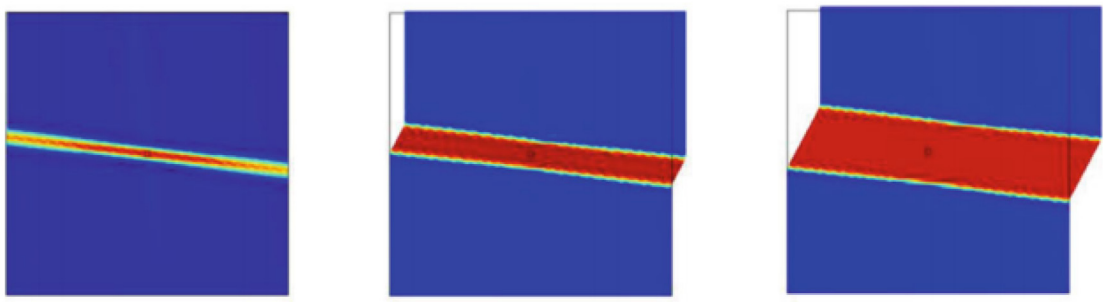

(a) $t = 3 \times 10^{-12}$s. (b) $t = 4 \times 10^{-12}$s. (c) $t = 5 \times 10^{-12}$s.

Fig. 4. Pattern of nucleus growth during martensite transformation under free stress: austenite is shown in blue and martensite in red (She et al., 2013). (For interpretation of the references to colour in this figure legend, the reader is referred to the web version of this article.)

$$m_i \ddot{r}_i = -\partial \Phi / \partial r_i, \tag{1}$$

where Φ is the potential energy of interaction between particles, and m_i and r_i are the mass and position vector of particle. The Verlet scheme is commonly used for time-discrete integration of this equation. The temperature of the system is usually obtained from the expression of an ideal gas law such that

$$T = \frac{2E_k}{3NK_b}, \tag{2}$$

where K_b is the Boltzmann constant, E_k is the total kinetic energy and N is the number of particles in the system. In MD, the supercell size and shape are assumed to change dynamically such that the internal stress $\boldsymbol{\sigma}^{int}$ equilibrates with the applied constant stress $\boldsymbol{\sigma}^{ext}$ (Parrinello and Rahman, 1981). The internal stress is related to the virial stress $\boldsymbol{\sigma}^{vir}$ (Parrinello and Rahman, 1981), that is equivalent to the Cauchy stress in continuum mechanics (Maranganti and Sharma, 2010), as follows:

$$\boldsymbol{\sigma}^{vir}(\boldsymbol{r}) = \frac{1}{J}\boldsymbol{h}\boldsymbol{\sigma}^{int}\boldsymbol{h}^{T} = \frac{1}{\Omega}\sum_i \left[- m_i \boldsymbol{v}_i \otimes \boldsymbol{v}_i + \sum_{i \neq j} \frac{\partial \Phi(r_{ij})}{\partial r_{ij}} \frac{\boldsymbol{r}_{ij} \otimes \boldsymbol{r}_{ij}}{r_{ij}} \right], \tag{3}$$

where, $\boldsymbol{h}$ is the cell tensor, J is the volume change, Ω is the current cell volume, $||\boldsymbol{v}_i||$ is the velocity vector of the ith atom and $\boldsymbol{r}_{ij} = \boldsymbol{r}_j - \boldsymbol{r}_i$ is the relative position vector of atom j with respect to atom i. A strain measure can be introduced at the atomic scale by analogy with the concept of the continuum Green strain (Saitoh and Liu, 2009). To this end, the infinitesimal segments between material points are substituted with interatomic segment vectors $\boldsymbol{r}_{ij}^{\alpha}$ between any two atoms i and j in a direction $\alpha = \{x,y,z\}$. The atomic strain measure is then given by

$$\varepsilon_{ij}^{\alpha\beta} = \frac{1}{2}\left(\frac{\partial u_{ij}^{\alpha}}{\partial r_{ij}^{\beta}(0)} + \frac{\partial u_{ij}^{\beta}}{\partial r_{ij}^{\alpha}(0)} \right) \approx \frac{1}{2\left[r_{ij}(0)\right]^2}\left(u_{ij}^{\alpha} r_{ij}^{\beta}(0) + u_{ij}^{\beta} r_{ij}^{\alpha}(0) \right), \tag{4}$$

where the current displacement u_{ij}^{α} is assumed to vary linearly with the initial interatomic distance $r_{ij}(0)$. Averaging (4) over a domain where atom i interacts with N others, the strain can be calculated at each atomic site as follows:

$$\varepsilon_i^{\alpha\beta} = \frac{1}{N}\sum_{j=1}^{N} \varepsilon_{ij}^{\alpha\beta}. \tag{5}$$

The difference between existing MD models for SMAs mainly resides in the choice of the potential, with most models using the Lennard–Jones (LJ) or embedded-atom-method (EAM) potentials.

2.2.1. Models using the EAM potential

The EAM potential was initially developed by Daw and Baskes (1984) for metals and later adapted for NiAl (Foiles and Daw, 1987; Chen et al., 1989; Rubini and Ballone, 1993; Farkas et al., 1995) and NiTi (Lai and Liu, 2000). For a system of atoms, it is expressed as follows:

$$\Phi = \sum_i F(\rho_i) + \frac{1}{2}\sum_i \sum_{j \neq i} \phi_i(r_{ij}), \tag{6}$$

where ϕ_{ij} describes the interaction between atoms i and j, r_{ij} is the spacial distance between atoms i and j, and $F(\rho_{ij})$ is an embedding function. A polynomial form was proposed by Rose et al. (1984) for F such that

$$F(\rho_i) = k_1\rho_i^{1/2} + k_2\rho_i + k_3\rho_i^2, \tag{7}$$

where ρ_i is the local electron density around the ith atom given by Clementi and Roetti (1974) as

$$\rho_i = \sum_{j\neq i}\tilde{\rho}(r_{ij}) = \sum_{j\neq i}\left(N^s\tilde{\rho}^s(r_{ij}) + N^d\tilde{\rho}^d(r_{ij})\right), \tag{8}$$

in which

$$\begin{aligned}\tilde{\rho}^s(r_{ij}) &= \tilde{\rho}^d(r_{ij}) = \frac{\left|\sum_l C_l R_l\right|^2}{4\pi},\\ R_l &= \frac{(2\zeta_l)^{n_l+\frac{1}{2}}}{[(2n_l)!]^{\frac{1}{2}}} r_{ij}^{n_l-1}(-\zeta_l r_{ij}).\end{aligned} \tag{9}$$

In Equation (9), C_l, ζ_l, N^d, N^s, n_l, k_1, k_2, k_3 are atom parameters. The following expression for ϕ_{ij} was proposed by Rubini and Ballone (1993):

$$\phi_{ij}(r_{ij}) = \frac{Z_i(r_{ij})Z_j(r_{ij})}{r_{ij}}, \tag{10}$$

where

$$Z(r_{ij}) = Z_0\left(1+\alpha r_{ij}^{\beta}\right)\exp\left(-\gamma r_{ij}\right), \tag{11}$$

and Z_0, α, β and γ are material parameters. The pressure is obtained from the virial theorem and controlled by the scaling method. The stress tensor is obtained and controlled using the Parrinello–Rahman (PR) method (Parrinello and Rahman, 1981). Sato et al. (2004), Uehara and Tamai (2006), Sato et al. (2008) and Ackland et al. (2008) modeled martensite transformation in NiTi using the EAM potential. Uehara et al. (2006) used the parameters proposed by Rose et al. (1984) to simulate the martensite transformation in a Ni68Al32 (at%) single crystal consisting of 864 atoms. The resulting stress–strain curve in Fig. 5(a) shows gradual zigzags with abrupt drops in stress corresponding to orientations of the variant layers. Smoother stress–strain behavior is obtained for larger models as shown in Fig. 5(b). Ishida and Hiwatari (2007) used a modified EAM

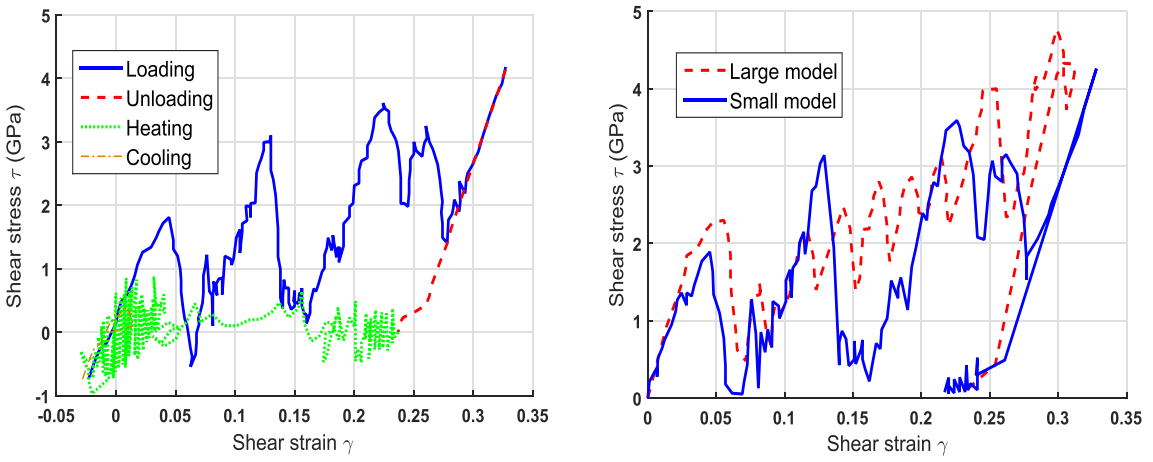

(a) stress-strain curve for the small model.

(b) comparison of stress-strain curves for the small and large models.

Fig. 5. Simulated stress–strain curves using an EAM potential (Uehara et al., 2006).

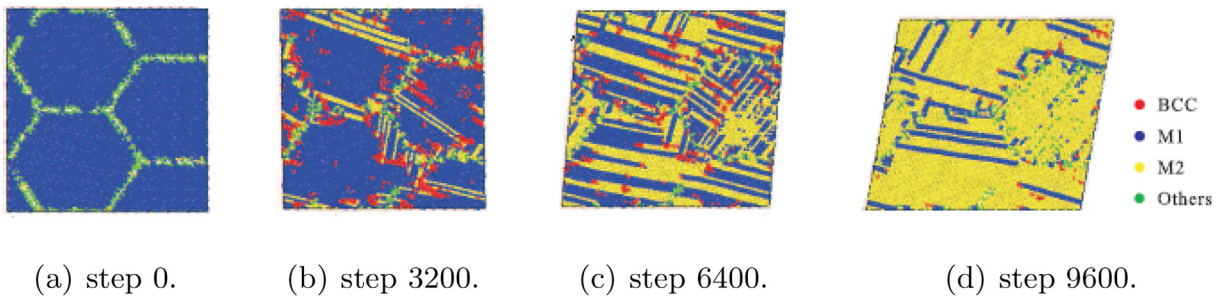

Fig. 6. Variation of the configuration of atoms for model P1: (a) initial state, (b) after relaxation, (c) during loading, and (d) after loading (Uehara et al., 2009).

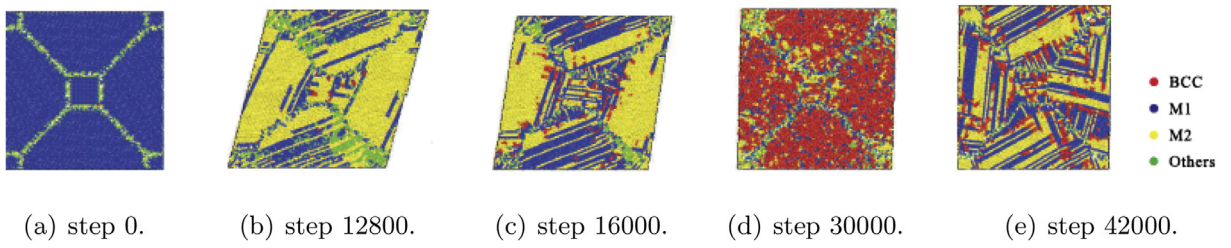

Fig. 7. Variation of the configuration of atoms for model P2: (a) initial state, (b) after loading, (c) after unloading, (d) after heating, and (e) after cooling (Uehara et al., 2009).

potential to show that the forward transformation temperature in NixTi $(1-x)$ (at%) varies instantaneously for $35 < x < 60$. Using this potential, Guo et al. (2007) pointed out the occurrence of MT at the crack tip in NiAl due to high stress concentration. Uehara et al. (2009) considered two NiAl polycrystals, P1 and P2, 16.6 nm × 15.6 nm × 1.5 nm in size and consisting of 31,000 atoms each. P1 comprised four hexagonal grains and P2 two square and two octagonal grains. Two martensite variants were considered: M1 with an alternating sequences of variant layers and M2 with a consecutive sequence. Starting with M1, the shape memory behavior was simulated as shown in Fig. 6 for P1 and in Fig. 7 for P2. It is interesting to note that the grain boundaries remained fixed during the simulation. Stress–strain curves obtained by Uehara et al. (2009) for P1 and P2 are shown in Fig. 8(a) and (b) for different loading conditions. The curves differ significantly from those obtained for single crystals and approach macroscopic experimental observations. Using a semi-empirical EAM potential, Saitoh and Liu (2009) analyzed the reversibility of martensite transformation in a Ni52.4Al47.6 (at%) system comprising 33,640 atoms. Fig. 9(a) shows the variation of the stress components with the longitudinal strain ε_{33}. The first part of the curve represents the

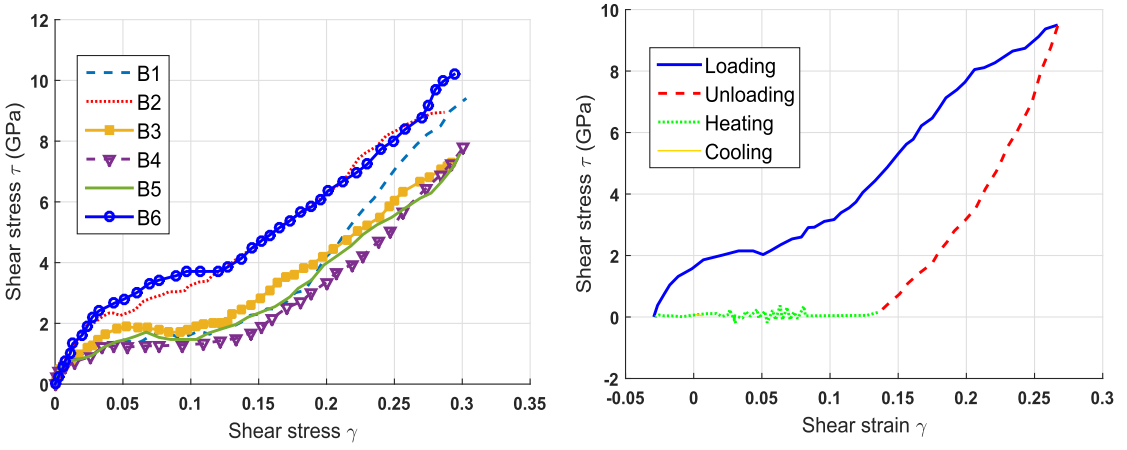

(a) pseudoelasticity for different variant orientations in P1.

(b) shape memory effect in P2.

Fig. 8. Stress–strain curves for the two polycrystals P1 and P2 (Uehara et al., 2009).

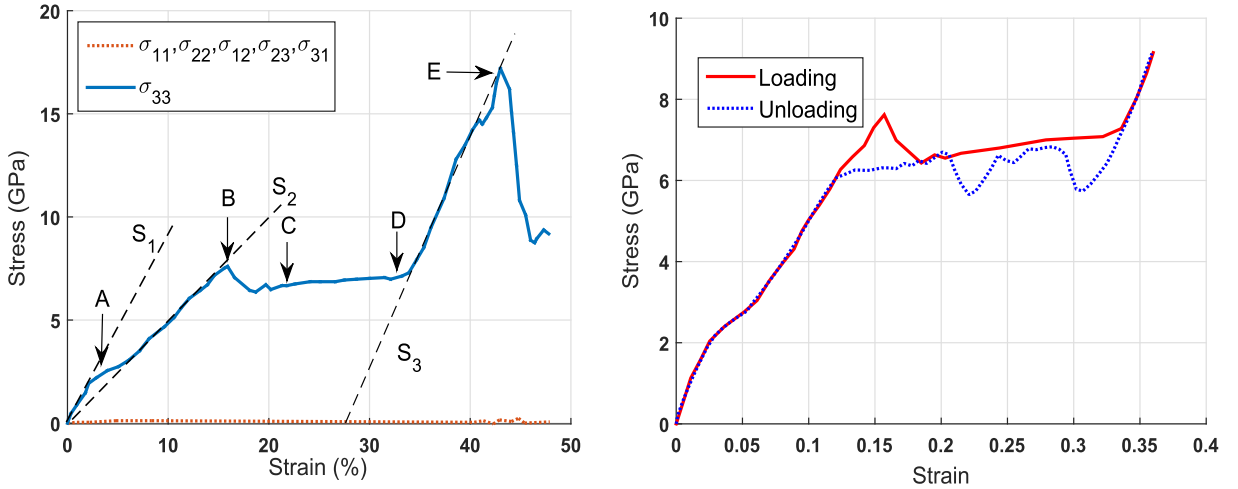

(a) tensile loading until failure.

(b) tensile loading cycle.

Fig. 9. Pseudoelastic response in a large 1D Ni–Al model of 33,640 atoms (Saitoh and Liu, 2009).

elastic behavior of austenite with Young's modulus varying between $E_A^{(1)} = 100$ GPa and $E_A^{(2)} = 47$ GPa, the second part corresponds to the forward phase transformation plateau, the third part represents the elastic behavior of martensite with $E_M = 113$ GPa, and the last part shows a sudden drop in stress at failure. The lower stiffness of austenite compared to martensite contradicts macroscopic experimental observations but is consistent with the nano-indentation measurements of Rajagopalan et al. (2005) where martensite was found to be 50% stiffer than austenite. Unloading the system before the breaking point leads to complete reverse transformation characterized by very small hysteresis (see Fig. 9(b)) due to the existence of a single minimum for the EAM potential corresponding to austenite. Mutter and Nielaba (2013) used a Finnis-Sinclair EAM potential (Finnis and Sinclair, 1984) to study the SME in a NiTi 3D nanomodel consisting of 90,000 atoms. The stress–strain tension curve at a loading rate $\dot{u} = 1$ m/s and $T = 1$ K are shown in Fig. 10(a) for Ni concentrations between 50% and 52%. The increase in Ni content was found to increase the elastic modulus of martensite and smoothen the transformation plateau due to increasing lattice instability. Contrary to the observations of Saitoh and Liu (2009) for NiAl, important hysteresis was found for the Nitinol nanomodel with a remanent strain between 5 and 5.6%. The strain–temperature curve during reverse transformation upon heating is shown in Fig. 10(b), where oriented martensite

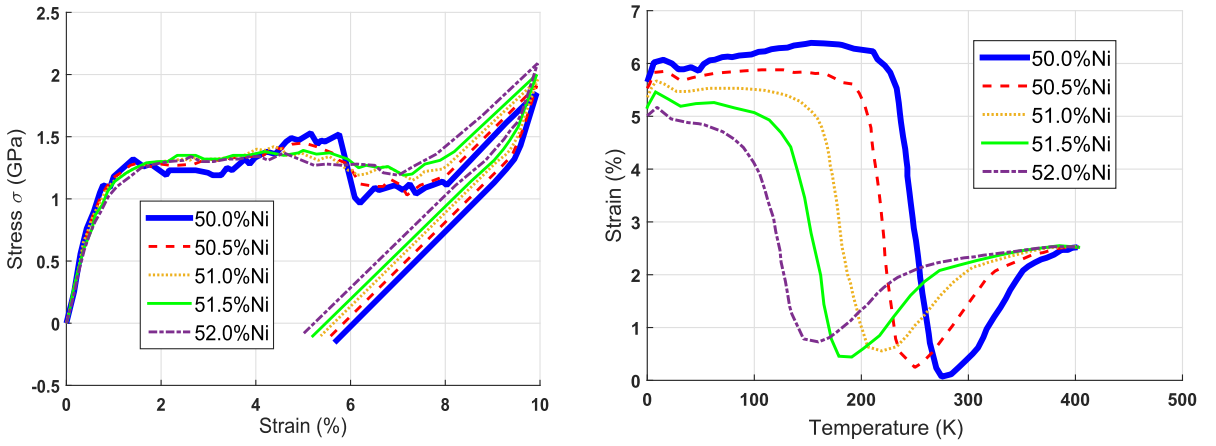

(a) tensile stress-strain curve of the NiTi nanomodel at $T = 1$ K.

(b) heating of the NiTi nanomodel to 400 K.

Fig. 10. Simulation of the SME in a NiTi nanoparticle using the Finnis-Sinclair EAM potential (Mutter and Nielaba, 2013).

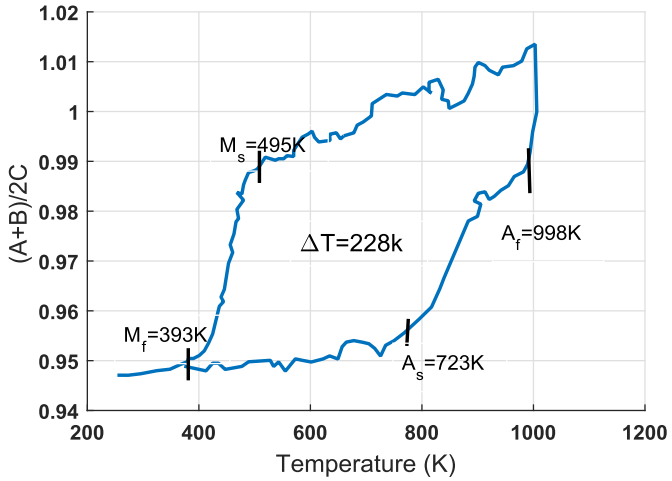

Fig. 11. Hysteresis in a heating–cooling cycle observed with a LJ potential (Ozgen and Adiguzel, 2004).

remains stable at the beginning of the heating stage before transforming back to austenite. An intermediate stage with a strain drop was observed due to the passage from a local minimum of the free energy corresponding to M_σ to a global minimum correspong to M_T. However, a final strain of 2.5% irrespective of the Ni percentage was finally found in the austenite phase. Recently, Mirzaeifar et al. (2014) successfully used a modified EAM potential to simulate the formation and reorientation of nanotwinned martensite in NiTi. The authors found that twinned martensite is stabilized by a propensity of the free surfaces to minimize their energy. In the absence of free surfaces, the pre-martensite or rhombohedral phase becomes stable.

2.2.2. Models using the Lennard–Jones potential

An alternative to EAM for the study of the atomistic austenite–martensite systems is to use the Lennard–Jones (LJ) potential, which has a simpler expression given by

$$\Phi = \frac{1}{2}\sum_i \sum_{j\neq i} \phi_{ij}(r_{ij}). \tag{12}$$

In Equation (12), the interaction energy $\phi_{ij}(r_{ij})$ between atoms i and j is given by

$$\phi_{ij}(r_{ij}) = 4\tilde{\varepsilon}_{ij}\left(\left(\frac{\tilde{\sigma}_{ij}}{r_{ij}}\right)^{12} - \left(\frac{\tilde{\sigma}_{ij}}{r_{ij}}\right)^{6}\right), \tag{13}$$

where $\tilde{\varepsilon}_{ij}$ is the depth of the potential well and $\tilde{\sigma}_{ij}$ represents the minimum possible distance between atoms i and j in the absence of interaction. Using the LJ potential, Suzuki and Shimono (2003) studied in detail the mechanisms of martensite transformation, including the formation of hexagonal close-packed (hcp) structures, nanocrystal size effect, etc. Ozgen and Adiguzel (2004) investigated the thermoelastic transformation of NixAl $(1-x)$ (at%) for $60 < x < 65$. They observed a thermal hysteresis of $\Delta T = 228$ K for $x = 62.5$ as shown in Fig. 11. Later, Kastner (2006) successfully simulated the thermodynamic properties of a small 2D assembly of 41 atoms, using the parameters listed in Table 1.

The phase composition was assumed to be stable for minimum values of the dimensionless free energy $\widehat{F}(T,\varepsilon)$ obtained by integrating the normalized load $\widehat{P}(T,\varepsilon')$ with respect to strain as follows:

$$\widehat{F}(T,\varepsilon) = \widehat{U}(T,\varepsilon) + T\widehat{S}(T,\varepsilon) = \widehat{F}(T,\varepsilon_0) + l_0 \int_{T,\varepsilon_0}^{T,\varepsilon} \widehat{P}(T,\varepsilon')d\varepsilon', \tag{14}$$

Table 1
Interaction parameters for the LJ potential in Kastner (2006).

	A1–A1	A2–A2	A1–A2
$\tilde{\varepsilon}_{ij}$	1.14	1.0	0.223
$\tilde{\sigma}_{ij}$	0.9	0.865	0.6

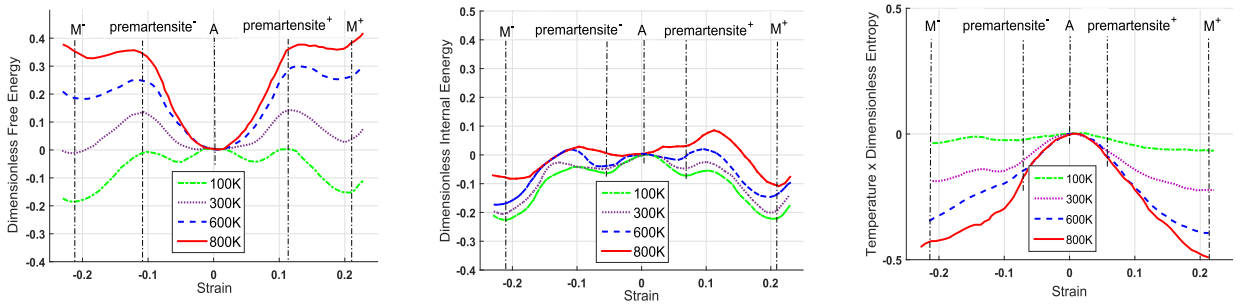

(a) free energy isotherms. (b) internal energy isotherms. (c) entropy isotherms.

Fig. 12. Simulated isotherms for the assembly of 41 atoms (Kastner, 2006).

where ε_0 is the initial strain, ε is the current strain, $\widehat{F}(T,\varepsilon_0)$ is a temperature-dependent parameter, l_0 is the reference length of the chain assembly, and $\widehat{S}(T,\varepsilon)$ and $\widehat{U}(T,\varepsilon)$ are the dimensionless entropy and internal energy of the system. In Fig. 12(a), $\widehat{F}(T,\varepsilon)$ is not convex and exhibits temperature-dependent minima. Fig. 12(b) and (c) show that martensite is stable for minimum internal energy, while austenite becomes stable for maximum entropy. For comparison, the author investigated the shape memory behavior in a large body corresponding to a sequence of 11 small clusters of 41-atoms connected diagonally. Martensite reorientation was found to occur at constant critical load in stress controlled simulation, which was not the case for strain controlled loading. Suzuki et al. (2006) and Deng et al. (2010) combined the Monte-Carlo method and MD to explain the underlying mechanisms of martensite stabilization and rubber-like behavior of SMAs. Using a similar approach, Zhong and Zhu (2012) simulated the patterning of nanotwins, including twin coarsening near the free surfaces, branching near the habit planes and substrate constraints. Kastner et al. (2011) investigated the evolution of the microstructure during cyclic transformations using a binary LJ potential. Martensite and austenite were favored at low and high values of the normalized parameters $\tilde{\varepsilon}_{ij}/\varepsilon_0$ and $\tilde{\sigma}_{ij}/\sigma_0$, respectively. When the system of 160,000 atoms was cooled down to 200 K, the martensite phase was found to nucleate and austenite was present around defects. The product morphology in Fig. 13(a) shows the formation of martensite plates. The potential energy field in Fig. 13(b) shows perfect compatibility between these micro-twins with no interface energy.

The above results demonstrate that molecular dynamics is a powerful and promising technique for modeling shape memory alloys at the microscopic level. However, accurate results require the use of large and complex models, which results in high computation cost.

3. Micro–macro models

The micro–macro models rely on micromechanics to describe the material behavior at the micro or meso scales. A scale transition is then used to derive macroscopic constitutive equations (Sun and Hwang, 1993; Huang et al., 2000; Blanc and Lexcellent, 2004; Sadjadpour and Bhattacharya, 2007; Levitas and Ozsoy, 2009). The development of micro–macro models

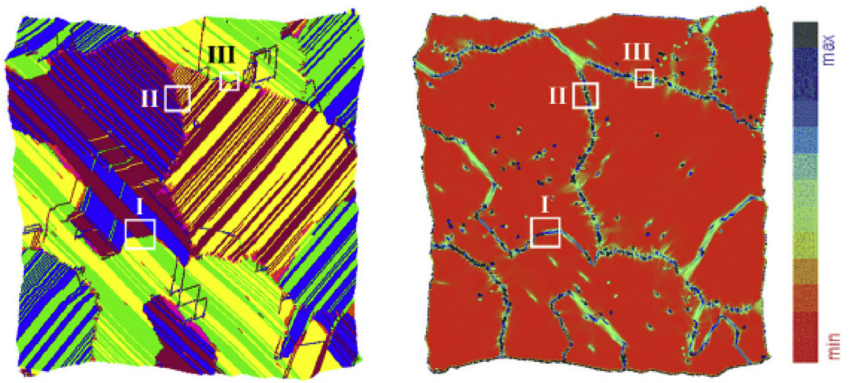

(a) product morphology. (b) potential energy field.

Fig. 13. Martensite transformation in a 160,000 atom SMA system (Kastner et al., 2011).

requires the use of suitable observable variables (OVs) and internal variables (IVs). The OVs usually consist of temperature T and external stress $\boldsymbol{\sigma}$ or strain $\boldsymbol{\varepsilon}$. The IVs usually comprise the volume fraction ξ of martensite and a mean transformation strain (MTS). Frémond (1987) developed one of the earliest constitutive models for SMAs using internal variables. Micromechanical and micro-plane/micro-sphere models are the two main micro–macro modeling approaches.

3.1. Models based on micromechanics

Micromechanical models rely on micromechanics to obtain an expression for the interaction energy within the material. The macroscopic behavior of the polycrystalline SMA is then obtained by averaging the behavior of single grains using scale transition techniques such as the Mori–Tanaka scheme (Mori and Tanaka, 1973; Siredey et al., 1999; Sun and Hwang, 1994), the self-consistent scheme (Patoor et al., 1988; Lu and Weng, 1998; Gall and Sehitoglu, 1999) and the uniform stress (Sachs) or strain (Taylor) mix approaches (Šittner and Novák, 2000; Thamburaja and Anand, 2001; Stupkiewicz and Petryk, 2002; Novák and Šittner, 2004; Hackl and Heinen, 2008). Alternatively, the scale transition can be accomplished numerically, e.g. using finite element techniques to account for the complex interaction between neighboring grains (Gall et al., 2000; Thamburaja and Anand, 2001; Lim and McDowell, 2002; Anand and Gurtin, 2003; Sengupta et al., 2009; Junker and Hackl, 2011). Early micromechanical models for SMAs were proposed among others by Delaey et al. (1987), Fischer and Tanaka (1992) and Raniecki et al. (1992). Micromechanical models considering plastic deformation were also proposed by Kudoh et al. (1985), Sun et al. (1991), Sadjadpour and Bhattacharya (2007), Wang et al. (2008) and Yu et al. (2012). Patoor et al. (1988, 1994) used crystallographic data to describe martensite transformation in polycrystal SMAs. The interaction energy was obtained from a 24×24 matrix called interaction matrix. The model accurately simulated pseudoelasticity but could not describe the self-accommodation of martensite. Lu and Weng (1997) developed a similar model with one martensite variant, while Goo and Lexcellent (1997) proposed a multivariant formulation considering both chemical and surface energies. Alternative expressions for the interaction energy in SMAs can be found in Huang and Brinson (1998) and Siredey et al. (1999). Gao et al. (2000) and Govindjee and Miehe (2001) proposed 3D multivariant models featuring a simplified interaction energy. The latter model was extended to finite strains by Stein and Sagar (2008). Other well-established micromechanical models were developed by Gall and Sehitoglu (1999), Lim and McDowell (2002), Wang and Yue (2006), Wang et al. (2008), Collard and Ben Zineb (2012), Yu et al. (2012), Levitas (2013), Guthikonda and Elliott (2013) and Zhu et al. (2014).

Hane and Shield (1999a) identified a set of 192 theoretically possible transformations systems in TixNi $(100 - x)$ (at%) with $x \in [49,50]$, of which only 24 have been observed experimentally. The habit planes are equally distributed between type I and type II that are normals in the {100} family and {110} family, respectively, with 24 symmetry. It is worth noting that the 192 habit planes represent only 36% of the total 528 theoretically possible solutions in NiTi. Compared to NiTi, Shield (1995) and Hane and Shield (1999b) showed that Cu–Al–Ni SMAs display 96 habit planes out of 120 that are theoretically possible. This corresponds to the total number of V-microstructures for which the variants pair (V_i, V_j') such that $i > j$ as reported by Stupkiewicz and Górzyńska-Lengiewicz (2012) who identified a total of 528 habit planes for the cubic-to-orthorhombic transformation, like in NiTi. For simplicity, most models and numerical simulations consider a maximum of 24 martensite variants. A notable exception is the work of Anand and Gurtin (2003) who simulated the superelastic stress–strain response of NiTi using the complete set of 192 martensite variants as well as the reduced set of 24 transformation systems. The authors found qualitatively similar curves for both systems with comparable hysteresis size. However, using the reduced set of 24 habit planes gave higher stress–strain curves compared to those predicted using the full set of 192 transformation systems. Considering the 24 variants of martensite in Cu-based and NiTi SMAs, the total martensite volume fraction and the transformation strain tensor are defined as the sum of contributions by the different variants, i.e.

$$\boldsymbol{\varepsilon}^{\mathrm{tr}} = \sum_{k=1}^{24} \xi_k \boldsymbol{\varepsilon}^{\mathrm{tr},k} \ \text{ and } \ 0 \le \xi = \sum_{k=1}^{24} \xi_k \le 1, \tag{15}$$

where ξ_k is the volume fraction of the kth martensite variant for which the local transformation strain tensor $\boldsymbol{\varepsilon}^{\mathrm{tr},k}$ is given by

$$\boldsymbol{\varepsilon}^{\mathrm{tr},k} = \frac{1}{2} g^{\mathrm{tr}} (\boldsymbol{n}_k \otimes \boldsymbol{m}_k + \boldsymbol{m}_k \otimes \boldsymbol{n}_k). \tag{16}$$

In the above equation, g^{tr} is the magnitude of the transformation, $\boldsymbol{n}_k$ is a unit vector normal to the habit plane and $\boldsymbol{m}_k$ is the unit vector indicating the transformation direction. The vectors $\boldsymbol{n}$ and $\boldsymbol{m}$ are given in Table 2 for Nitinol and in Table 3 for CuZnAl SMAs.

The energy due to the interaction between all 24 martensite variants is given by

$$\Phi_{\mathrm{intervariant}} = \frac{1}{2} \sum_{i,j=1}^{24} H^{ij} \xi^i \xi^j, \tag{17}$$

where H^{ij} couples variants ith and jth in the interaction matrices given in Table 4 for NiTi and in Table 5 for CuZnAl and CuAlBe.

Table 2
Crystallographic data for the 24 martensite variants in NiTi (Wang et al., 2008).

Variant	$\boldsymbol{n}$			$\boldsymbol{m}$			Variant	$\boldsymbol{n}$			$\boldsymbol{m}$		
1	−0.8889	−0.4044	0.2152	0.4114	−0.4981	0.7633	13	−0.2152	0.8889	−0.4044	−0.7633	−0.4114	−0.4981
2	−0.4044	−0.8889	−0.2152	−0.4981	0.4114	−0.7633	14	−0.2152	−0.8889	0.4044	−0.7633	0.4114	0.4981
3	0.8889	0.4044	0.2152	−0.4114	0.4981	0.7633	15	0.2152	0.4044	−0.8889	0.7633	0.4981	0.4114
4	0.4044	0.8889	−0.2152	0.4981	−0.4114	−0.7633	16	0.2152	−0.4044	0.8889	0.7633	−0.4981	−0.4114
5	−0.8889	0.4044	−0.2152	0.4114	0.4981	−0.7633	17	0.8889	−0.2152	0.4044	−0.4114	−0.7633	0.4981
6	0.4044	−0.8889	0.2152	0.4981	0.4114	0.7633	18	−0.8889	−0.2152	−0.4044	0.4114	−0.7633	−0.4981
7	0.8889	−0.4044	−0.2152	−0.4114	−0.4981	−0.7633	19	0.4044	0.2152	0.8889	0.4981	0.7633	−0.4114
8	−0.4044	0.8889	0.2152	−0.4981	−0.4114	0.7633	20	−0.4044	0.2152	−0.8889	−0.4981	0.7633	0.4114
9	0.2152	0.8889	0.4044	0.7633	−0.4114	0.4981	21	0.8889	0.2152	−0.4044	−0.4114	0.7633	−0.4981
10	0.2152	−0.8889	−0.4044	0.7633	0.4114	−0.4981	22	−0.8889	0.2152	0.4044	0.4114	0.7633	0.4981
11	−0.2152	−0.4044	−0.8889	−0.7633	−0.4981	0.4114	23	−0.4044	−0.2152	0.8889	−0.4981	−0.7633	−0.4114
12	−0.2152	0.4044	0.8889	−0.7633	0.4981	−0.4114	24	0.4044	−0.2152	−0.8889	0.4981	−0.7633	0.4114

Table 3
Crystallographic data for the 24 martensite variants in CuZnAl (De Vos et al., 1978; Patoor et al., 1994).

Variant	$\boldsymbol{n}$			$\boldsymbol{m}$			Variant	$\boldsymbol{n}$			$\boldsymbol{m}$		
1	−0.182	0.669	0.721	−0.165	−0.737	0.665	13	0.721	−0.182	0.669	0.665	−0.165	−0.737
2	−0.182	0.721	0.669	−0.165	0.665	−0.737	14	0.669	−0.182	0.721	−0.737	−0.165	0.665
3	0.182	0.669	0.721	0.165	−0.737	0.665	15	0.721	0.182	0.669	0.665	0.165	−0.737
4	0.182	0.721	0.669	0.165	0.665	−0.737	16	0.669	0.182	0.721	−0.737	0.165	0.665
5	−0.669	−0.182	0.721	0.737	−0.165	0.665	17	0.669	−0.721	0.182	−0.737	−0.665	0.165
6	−0.721	−0.182	0.669	−0.665	−0.165	−0.737	18	0.721	−0.669	0.182	0.665	0.737	0.165
7	−0.669	0.182	0.721	0.737	0.165	0.665	19	−0.669	0.721	0.182	0.737	0.665	0.165
8	−0.721	0.182	0.669	−0.665	0.165	−0.737	20	−0.721	0.669	0.182	−0.665	−0.737	0.165
9	−0.182	−0.669	0.721	−0.165	0.737	0.665	21	−0.721	−0.669	0.182	−0.665	0.737	0.165
10	−0.182	−0.721	0.669	−0.165	−0.665	−0.737	22	−0.669	−0.721	0.182	0.737	−0.665	0.165
11	0.182	−0.669	0.721	0.165	0.737	0.665	23	0.721	0.669	0.182	0.665	−0.737	0.165
12	0.182	−0.721	0.669	0.165	−0.665	−0.737	24	0.669	0.721	0.182	−0.737	0.665	0.165

A general expression for the complementary free energy in a micromechanical model can be written as follows (Wang et al., 2008):

$$\Psi\left(\boldsymbol{\sigma}, T, \xi^n, \boldsymbol{\varepsilon}^{\mathrm{pl}}\right) = \frac{1}{2}\boldsymbol{\sigma} : \boldsymbol{S} : \boldsymbol{\sigma} + \boldsymbol{\sigma} : \boldsymbol{\varepsilon}^{\mathrm{pl}} + \boldsymbol{\sigma} : \sum_{n=1}^{24} \boldsymbol{\varepsilon}^n \xi^n - \frac{1}{2}\sum_{n=1}^{24} H^{mn}\xi^m\xi^n - B(T - T_0)\sum_{n=1}^{24}\xi^n, \tag{18}$$

where $\boldsymbol{\varepsilon}^n$ is the transformation strain of the nth martensite variant, T_0 is the reference temperature, B a parameter related to the chemical energy (Bekker and Brinson, 1998), $\boldsymbol{S}$ is the fourth-order stiffness tensor and $\boldsymbol{\varepsilon}^{\mathrm{pl}}$ is the plastic strain tensor.

Table 4
Interaction matrix for NiTi (Wang et al., 2008).

Variant	1	2	3	4	5	6	7	8	9	10	11	12	13	14	15	16	17	18	19	20	21	22	23	24
1	C	C	C	C	C	I	C	I	I	I	I	C	I	I	C	I	C	I	I	I	C	I	I	I
2	C	C	C	C	I	C	I	C	C	I	I	I	C	I	I	I	I	I	C	I	I	I	I	C
3	C	C	C	C	C	I	C	I	I	I	C	I	I	I	I	C	I	C	I	I	I	C	I	I
4	C	C	C	C	I	C	I	C	I	C	I	I	I	C	I	I	I	I	I	C	I	I	C	I
5	C	I	C	I	C	C	C	C	I	I	C	I	I	I	I	C	C	I	I	I	C	I	I	I
6	I	C	I	C	C	C	C	C	C	I	I	I	C	I	I	I	I	I	I	C	I	I	C	I
7	C	I	C	I	C	C	C	C	I	I	I	C	I	I	C	I	I	C	I	I	C	I	I	I
8	I	C	I	C	C	C	C	C	I	C	I	I	I	C	I	I	I	I	C	I	I	I	I	C
9	I	C	I	I	I	C	I	I	C	C	C	C	C	C	I	I	I	C	I	I	C	I	I	I
10	I	I	I	C	I	I	I	C	C	C	C	C	C	C	I	I	C	I	I	I	I	C	I	I
11	I	I	C	I	C	I	I	I	C	C	C	C	I	I	C	C	I	I	C	I	I	I	C	I
12	C	I	I	I	I	I	C	I	C	C	C	C	I	I	C	C	I	I	I	C	I	I	I	C
13	I	C	I	I	I	C	I	I	C	C	I	I	C	C	C	C	C	I	I	I	I	C	I	I
14	I	I	I	C	I	I	I	C	C	C	I	I	C	C	C	C	I	C	I	I	C	I	I	I
15	C	I	I	I	I	I	C	I	I	I	C	C	C	C	C	C	I	I	C	I	I	I	C	I
16	I	I	C	I	C	I	I	I	I	I	C	C	C	C	C	C	I	I	I	C	I	I	I	C
17	C	I	I	I	C	I	I	I	I	C	I	I	C	I	I	I	C	C	C	C	C	C	I	I
18	I	I	C	I	I	I	C	I	C	I	I	I	I	C	I	I	C	C	C	C	C	C	I	I
19	I	C	I	I	I	I	I	C	I	I	C	I	I	I	C	I	C	C	C	C	I	I	C	C
20	I	I	I	C	I	C	I	I	I	I	I	C	I	I	I	C	C	C	C	C	I	I	C	C
21	C	I	I	I	C	I	I	I	C	I	I	I	I	C	I	I	C	C	I	I	C	C	C	C
22	I	I	C	I	I	I	C	I	I	C	I	I	C	I	I	I	C	C	I	I	C	C	C	C
23	I	I	I	C	I	C	I	I	I	I	C	I	I	I	C	I	I	I	C	C	C	C	C	C
24	I	C	I	I	I	I	I	C	I	I	I	C	I	I	I	C	I	I	C	C	C	C	C	C

$C = G_A/3000$, $I = G_A/750$, where G_A is the shear modulus of austenite.

Table 5
Interaction matrix for CuZnAl SMA (Patoor et al., 1994; Niclaeys et al., 2002).

Variant	1	2	3	4	5	6	7	8	9	10	11	12	13	14	15	16	17	18	19	20	21	22	23	24
1	C	C	C	C	I	I	C	I	C	I	C	I	I	C	I	I	I	I	I	C	C	I	I	I
2	C	C	C	C	I	I	I	C	I	C	I	C	C	I	I	I	I	I	C	I	I	C	I	I
3	C	C	C	C	C	I	I	I	C	I	C	I	I	I	I	C	I	C	I	I	I	I	C	I
4	C	C	C	C	I	C	I	I	I	C	I	C	I	I	C	I	C	I	I	I	I	I	I	C
5	I	I	C	I	C	C	C	C	C	I	I	I	I	C	I	C	C	I	I	I	I	C	I	I
6	I	I	I	C	C	C	C	C	I	C	I	I	C	I	C	I	I	C	I	I	C	I	I	I
7	C	I	I	I	C	C	C	C	I	I	C	I	I	C	I	C	I	I	C	I	I	I	I	C
8	I	C	I	I	C	C	C	C	I	I	I	C	C	I	C	I	I	I	I	C	I	I	C	I
9	C	I	C	I	C	I	I	I	C	C	C	C	I	I	I	C	I	I	I	C	C	I	I	I
10	I	C	I	C	I	C	I	I	C	C	C	C	I	I	C	I	I	I	C	I	I	C	I	I
11	C	I	C	I	I	I	C	I	C	C	C	C	I	C	I	I	I	C	I	I	I	I	C	I
12	I	C	I	C	I	I	I	C	C	C	C	C	C	I	I	I	C	I	I	I	I	I	I	C
13	I	C	I	I	I	C	I	C	I	I	I	C	C	C	C	C	I	C	I	C	I	I	I	I
14	C	I	I	I	C	I	C	I	I	I	C	I	C	C	C	C	C	I	I	I	I	C	I	I
15	I	I	I	C	I	C	I	C	I	C	I	I	C	C	C	C	I	I	I	C	I	I	C	I
16	I	I	C	I	C	I	C	I	C	I	I	I	C	C	C	C	I	I	C	I	I	I	I	C
17	I	I	I	C	C	I	I	I	I	I	I	C	I	C	I	I	C	C	C	C	I	C	I	C
18	I	I	C	I	I	C	I	I	I	I	C	I	C	I	I	I	C	C	C	C	C	I	C	I
19	I	C	I	I	I	I	C	I	I	C	I	I	I	I	I	C	C	C	C	C	I	C	I	C
20	C	I	I	I	I	I	I	C	C	I	I	I	I	I	C	I	C	C	C	C	C	I	C	I
21	C	I	I	I	I	C	I	I	C	I	I	I	C	I	I	I	I	C	I	C	C	C	C	C
22	I	C	I	I	C	I	I	I	I	C	I	I	I	C	I	I	C	I	C	I	C	C	C	C
23	I	I	C	I	I	I	I	C	I	I	C	I	I	I	C	I	I	C	I	C	C	C	C	C
24	I	I	I	C	I	I	C	I	I	I	I	C	I	I	I	C	C	I	C	I	C	C	C	C

$C \approx \mu/1000 \approx 40$ MPa, and $I \approx \mu/150 \approx 270$ MPa, where μ is the shear modulus of austenite.

Stupkiewicz and Petryk (2010b) observed that the simple Taylor homogenization can be as accurate as FEM averaging if its strong internal kinematic constraints are relaxed. Therefore, they considered the polycrystal as an assembly of bi-crystals consisting of pairs of contiguous grains, instead of aggregates of individual grains. To account for interaction, the grain pairs were assumed to satisfy the conditions of traction continuity and kinematic compatibility at their planar interface of orientation $\boldsymbol{n}$ so that

$$\begin{aligned} &\bar{\boldsymbol{\varepsilon}}_{(2)} - \bar{\boldsymbol{\varepsilon}}_{(1)} = \frac{1}{2}(\boldsymbol{n}\otimes\boldsymbol{c} + \boldsymbol{c}\otimes\boldsymbol{n}), \\ &\left(\bar{\boldsymbol{\sigma}}_{(2)} - \bar{\boldsymbol{\sigma}}_{(1)}\right)\cdot\boldsymbol{n} = \boldsymbol{0}. \end{aligned} \tag{19}$$

In this equation, $\bar{\boldsymbol{\varepsilon}}_{(i)}$ is the average strain of the i^{th} grain ($i = 1, 2$) in the bi-crystal, $\bar{\boldsymbol{\sigma}}_{(i)}$ is the average stress and $\boldsymbol{c}$ is an arbitrary vector. The average stress tensor, strain tensor $\bar{\boldsymbol{\varepsilon}}_{\text{bi}}$, free energy density and dissipation density in the bi-crystal were then obtained by a Voigt mixture rule from those of the two grains. In the Taylor transition technique, $\bar{\boldsymbol{\varepsilon}}_{\text{bi}}$ is assumed equal to the macroscopic strain and the macroscopic stress is given by averaging $\bar{\boldsymbol{\sigma}}_{\text{bi}}$, while the Sachs homogenization technique considers $\bar{\boldsymbol{\sigma}}_{\text{bi}}$ to be equal to the macroscopic stress and averages $\bar{\boldsymbol{\varepsilon}}_{\text{bi}}$. Using the bi-crystal approach, Stupkiewicz and Petryk (2010b) simulated pseudoelasticity, martensite reorientation and tension-compression asymmetry in a NiTi polycrystal. Fig. 14 shows the stress–strain behavior of textured NiTi obtained using the Taylor and Sachs techniques using contiguous grain interaction versus single-grain averaging. For [1 1 1] textured NiTi subjected to uniaxial loading along the drawing direction, a very small difference was observed between the predictions of the Taylor and Sachs models based on bi-crystals. The model was validated against the experimental results of McNaney et al. (2003) and adopted by Stupkiewicz and Petryk (2010a). To account for transformation ratcheting of pseudoelastic NiTi, Yu et al. (2013) developed a crystal plasticity based constitutive model considering 24 friction slip systems at the austenite–martensite interface and the accumulation of pinned martensite during cyclic loading. Their work was extended by Yu et al. (2014) to account for loading rate effects during cyclic deformation and by Yu et al. (2015) to investigate the effect of reorientation-induced plasticity on non-proportional multi-axial transformation ratcheting of pseudoelastic NiTi SMAs.

3.2. Micro-plane and micro-sphere models

The micro-plane theory initiated by Taylor (1938) describes the multiaxial macroscopic behavior of SMAs as a superposition of uniaxial responses within several planes of different orientations called “micro-planes” under the assumption of static constraints (Batdorf and Budiansky, 1949) or kinematic constraints (Bažant, 1984; Bažant and Oh, 1985).

The static constraint method considers a unit vector $\boldsymbol{n}$ to define the normal direction $\boldsymbol{N}$ to the micro-plane. In-plane unit vectors $\boldsymbol{m}$ and $\boldsymbol{l}$ of components m_i and l_i, $i = 1$ to 3, are used to define the shear directions $\boldsymbol{M}$ and $\boldsymbol{L}$. The stress components

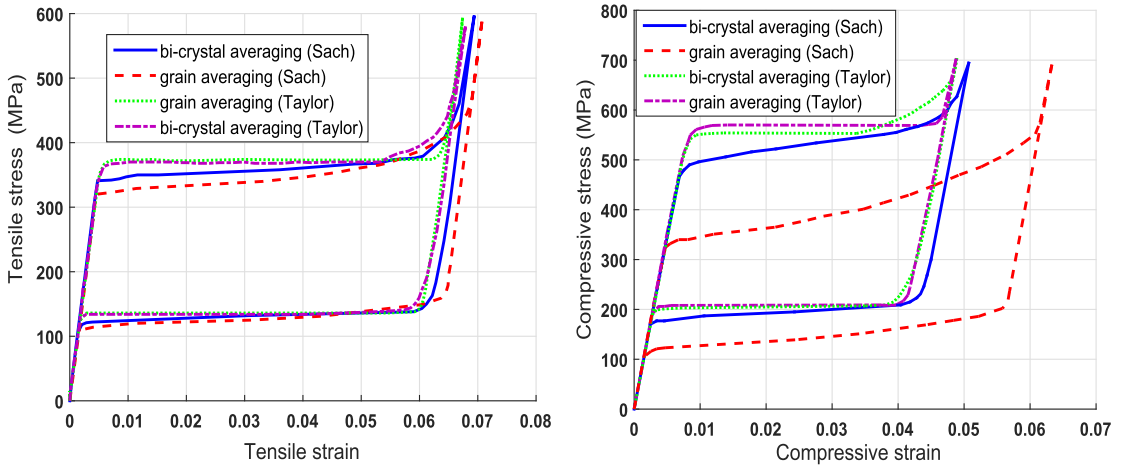

(a) uniaxial tension of textured NiTi. (b) uniaxial compression of textured NiTi.

Fig. 14. Pseudoelastic simulations of NiTi using bi-crystal Taylor-based and Sachs-based micromechanical models (Stupkiewicz and Petryk (2010b)).

along these directions are obtained in each micro-plane from the projections of the macroscopic stress tensor (Carol and Prat, 1990; Brocca et al., 2002) as follows:

$$\sigma_N = N_{ij}\sigma_{ij}, \sigma_M = M_{ij}\sigma_{ij} \text{ and } \sigma_L = L_{ij}\sigma_{ij}, \tag{20}$$

where $N_{ij} = n_i n_j$, $M_{ij} = (m_i n_j + m_j n_i)/2$ and $L_{ij} = (l_i n_j + l_j n_i)/2$ are the Schmid tensors. From (20), the constitutive relation yields the micro-plane strains that, in turn, give the macroscopic strain components by means of the principle of virtual work (PVW)

$$\varepsilon_{ij} = \frac{3}{2\pi}\int_{\Omega} \varepsilon_N n_i n_j d\Omega + \frac{3}{2\pi}\int_{\Omega} \frac{\varepsilon^{\mathrm{tr}}}{2}\left(n_i\delta_{rj} + n_j\delta_{ri}\right)d\Omega, \tag{21}$$

where Ω is the surface of a unit hemisphere and δ_{ij} is the Kronicker delta.

For the kinematic constraint method, the macroscopic strain tensor $\boldsymbol{\varepsilon}$ is projected on the micro-plane to give the normal strain ε_N and the in-plane strains ε_{M} and ε_{L} as follows:

$$\varepsilon_N = N_{ij}\varepsilon_{ij}, \varepsilon_{\mathrm{M}} = M_{ij}\varepsilon_{ij} \text{ and } \varepsilon_{\mathrm{L}} = L_{ij}\varepsilon_{ij}. \tag{22}$$

The local stresses σ_{N}, σ_{M} and σ_{L} are then obtained using the PVW

$$\sigma_{ij} = \frac{3}{2\pi}\int_{\Omega} \sigma_N n_i n_j d\Omega + \frac{3}{2\pi}\int_{\Omega} \frac{\sigma^{\mathrm{tr}}}{2}\left(n_i\delta_{rj} + n_j\delta_{ri}\right)d\Omega. \tag{23}$$

The static and kinematic constraints are sometimes combined to get a so-called double constrained model (Carol and Bazant, 1997; Bažant et al., 2000). Bažant and Oh (1986) proposed an efficient and accurate numerical integration scheme of these models using a single Gauss integration point on each of the 21 micro-planes. Brocca et al. (2002) developed the first micro-plane model (MPM) for polycrystalline SMAs. Using the static constraint method and following Brinson and Huang (1996), they defined the following uniaxial stress–strain relation in a micro-plane:

$$\tau = G(\gamma - \varepsilon_{\mathrm{L}}\xi), \tag{24}$$

where τ is the shear stress, G is the shear modulus, γ is the shear strain along $\boldsymbol{l}$ or $\boldsymbol{m}$, ε_{L} is the maximum transformation strain and ξ is the martensite volume fraction. Despite neglecting the thermal expansion and using identical elastic moduli for austenite and martensite, the model of Brocca et al. (2002) allowed proper simulation of pseudoelasticity in NiTi accounting for minor hysteresis loops as well as tension-compression asymmetry. A Volumetric–Deviatoric–Tangential (VDT) split of the stress and strain was proposed by Bažant et al. (2000), Carol et al. (2001) and Kuhl et al. (2001, 2001) found that the macroscopic stress and strain derived from the PVW may not respect the second principle of thermodynamics. This was

confirmed by Leukart and Ramm (2003), Leukart (2005) and Kadkhodaei et al. (2008) using a volumetric–deviatoric (VD) split. The latter authors demonstrated that MPM with two shear directions may give unrealistic results and remarked that this can be avoided by themodynamically consistent MPM. In this line of thought, Mehrabi et al. (2012) and Mehrabi and Kadkhodaei (2013) proposed a 3D phenomenological micro-plane model using VDT split. Their models accurately predicted the reorientation of martensite under multiaxial loading. Recently, Mehrabi et al. (2014) developed a thermodynamically consistent MPM using VD split. They defined a macroscopic Gibbs free energy by integrating the potential over the micro-planes of all orientations and described the evolution of detwinned martensite in a way similar to Brinson (1993):

$$\begin{aligned}\psi^{\mathrm{mac}}(\sigma,T,\xi) &= \frac{3}{2\pi}\int_{\Omega}\psi^{\mathrm{mic}}(\sigma,T,\xi)d\Omega,\\ \psi^{\mathrm{mic}}(\boldsymbol{\sigma},T,\xi) &= -\frac{1}{2\rho}\boldsymbol{\sigma}:\boldsymbol{S}:\boldsymbol{\sigma}+c\left[(T-T_0)-T\ln\left(\frac{T}{T_0}\right)\right]-s_0T+u_0+\frac{1}{\rho}f(\xi).\end{aligned} \tag{25}$$

Here, $\boldsymbol{S}$ is the fourth-order compliance tensor, c is the effective specific heat, T_0 is the equilibrium temperature, u_0 and s_0 are the specific internal energy and entropy and $f(\xi)$ is a transformation kinetic function where ξ is constrained in [0,1]. Mehrabi et al. (2014) simulated the pseudoelastic behavior of a thin-walled NiTi tube. The comparison with their experimental results shows that both VDT and VD split formulations give good results in uniaxial tension (see Fig. 15(a)) and pure torsion tests (see Fig. 15(b)), with the VD split being less intensive computationally.

Like in micro-plane models, micro-sphere models are based on the projection of the macroscopic strain or stress onto directions that are normal to a micro-sphere (Ostwald et al., 2010b,a). To this end, the authors adopted the 1D constitutive model proposed by Govindjee and Hall (2000) and used statistical physics to obtain the evolution of the volume fractions of the different phases. Using kinematic constraints, the one-dimensional microscopic radial strain $\varepsilon^{\mathrm{mic}}$ was given by

$$\varepsilon^{\mathrm{mic}} = [\boldsymbol{r}\otimes\boldsymbol{r}]:\boldsymbol{\varepsilon}^{\mathrm{mac}}, \tag{26}$$

where $\boldsymbol{r}$ is an underlying integration direction. The microscopic free energy Ψ^{mic} as well as the calculated microscopic stress σ^{mic} and volume ξ^{α} of a phase α are transferred to the macro-level as follows:

$$\begin{aligned}\boldsymbol{\sigma}^{\mathrm{mac}} &= \frac{1}{4\pi}\int_{\Omega}\sigma^{\mathrm{mic}}[\boldsymbol{r}\otimes\boldsymbol{r}\mathrm{d}]\Omega \approx \sum_{i=1}^{n_r}\overline{w}_i\sigma_i^{\mathrm{mic}}[\boldsymbol{r}_i\otimes\boldsymbol{r}_i],\\ \Psi^{\mathrm{mac}} &= \frac{1}{4\pi}\int_{\Omega}\Psi^{\mathrm{mic}}\mathrm{d}\Omega \approx \sum_{i=1}^{n_r}\overline{w}_i\Psi_i^{\mathrm{mic}},\\ \xi_{\alpha}^{\mathrm{mac}} &= \frac{1}{4\pi}\int_{\Omega}\xi_{\alpha}^{\mathrm{mic}}\mathrm{d}\Omega \approx \sum_{i=1}^{n_r}\overline{w}_i\xi_i^{\alpha,\mathrm{mic}},\end{aligned} \tag{27}$$

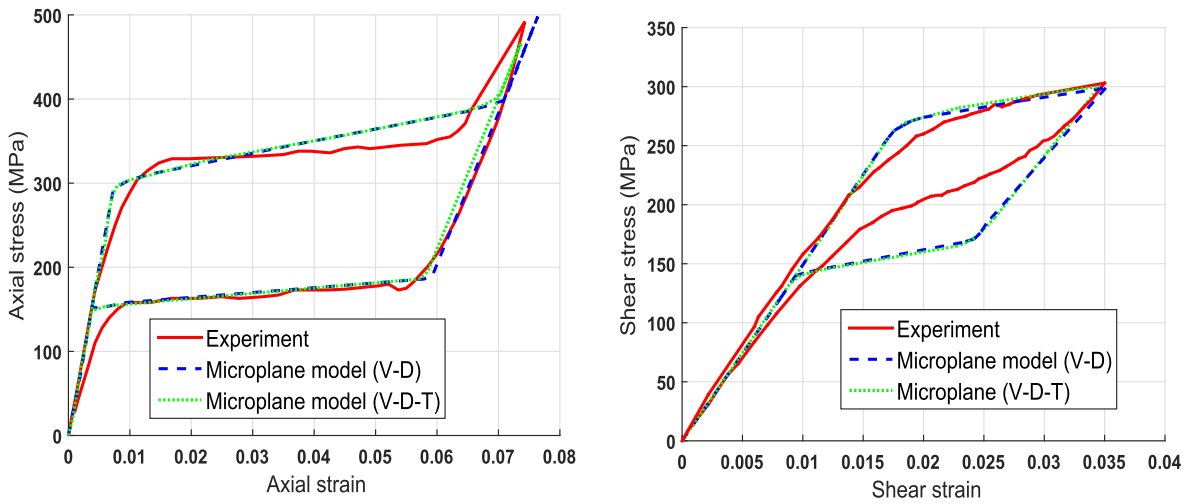

(a) uniaxial loading.

(b) pure torsion loading.

Fig. 15. Comparison of simulation results using VD and VDT split micro-plane models with experimental data (Mehrabi et al., 2014).

where ξ_i^{α} is the volume fraction of phase α at the ith integration direction $\boldsymbol{r}_i$ and $\overline{w}_i$ is the corresponding weighting factor which depends on the integration scheme, and n_r is the total number of integration directions. Ostwald et al. (2010b) used 42 integration directions while Ostwald et al. (2010a) used 21 integration directions for numerical simulations. The projection of macroscopic strain $\widehat{\boldsymbol{\varepsilon}}^{\mathrm{mac}}(t) = k(t)\varepsilon_0 \boldsymbol{e}_1 \otimes \boldsymbol{e}_1$ with $k = \widehat{k}(t) \in [-1, 1]$ is shown in Fig. 16(a) and the resulting microstress in Fig. 16(b). The distribution of the volume fractions of the underlying 1D model after several loading cycles at $k\varepsilon_0 = 0.05$ is illustrated in Fig. 16(c) and shows no transformation in the orthogonal YZ plane. The affine micro-sphere model of Ostwald et al. (2010a) was later extended to account for the interaction between phase transformation an plasticity by Ostwald et al. (2011, 2014) who distinguished the contributions of the deviatoric and volumetric parts of the strain. The purely deviatoric macroscopic plastic strain in phase α was expressed as follows:

$$\boldsymbol{\varepsilon}_{\mathrm{dev,pl}}^{\alpha,\mathrm{mac}} = \frac{1}{4\pi} \int_{\Omega} \boldsymbol{\varepsilon}_{\mathrm{pl}}^{\alpha,\mathrm{mic}} \left[\boldsymbol{r} \otimes \boldsymbol{r} - \frac{1}{3} \mathbb{1} \right] \mathrm{d}\Omega \approx \sum_{i=1}^{n_r} \boldsymbol{\varepsilon}_{\mathrm{pl},i}^{\alpha,\mathrm{mic}} \overline{w}_i \left[\boldsymbol{r}_i \otimes \boldsymbol{r}_i - \frac{1}{3} \mathbb{1} \right]. \tag{28}$$

Using this approach, Ostwald et al. (2014) simulated the pseudoplastic and pseudoelastic behaviors, stress–strain–temperature curves, and stress–strain minor loops observed experimentally Helm and Haupt (2001). Their work was extended recently by Ostwald et al. (2015) to investigate the effect of cyclic loading on SMAs and successfully simulate the shear behavior of SMA plates with holes.

Micro–macro models allow accurate simulations that are well founded in terms of physics. However, they tend to feature many state variables and material parameters, which make them challenging to characterize and computationally expensive.

4. Macroscopic models

Macroscopic models describe the behavior of polycrystalline SMAs based on phenomenological considerations, simplified micro–macro thermodynamics or direct experimental data fitting. Tanaka and Nagaki (1982) established the first macroscopic phenomenological model using internal variables to describe thermoplastic phase transformation in SMAs subjected to uniaxial loading. This work was extended by Tanaka (1986) to feature exponential transformation hardening functions. To circumvent the need for explicit constraints on the volume fractions of the different phases involved, Liang and Rogers (1990) proposed a 3D model using cosine evolution functions for ξ. Brinson (1993) and Brinson and Lammering (1993) extended this model by splitting the volume fraction into a temperature-induced part ξ_T and a stress-induced part ξ_σ. Lagoudas et al. (1996) compared the exponential and cosine models to their own polynomial approach in simulating pseudoelasticity for active metal matrix composites. The exponential model was found to be less satisfactory in predicting the stress–strain behavior and heat energy rate curves, compared to the other two models. Boyd and Lagoudas (1996) proposed the first model that accounts for martensite reorientation by introducing an inelastic strain tensor. However, the authors focused only on proportional loading and did not compare their numerical results with experimental data. The first 3D phenomenological model for SMAs is attributed to Bertram (1983). Other pioneering 3D phenomenological models are those of Raniecki et al. (1992); Raniecki and Lexcellent (1994, 1998), Auricchio et al. (1997) and Souza et al. (1998). The above models led the way to significant developments in phenomenological modeling for SMAs by several research groups worldwide.

4.1. Models based on the theory of plasticity

In these models, processes such as phase transformation and detwinning are governed by loading functions and flow rules analogous to those of classical plasticity. The evolution rules commonly have a normality structure and obey conditions of consistency with the definition of the loading functions.

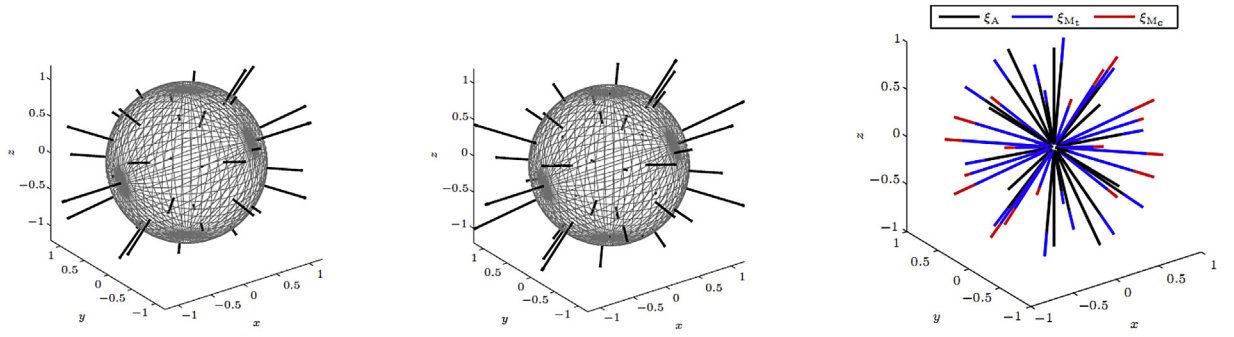

(a) strain projections. (b) calcultated stresses. (c) volume fractions of the phases.

Fig. 16. Volume fraction of autenite, tension-induced martensite M_t and compression-induced martensite M_c by Ostwald et al. (2010b).

4.1.1. The model of Souza et al. (1998)

Souza et al. (1998) proposed a 3D phenomenological model that can simulate the behavior of polycrystalline CuZnAlMn experimentally observed by Sittner et al. (1995). The Helmholtz free energy used to derive the model is written in terms of the total strain $\boldsymbol{\varepsilon}$, transformation strain $\boldsymbol{\varepsilon}^{\mathrm{tr}}$, elastic strain $\boldsymbol{\varepsilon}^{\mathrm{el}}$ and temperature T as follows:

$$\Phi(\boldsymbol{\varepsilon},\boldsymbol{\varepsilon}^{\mathrm{tr}},T)=\frac{1}{2}\kappa(\mathrm{Tr}(\boldsymbol{\varepsilon}))^2+G\left\|\boldsymbol{e}^{\mathrm{el}}\right\|^2+\tau_{\mathrm{m}}(T)\left\|\boldsymbol{e}^{\mathrm{tr}}\right\|+\frac{h}{2}\left\|\boldsymbol{e}^{\mathrm{tr}}\right\|^2+I_{0,\varepsilon^{\mathrm{tr}}_{\max}}(\boldsymbol{\varepsilon}^{\mathrm{tr}}), \tag{29}$$

where $\boldsymbol{e}^{\mathrm{el}}$ and $\boldsymbol{e}^{\mathrm{tr}}$ are the deviatoric parts of the elastic and transformation strain tensors, κ is the bulk modulus, G is the shear modulus of the SMA, $\|\cdot\|$ is the Euclidean norm and h is a transformation hardening parameter. The chemical energy $\tau_{\mathrm{m}}(T)$ that appears in (29) is a positive increasing function of temperature given by

$$\tau_{\mathrm{m}}(T)=\begin{cases}\beta(T-T_0) & \text{if } 0\le\left\|\boldsymbol{e}^{\mathrm{tr}}\right\|\le\boldsymbol{\varepsilon}^{\mathrm{tr}}_{\max},\\ +\infty & \text{otherwise.}\end{cases} \tag{30}$$

$I_{0,\varepsilon^{\mathrm{tr}}_{\max}}$ is an indicator function that accounts for the requirement on $\|\boldsymbol{\varepsilon}^{\mathrm{tr}}\|$ not to exceed $\boldsymbol{\varepsilon}^{\mathrm{tr}}_{\max}$ and is defined as

$$I_{0,\varepsilon^{\mathrm{tr}}_{\max}}=\begin{cases}0 & \text{if } 0\le\left\|\boldsymbol{\varepsilon}^{\mathrm{tr}}\right\|\le\boldsymbol{\varepsilon}^{\mathrm{tr}}_{\max},\\ +\infty & \text{otherwise.}\end{cases} \tag{31}$$

The model of Souza et al. (1998) was improved by Auricchio and Petrini (2002) who proposed a robust algorithm to simulate the SME and PE under non-proportional loading. This work was later extended by Evangelista et al. (2009) who developed 3D and 1D consistent models where the role of the different material parameters is highlighted. Their model was validated against the experimental data obtained by Airoldi et al. (1995) and was used to simulate the OWSME (see Fig. 17(a)) and PE (see Fig. 17(b)) in a 2D cantiliver beam subjected to bending using a new beam finite element. Further generalization of the work of Souza et al. (1998) was carried out by Auricchio and Petrini (2004) who introduced a thermal energy term $\Phi_T(T)$ into the Helmholtz free energy expression in (29) given by

$$\Phi_T(T)=-3\alpha_T\kappa(T-T_0)\mathrm{Tr}(\boldsymbol{\varepsilon})+(u_0-Ts_0)+c\left[(T-T_0)-T\ln\left(\frac{T}{T_0}\right)\right], \tag{32}$$

where c is the heat capacity of the SMA, α_T is the thermal expansion coefficient, u_0 and s_0 are the internal energy and entropy at the reference temperature T_0. This work was extended by Auricchio and Reali (2007) in 1D and by Auricchio et al. (2007) in 3D to simulate the coupling between plasticity and phase transformation. Auricchio et al. (2009) also proposed a 1D formulation of the model of Auricchio and Petrini (2004) to account for tension-compression asymmetry. Mahnken and Wilmanns (2008) further considered the possibility of simultaneous tension-induced, compression-induced and shear-induced martensite. The second and third terms in (29) were accordingly modified as follows:

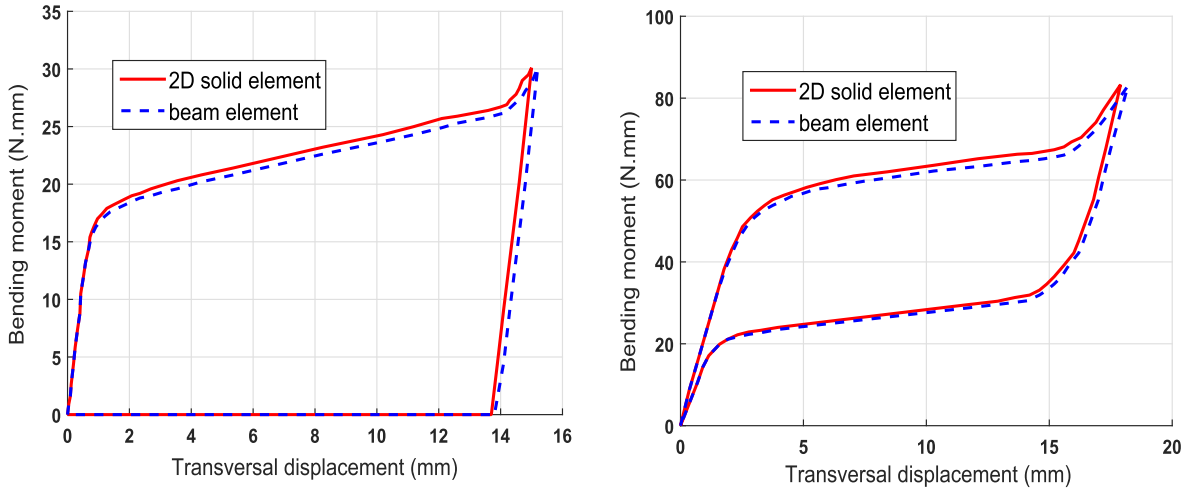

(a) shape memory behavior. (b) pseudoelastic behavior.

Fig. 17. 2D Numerical simulation of pure bending of a cantilever SMA beam (Evangelista et al., 2009).

$$\Phi^{\mathrm{tr}} = \sum_{i=1}^{n}\left(q_i\left(e_i + \frac{1}{b_i}\exp\left(-b_i e_i\right)\right) - \frac{q_i}{e_i} + \frac{1}{2}h_i\left\|\boldsymbol{e}^{\mathrm{tr}}\right\|^2 + \tau_{m_i}\left\|\boldsymbol{e}^{\mathrm{tr}}\right\|\right), \tag{33}$$

where q_i, b_i, and h_i are material parameters that influence transformation hardening. The above equation generalizes the model of Souza et al. (1998) and Auricchio and Petrini (2002) that are retrieved for $n = 1$ and $q_i = 0$. From the work of Auricchio et al. (2007), Arghavani et al. (2010b) proposed a 3D model where martensite reorientation and phase transformation are decoupled. The model introduces the following Lagrangian:

$$L(\boldsymbol{\varepsilon}, \boldsymbol{\varepsilon}^{\mathrm{tr}}, T) = \Phi(\boldsymbol{\varepsilon}, \boldsymbol{\varepsilon}^{\mathrm{tr}}, T) + \Phi_T(T) + \lambda(\|N\| - 1), \tag{34}$$

where $\boldsymbol{N} = \frac{\boldsymbol{\varepsilon}^{\mathrm{tr}}}{\|\boldsymbol{\varepsilon}^{\mathrm{tr}}\|}$ and λ is a Lagrange multiplier. From (34), the authors derived the thermodynamic forces A_ξ and $\boldsymbol{A}_{\mathrm{re}}$ governing phase transformation and martensite reorientation, which were found to be

$$\begin{aligned} A_\xi &= 2G\left(\boldsymbol{e}^{\mathrm{el}} : \boldsymbol{N}\right) - \left(\tau_{\mathrm{M}}(T) + h\left\|\boldsymbol{e}^{\mathrm{tr}}\right\| + \gamma\right), \\ \boldsymbol{A}_{\mathrm{re}} &= 2G\boldsymbol{e}^{\mathrm{el}} - 2G\left(\boldsymbol{e}^{\mathrm{el}} : \boldsymbol{N}\right)\boldsymbol{N}. \end{aligned} \tag{35}$$

Recently, Auricchio and Bonetti (2013) generalized the work of Souza et al. (1998) by considering an expression proposed by Frémond (2002) to derive a 3D model that accounts for martensite reorientation and tension-compression asymmetry. This work was extended by Auricchio et al. (2014) to represent the smooth thermomechanical response of SMAs with transformation-dependent elastic properties, martensite reorientation and low-stress phase transformations. Recently, the initial work of Souza et al. (1998) and its extensions by Auricchio and Petrini (2004) and Arghavani et al. (2011a) were generalized for porous SMAs by Ashrafi et al. (2015a,b) who derived 3D models for pressure-dependent phase transformation of porous NiTi SMAs under proportional and non-proportional multiaxial loadings. Ashrafi et al. (2015b) validated their model against the experimental data of Zhao et al. (2005) and showed that the recoverable strain in porous SMAs increases with porosity under uniaxial or hydrostatic loading, while the critical force for phase transformation decreases. The Souza–Auricchio model was further extended to account for the magnetic effects in SMAs like in (Auricchio et al., 2011, 2015; Grandi and Stefanelli, 2015). A summary of the constitutive equations of the Auricchio and Petrini (2004) model is given in Table 6.

4.1.2. *The model of Boyd and Lagoudas (1996)*

Boyd and Lagoudas (1996) developed a phenomenological SMA model that was validated experimentally by Lagoudas et al. (1996). The model is derived from the following Gibbs free energy expression:

$$\Psi\left(\boldsymbol{\sigma}, T, \xi, \boldsymbol{\varepsilon}^{\mathrm{tr}}\right) = (1-\xi)\Psi_{\mathrm{A}}(\boldsymbol{\sigma}, T) + \xi\Psi_{\mathrm{M}}(\boldsymbol{\sigma}, T) + \Psi^{\mathrm{mix}}\left(\xi, \boldsymbol{\varepsilon}^{\mathrm{tr}}\right), \tag{36}$$

where Ψ_{A} and Ψ_{M} are the free energies of austenite and martensite, and Ψ^{mix} is a mixing energy term reflecting the interactions between the different phases. Ψ_α (α = A,M) were defined as follows:

$$\Psi_\alpha(\boldsymbol{\sigma}, T) = -\frac{1}{2\rho}(\boldsymbol{\sigma} : \boldsymbol{S}^\alpha : \boldsymbol{\sigma}) - \frac{1}{\rho}\left(\boldsymbol{\alpha}_T^\alpha : \boldsymbol{\sigma}\right)(T - T_0) + c^\alpha\left[(T - T_0) - T\ln\left(\frac{T}{T_0}\right)\right] - s_0^\alpha T + u_0^\alpha. \tag{37}$$

In Equation (37), s_0^α and u_0^α are the effective specific entropy and internal energy, respectively, at the reference temperature T_0, c^α is the effective specific heat and $\boldsymbol{\alpha}_T^\alpha$ is the thermal expansion coefficients tensor. The subsequent evolutions of the model of Boyd and Lagoudas (1996) mainly focused on improving the definition of the mixing energy and/or the introduction of permanent plastic deformation. For example, Lagoudas et al. (2006) proposed the following mixing energy:

Table 6
Summary of constitutive relations for the Auricchio and Petrini (2004) model.

Stress–strain relation
$\boldsymbol{\sigma} = 2G\ \mathrm{dev}\ (\boldsymbol{\varepsilon} - \boldsymbol{\varepsilon}^{\mathrm{tr}}) + \kappa[\mathrm{Tr}\ (\boldsymbol{\varepsilon}) - 3\alpha(T - T_0)]1,$
$\boldsymbol{X} = \boldsymbol{\sigma}^{\mathrm{d}} - \beta < T - M_{\mathrm{f}} > \frac{\boldsymbol{\varepsilon}^{\mathrm{tr}}}{\|\boldsymbol{\varepsilon}^{\mathrm{tr}}\|} + h\boldsymbol{\varepsilon}^{\mathrm{tr}}.$
Loading function
$\mathcal{F}_{\mathrm{tr}} = \sqrt{2J_2(\boldsymbol{X})} + m\frac{J_3(\boldsymbol{X})}{J_2(\boldsymbol{X})} - R \le 0, \quad \text{with } m = \sqrt{\frac{27}{2}}\frac{\sigma_{\mathrm{c}} - \sigma_{\mathrm{t}}}{\sigma_{\mathrm{c}} + \sigma_{\mathrm{t}}} \text{ and } R = 2\sqrt{\frac{2}{3}}\frac{\sigma_{\mathrm{c}}\sigma_{\mathrm{t}}}{\sigma_{\mathrm{c}} + \sigma_{\mathrm{t}}}.$
Consistency conditions and flow rule
$\dot{\zeta}\dot{\mathcal{F}}_{\mathrm{tr}} = 0, \dot{\boldsymbol{\varepsilon}}^{\mathrm{tr}} = \dot{\zeta}\frac{\partial\mathcal{F}_{\mathrm{tr}}}{\partial\boldsymbol{\sigma}}, \dot{\zeta} \ge 0, \dot{\mathcal{F}}_{\mathrm{tr}} \le 0.$
Additional constraints
$0 \le \xi \le 1, \text{ and } \|\boldsymbol{\varepsilon}^{\mathrm{tr}}\| <= \varepsilon_{\mathrm{L}}.$

$$\psi^{\mathrm{mix}} = -\frac{1}{\rho}\left(\boldsymbol{\sigma} : \boldsymbol{\varepsilon}^{\mathrm{tr}}\right) + f(\xi), \tag{38}$$

where $f(\xi)$ is the transformation hardening function given by

$$f(\xi) = \begin{cases} f^{\mathrm{M}}(\xi) & \text{for A}\rightarrow\text{M}, \\ f^{\mathrm{A}}(\xi) & \text{for M}\rightarrow\text{A}, \end{cases} \tag{39}$$

and where f^{M} and f^{A} are expressed in one of the following ways:

- Using the exponential model of Tanaka (1986),

$$\begin{aligned} f^{\mathrm{M}} &= \frac{\rho\Delta s_0}{a_{\mathrm{e}}^{\mathrm{M}}}\left[(1-\xi)\ln(1-\xi)+\xi\right] + \left(\mu_1^{\mathrm{e}} + \mu_2^{\mathrm{e}}\right)\xi, \\ f^{\mathrm{A}} &= \frac{\rho\Delta s_0}{a_{\mathrm{e}}^{\mathrm{A}}}\xi\left[\ln(\xi) - 1\right] + \left(\mu_1^{\mathrm{e}} - \mu_2^{\mathrm{e}}\right)\xi, \end{aligned} \tag{40}$$

where $a_{\mathrm{e}}^{\mathrm{A}}$, $a_{\mathrm{e}}^{\mathrm{M}}$, μ_1^{e} and μ_2^{e} are material parameters and Δs_0 is related to the entropy of the phases,

- Using the cosine evolution rule of Liang and Rogers (1990),

$$\begin{aligned} f^{\mathrm{M}} &= \int_0^{\xi} -\frac{\rho\Delta s_0}{a_{\mathrm{c}}^{\mathrm{M}}}\left[\pi - \cos^{-1}\left(2\widehat{\xi} - 1\right)\right] d\widehat{\xi} + \left(\mu_1^{\mathrm{c}} + \mu_2^{\mathrm{c}}\right)\xi, \\ f^{\mathrm{A}} &= \int_0^{\xi} -\frac{\rho\Delta s_0}{a_{\mathrm{c}}^{\mathrm{A}}}\left[\pi - \cos^{-1}\left(2\widehat{\xi} - 1\right)\right] d\widehat{\xi} + \left(\mu_1^{\mathrm{c}} - \mu_2^{\mathrm{c}}\right)\xi, \end{aligned} \tag{41}$$

where $a_{\mathrm{c}}^{\mathrm{A}}$, $a_{\mathrm{c}}^{\mathrm{M}}$, μ_1^{c} and μ_2^{c} are material parameters,

- Using the polynomial model of Lagoudas et al. (1996),

$$\begin{aligned} f^{\mathrm{M}} &= \frac{1}{2}\rho b^{\mathrm{M}}\xi^2 + \left(\mu_1^{p} + \mu_2^{p}\right)\xi, \\ f^{\mathrm{A}} &= \frac{1}{2}\rho b^{\mathrm{A}}\xi^2 + \left(\mu_1^{p} - \mu_2^{p}\right)\xi, \end{aligned} \tag{42}$$

where b^{A}, b^{M}, μ_1^{p} and μ_2^{p} are four material parameters.

Later, Lagoudas et al. (2012) proposed a model that accounts for smooth response of polycrystalline SMA using nonlinear hardening functions. Mollica et al. (2001) proposed generalized expressions for the hardening functions of Lagoudas et al. (1996) as follows:

$$\begin{aligned} f^{\mathrm{M}} &= \frac{1}{2}a_1\left(1 + \xi^{n_1} - (1-\xi)^{n_2}\right) + a_3, \\ f^{\mathrm{A}} &= \frac{1}{2}a_2\left(1 + \xi^{n_3} - (1-\xi)^{n_4}\right) - a_3, \end{aligned} \tag{43}$$

where n_1, n_2, n_3 and n_4 are real numbers in (0,1], and a_1, a_2 and a_3 are material parameters. This nonlinear model was validated against the experimental results of Wu et al. (2003) for SMAs subjected to cyclic temperature variations and was found to give better results than the model of Boyd and Lagoudas (1996) (see Fig. 18(a)). Fig. 18(b) shows that this nonlinear model further captures the variation of transformation strain with the applied stress and the smoothness of the stress–strain and strain–temperature curves with good accuracy. The associated flow rule for the transformation strain given in Lagoudas et al. (1996), and Qidwai and Lagoudas (2000a,b) can be written as

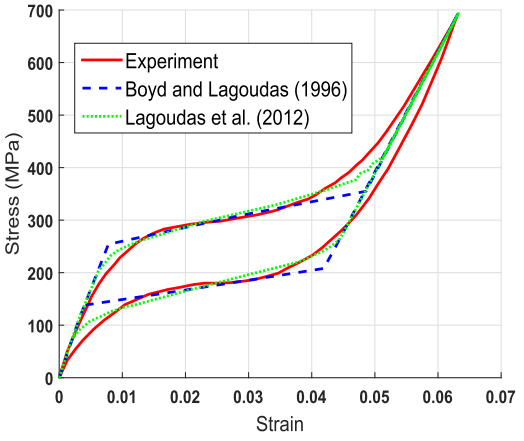

(a) comparison of the linear model of Boyd and Lagoudas (1996) and the nonlinear model of Lagoudas et al. (2012).

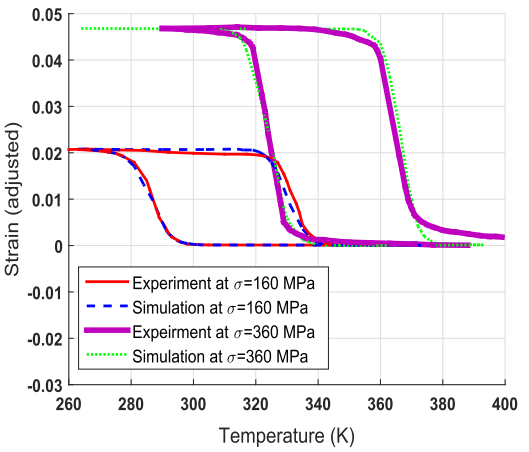

(b) experiments (Wu et al., 2003) and simulations (Lagoudas et al., 2012) of the transformation strain-temperature response for equiatomic NiTi.

Fig. 18. Simulation of the thermomechanical behavior of NiTi SMA (Lagoudas et al., 2012).

$$\dot{\boldsymbol{\epsilon}}^{\mathrm{tr}} = \boldsymbol{\Lambda}^{\mathrm{tr}}\dot{\xi}, \tag{44}$$

where the transformation direction $\boldsymbol{\Lambda}^{\mathrm{tr}}$ is obtained from considerations of maximum dissipation of phase transformation by analogy with plasticity as follows:

$$\boldsymbol{\Lambda}^{\mathrm{tr}} = \frac{\partial \widehat{\Phi}}{\partial \boldsymbol{\sigma}}, \tag{45}$$

where $\widehat{\Phi}$ is the transformation function. Using (44) the thermodynamic force of phase transformation was obtained as

$$\pi = \boldsymbol{\sigma} : \boldsymbol{\Lambda}^{\mathrm{tr}} - \rho\frac{\partial \Psi}{\partial \xi}. \tag{46}$$

Lagoudas et al. (2006) defined the loading functions for forward and reverse transformations as

$$\begin{aligned} F^{\mathrm{F}} &= \widehat{\Phi}(\boldsymbol{\sigma}) + \rho\frac{\partial \Psi}{\partial \xi} - \widehat{Y}, \quad \text{for A}\rightarrow\text{M}, \\ F^{\mathrm{R}} &= -\widehat{\Phi}(\boldsymbol{\sigma}) - \rho\frac{\partial \Psi}{\partial \xi} - \widehat{Y}, \quad \text{for M}\rightarrow\text{A}, \end{aligned} \tag{47}$$

where $\widehat{Y}$ is a material parameter. To analyze the behavior of thick walled SMA cylinders under internal pressure, Mirzaeifar et al. (2011) use the model of Qidwai and Lagoudas (2000b) who identified three main forms of the transformation function $\widehat{\Phi}(\boldsymbol{\sigma})$:

- The first form of $\widehat{\Phi}$ used by Lagoudas et al. (1996) and Hartl and Lagoudas (2009) depends only on the second invariant J_2 of the stress deviator and is given by

$$\widehat{\Phi}(\sigma) = \alpha\sqrt{3J_2} \ \text{ with } \ \boldsymbol{\Lambda}^{\mathrm{tr}} = \frac{3}{2}\alpha\frac{\mathrm{dev}\,(\boldsymbol{\sigma})}{||\mathrm{dev}\,(\boldsymbol{\sigma})||}, \tag{48}$$

where α corresponds to the maximum transformation strain ε_{L}. Popov and Lagoudas (2007) used two different values of α that were denoted α^{SA} for twinned martensite and α^{ori} for oriented martensite.

The flow rule in (48) cannot be used for stress-free temperature-induced reverse transformation. another expression was therefore introduced by Hartl et al. (2010) in which the flow direction is parallel to the transformation strain tensor at reversal

$\boldsymbol{\varepsilon}^{\mathrm{tr}}_{\mathrm{rev}}$. Based on the work of Boyd and Lagoudas (1996), and Lagoudas and Entchev (2004), Hartl et al. (2010) considered additional inelastic deformations by means of transformation induced plasticity (TRIP) and viscoplasticity for which the strain rates are given by

$$\dot{\boldsymbol{\varepsilon}}^{\mathrm{trip}} = \dot{\xi}\boldsymbol{\Lambda}^{\mathrm{trip}} \text{ and } \dot{\boldsymbol{\varepsilon}}^{\mathrm{vp}} = ||\dot{\boldsymbol{\varepsilon}}^{\mathrm{vp}}||\boldsymbol{\Lambda}^{\mathrm{vp}}. \tag{49}$$

The flow directions $\boldsymbol{\Lambda}^{\mathrm{tr}}_{\mathrm{rev}}$ for reverse transformation, $\boldsymbol{\Lambda}^{\mathrm{trip}}$ for TRIP and $\boldsymbol{\Lambda}^{\mathrm{vp}}$ for viscoplasticity are taken as

$$\begin{aligned}
\boldsymbol{\Lambda}^{\mathrm{tr}}_{\mathrm{rev}} &= \frac{\boldsymbol{\varepsilon}^{\mathrm{tr}}_{\mathrm{rev}}}{\xi_{\mathrm{rev}}},\\
\boldsymbol{\Lambda}^{\mathrm{vp}} &= \frac{3}{2}\frac{\mathrm{dev}\,(\boldsymbol{\sigma})}{\sigma_{\mathrm{vm}}},\\
\boldsymbol{\Lambda}^{\mathrm{trip}} &= \mathrm{sgn}\,(\dot{\xi})\left[p_1 - p_2\frac{\sigma_{\mathrm{vm}}}{E_{\mathrm{A}}} + p_3\left(\frac{\sigma_{\mathrm{vm}}}{E_{\mathrm{A}}}\right)^2\right]\boldsymbol{\Lambda}^{\mathrm{vp}},
\end{aligned} \tag{50}$$

where E_{A} is the elastic modulus of austenite, ξ_{rev} is the martensite volume fraction at reversal, σ_{vm} is the effective von Mises stress, and p_1, p_2 and p_3 are three material constants. Associated flow rules constructed with a single martensite volume fraction were found to give spurious residual strains in presence of multiaxial non-proportional loading. To address this issue, Popov and Lagoudas (2007) used (48) for direct transformation and adopted the following flow direction for reverse phase change:

$$\boldsymbol{\Lambda}^{\mathrm{tr}}_{\mathrm{rev}} = \frac{3}{2}\varepsilon_{\mathrm{sat}}\frac{\mathrm{dev}\,(\boldsymbol{\varepsilon})}{\|\mathrm{dev}\,(\boldsymbol{\varepsilon})\|}, \tag{51}$$

where $\varepsilon_{\mathrm{sat}}$ is the maximum uniaxial transformation strain. The 3D model of Hartl et al. (2010) further accounts for rate-independent irrecoverable deformation in SMAs at high temperature. It was recently extended by Chemisky et al. (2014) to simulate the cyclic actuation behavior of high temperature shape memory alloys (HTMAs). Like in (Hartl et al., 2010) and (Lagoudas et al., 2012), the authors replaced $\varepsilon_{\mathrm{sat}}$ in (51) by a function α defined as follows:

$$\alpha = \begin{cases} \varepsilon_{\mathrm{min}} & \text{for } \sigma_{\mathrm{vm}} < \overline{\sigma}_{\mathrm{crit}},\\ \varepsilon_{\mathrm{min}} + (\varepsilon_{\mathrm{sat}} - \varepsilon_{\mathrm{min}})\left(1 - \mathrm{e}^{-k(\sigma_{\mathrm{vm}} - \overline{\sigma}_{\mathrm{crit}})}\right) & \text{for } \sigma_{\mathrm{vm}} \geq \overline{\sigma}_{\mathrm{crit}}, \end{cases} \tag{52}$$

where k is a parameter used to calibrate α given the minimum and maximum transformation strains, $\varepsilon_{\mathrm{min}}$ and $\varepsilon_{\mathrm{sat}}$, and $\overline{\sigma}_{\mathrm{crit}}$ represents the value of σ_{vm} when $\alpha = \varepsilon_{\mathrm{min}}$.

- The second form of $\widehat{\Phi}$ uses the first invariant I_1 of stress and the second invariant J_2 of the stress deviator such that

$$\begin{aligned}
\widehat{\Phi}(\boldsymbol{\sigma}) &= \alpha\sqrt{3J_2} + \beta I_1,\\
\boldsymbol{\Lambda}^{\mathrm{tr}} &= \frac{3}{2}\alpha\frac{\mathrm{dev}\,(\boldsymbol{\sigma})}{\sigma_{\mathrm{vm}}} + \beta\mathbb{1},
\end{aligned} \tag{53}$$

where $\mathbb{1}$ is the second-order identity tensor and β is a parameter that accounts for either volumetric transformation strain or tension-compression asymmetry, but not both simultaneously.

- The third form of $\widehat{\Phi}$ is given in terms of the first, second and third stress invariants I_1, J_2 and J_3 such that

$$\begin{aligned}
\widehat{\Phi}(\boldsymbol{\sigma}) &= \eta\sqrt{3J_2}\left[1 + \theta\frac{J_3}{(3J_2)^{3/2}}\right] + \omega I_1,\\
\boldsymbol{\Lambda}^{\mathrm{tr}} &= \eta\left[\frac{2\mathrm{dev}\,(\boldsymbol{\sigma})}{2\sqrt{3J_2}} + \theta\frac{\sqrt{3J_2}(\mathrm{dev}\,(\boldsymbol{\sigma}) : \mathrm{dev}\,(\boldsymbol{\sigma}) - 2/3J_2\mathbb{1}) - 3J_3\mathrm{dev}\,(\sigma)}{(3J_2)^2}\right] + \omega\mathbb{1},
\end{aligned} \tag{54}$$

where ω is one-third the volumetric transformation strain, and η and θ are material parameters obtained by calibrating the maximum transformation strain in tension and in compression. A summary of the constitutive equations of the Boyd and Lagoudas (1996) model is given in Table 7.

4.2. Models derived from thermodynamic potentials

For these models, an energy potential is first constructed directly from microscopic, phenomenological or physical considerations. Constitutive relations are then derived in accordance with thermodynamic principles.

4.2.1. The ZM model of Zaki and Moumni (2007a)

Zaki and Moumni (2007a,b) and Moumni et al. (2008b) developed a phenomenological model for NiTi SMAs within the framework of generalized standard materials with internal constraints (Halphen and Nguyen, 1974). The state variables used in the ZM model include the temperature T, martensite volume fraction ξ, local transformation strain tensors for austenite $\boldsymbol{\varepsilon}_A$ and martensite $\boldsymbol{\varepsilon}_M$, and local martensite orientation strain tensor $\boldsymbol{\varepsilon}^{ori}$. The state equations of the ZM model are derived from a Helmholtz free energy potential given by

$$\Phi\left(T, \boldsymbol{\varepsilon}_A, \boldsymbol{\varepsilon}_M, \boldsymbol{\varepsilon}^{ori}, \xi\right) = (1-\xi)\Phi_A + \xi\Phi_M + I_{AM}. \tag{55}$$

In the above equation, Φ_A is the free energy of austenite taken as

$$\Phi_A(\boldsymbol{\varepsilon}_A) = \frac{1}{2}\boldsymbol{\varepsilon}_A : \boldsymbol{K}_A : \boldsymbol{\varepsilon}_A, \tag{56}$$

where $\boldsymbol{K}_A$ is the elastic stiffness tensor of austenite. The free energy Φ_M of martensite is given by

$$\Phi_M\left(\boldsymbol{\varepsilon}_M, \boldsymbol{\varepsilon}^{ori}, T\right) = \frac{1}{2}\left(\boldsymbol{\varepsilon}_M - \boldsymbol{\varepsilon}^{ori}\right) : \boldsymbol{K}_M : \left(\boldsymbol{\varepsilon}_M - \boldsymbol{\varepsilon}^{ori}\right) + C(T), \tag{57}$$

where $\boldsymbol{\varepsilon}^{ori}$ is the martensite orientation strain tensor, $\boldsymbol{K}_M$ is the elastic stiffness tensor of martensite and $C(T)$ is the heat density of phase transformation given by

$$C(T) = C_0 + \zeta\left(T - A_f^0\right). \tag{58}$$

In this equation, C_0 is the value of $C(T)$ for $T = A_f^0$ and $\boldsymbol{\sigma} = 0$, while ζ controls the influence of temperature on the transformation stress. The interaction energy I_{AM} is constructed as the summation of three terms as follows:

$$I_{AM} = G\frac{\xi^2}{2} + b_1\frac{\xi^2}{2}\left(\frac{2}{3}\boldsymbol{\varepsilon}^{tr} : \boldsymbol{\varepsilon}^{tr}\right) + b_2\frac{\xi}{2}(1-\xi)\left(\frac{2}{3}\boldsymbol{\varepsilon}^{tr} : \boldsymbol{\varepsilon}^{tr}\right). \tag{59}$$

The first term on the right-hand side accounts for intervariant interaction, the second term is the interaction energy between martensite plates, and the third is the interaction energy between austenite and martensite. The martensite elastic modulus E_M as well as b_1, b_2 and Y are determined from a martensite orientation test, while the austenite Young's modulus E_A, and a, b, G, C_0 and ζ are obtained from a uniaxial tension experiment in the pseudoelastic range. From considerations of physical constraints on ξ, $\boldsymbol{\varepsilon}_A$, $\boldsymbol{\varepsilon}_M$ and the maximum transformation strain ε_{max}^{tr} the authors defined the following constraints potential:

Table 7
Summary of constitutive relations for the Boyd and Lagoudas (1996) model.

Stress-strain relation
$\boldsymbol{\sigma} = [\xi\boldsymbol{S}_M + (1-\xi)\boldsymbol{S}_A]^{-1} : [\boldsymbol{\varepsilon} - \boldsymbol{\varepsilon}^{tr} - \boldsymbol{\alpha}(T - T_0)]$.
Loading functions
$\mathcal{F}^F = \varepsilon_L\sqrt{3J_2} - \rho\frac{\partial\Psi}{\partial\xi} - \widehat{Y} \le 0, \quad \text{for } \dot{\xi} > 0,$
$\mathcal{F}^R = -\varepsilon_L\sqrt{3J_2} + \rho\frac{\partial\Psi}{\partial\xi} - \widehat{Y} \le 0, \quad \text{for } \dot{\xi} < 0.$
Consistency conditions and flow rules
$\dot{\xi}\dot{\mathcal{F}}^F = 0, \dot{\xi} \ge 0, \dot{\mathcal{F}}^F \le 0, \quad \text{for } \dot{\xi} > 0,$
$-\dot{\xi}\dot{\mathcal{F}}^R = 0, -\dot{\xi} \ge 0, \dot{\mathcal{F}}^R \le 0, \quad \text{for } \dot{\xi} < 0,$
$\dot{\boldsymbol{\varepsilon}}^{tr} = \frac{3}{2}\varepsilon_L\dot{\xi}\frac{\mathrm{dev}(\boldsymbol{\sigma})}{\sigma_{vm}}$.
Additional constraints
$0 \le \xi \le 1$, and $\| \boldsymbol{\varepsilon}^{tr} \| <= \varepsilon_L$.

$$\Phi_{KT} = \lambda_1\xi + \lambda_2(1-\xi) + \lambda_3\left(\varepsilon^{tr}_{max} - \sqrt{\frac{2}{3}\boldsymbol{\varepsilon}^{tr}:\boldsymbol{\varepsilon}^{tr}}\right) + \boldsymbol{\lambda}:[(1-\xi)\boldsymbol{\varepsilon}_A + \xi\boldsymbol{\varepsilon}_M - \boldsymbol{\varepsilon}], \tag{60}$$

where $\boldsymbol{\varepsilon}$ is the macroscopic strain, and λ_1, λ_2, λ_3 and $\boldsymbol{\lambda}$ are Lagrange multipliers associated with the following Kuhn–Tucker conditions:

$$\begin{aligned}
&\lambda_1 \geq 0, \ \text{and} \ \lambda_1\xi = 0,\\
&\lambda_2 \geq 0, \ \text{and} \ \lambda_2(1-\xi) = 0,\\
&\lambda_3 \geq 0, \ \text{and} \ \lambda_3\left(\varepsilon^{tr}_{max} - \sqrt{\frac{2}{3}\boldsymbol{\varepsilon}^{ori}:\boldsymbol{\varepsilon}^{ori}}\right) = 0.
\end{aligned} \tag{61}$$

The derivation of the constitutive equations is then reduced to an optimization problem of the Lagrangian

$$L\left(T,\xi,\boldsymbol{\varepsilon},\boldsymbol{\varepsilon}_A,\boldsymbol{\varepsilon}_M,\boldsymbol{\varepsilon}^{ori}\right) = (1-\xi)\Phi_A + \xi\Phi_M + I_{AM} + \Phi_{KT}. \tag{62}$$

Within the framework of generalized standard materials, the authors considered the thermodynamic forces for phase transformation, $A_\xi = -\partial L/\partial\xi$ and orientation, $\boldsymbol{A}_{tr} = -\partial L/\partial\boldsymbol{\varepsilon}^{tr}$ to be sub-gradients of the following positive and convex pseudo-potential of dissipation D_p:

$$D_p = [a_1(1-\xi) + a_2\xi]|\dot{\xi}| + \xi^2\sigma^{ori}\sqrt{\frac{2}{3}\dot{\boldsymbol{\varepsilon}}^{tr}:\dot{\boldsymbol{\varepsilon}}^{tr}}. \tag{63}$$

In (63), the material parameters a_1 and a_2 control the width of the pseudoelastic hysteresis loop for $\xi = 0$ and $\xi = 1$, and σ^{ori} is the critical stress for martensite orientation. This allows the definition of loading functions for forward transformation, reverse transformation and orientation that are respectively given by

$$\begin{aligned}
&F^F_\xi = A_\xi - [a_1(1-\xi) + a_2\xi],\\
&F^R_\xi = -A_\xi - [a_1(1-\xi) + a_2\xi],\\
&F_{ori} = \frac{F_{tr}}{\xi} = \left\|\frac{\boldsymbol{A}_{tr}}{\xi}\right\| - \xi Y, \quad \text{for} \ \xi > 0.
\end{aligned} \tag{64}$$

These loading functions govern the activation of different mechanisms as follows:

- If $F^F_\xi < 0$ and $F^R_\xi < 0$, no phase transformation takes place and therefore $\dot{\xi} = 0$.
- If $F^F_\xi = 0$, the onset of forward phase transformation is reached. In this case $\dot{\xi} = 0$ if $\dot{F}^F_\xi < 0$, or given by the consistency condition $\dot{F}^F_\xi = 0$ otherwise.
- If $F^R_\xi = 0$, the onset of reverse phase transformation is reached. In this case $\dot{\xi} = 0$ if $\dot{F}^R_\xi < 0$, or given by the consistency condition $\dot{F}^R_\xi = 0$ otherwise.
- If $F_{ori} = 0$, the onset of martensite orientation is reached. The evolution of the martensite orientation strain follows the normality condition

$$\dot{\boldsymbol{\varepsilon}}^{tr} = \eta\frac{\partial F_{ori}}{\partial \boldsymbol{X}}, \tag{65}$$

where $\boldsymbol{X}$ is the deviatoric part of $\mathrm{dev}(\boldsymbol{A}^{tr})/\xi$ and η is a positive scalar that satisfies the Kuhn–Tucker conditions

$$\eta \geq 0, F_{ori} \leq 0, \ \text{and} \ \eta F_{ori} = 0. \tag{66}$$

Using the experimental results of Shaw and Kyriakides (1995), Zaki and Moumni (2007a) identified the NiTi parameters to validate their model. The numerical predictions show good agreement with the experimental data for both pseudoelasticity and orientation of self-accommodated martensite (Fig. 19). A significant deviation was observed nevertheless for $T \in [10\,^\circ\text{C}, 30\,^\circ\text{C}]$, which was explained by the formation of a rhombohedral phase (R-phase) not considered by the model. The best results were obtained in the temperature range 50 °C to 80 °C. For temperatures above 90 °C, the experimental results display permanent plastic strains that were not captured by the initial ZM model. The model was later extended to account for plastic yielding (Zaki et al., 2010b), tension-compression asymmetry (Zaki, 2010; Zaki et al., 2011), thermomechanical coupling (Zaki et al., 2010a; Morin et al., 2011a,d) and cyclic loading effects (Moumni et al., 2008a, 2009; Morin et al., 2011b,c; Morin, 2011). Moreover, Zaki (2012a, 2012b, 2012c) developed a new algorithm to simulate martensite reorientation in SMAs under

multiaxial loading using an implicit Newton–Raphson scheme. Zaki et al. (2014) and Gu et al. (2015) later implemented the ZM model using an explicit closed-form expression of the material jacobian to simulate the multiaxial non-proportional loading response of SMAs. Hazar et al. (2013) and more recently Hazar et al. (2015) combined the ZM model with a non-local stationary method to analyze phase transformation around the tip of a stable growing edge crack in a semi-infinite Nitinol plate. Moumni et al. (2015) proposed two approach for the modeling of solids undergoing phase transformations assuming the solid phases to be finely mixed in the first case and as heterogeneous solution in the second case. The work was carried out within the thermodynamic framework of generalized standard materials with physical constraints on the state variable but did not use the ZM model. The constitutive equations of the ZM model (Zaki and Moumni, 2007a) are summarized in Table 8.

4.2.2. The model of Peultier et al. (2006)

Assuming identical elastic properties for austenite and martensite, Peultier et al. (2006) decomposed the total strain into an elastic part $\boldsymbol{\varepsilon}^{\mathrm{el}}$ and a transformation part $\boldsymbol{\varepsilon}^{\mathrm{tr}}$ as follows:

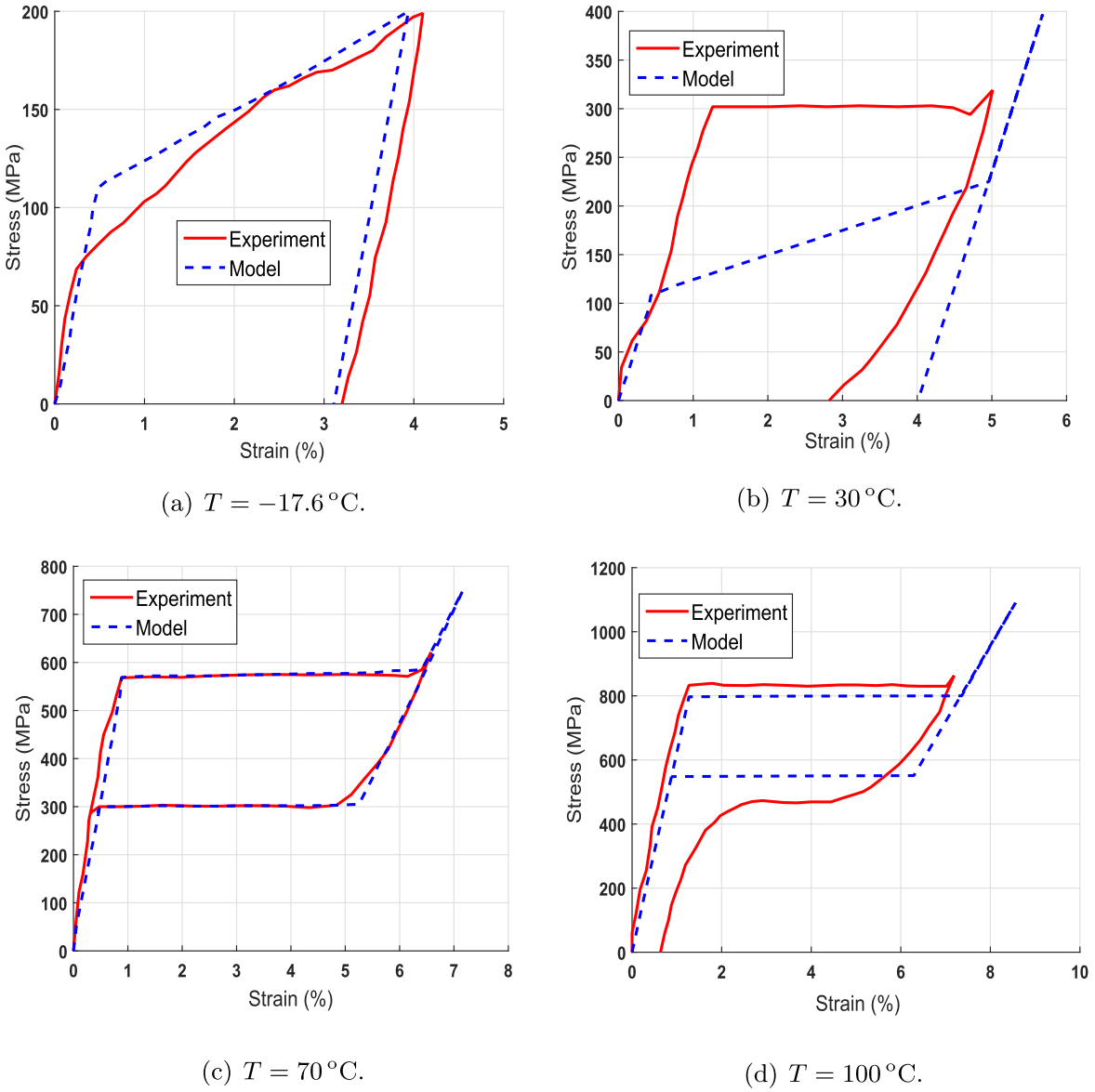

Fig. 19. Numerical vs experimental stress–strain curves in uniaxial tension at different temperatures (Zaki and Moumni, 2007a).

Table 8
Summary of constitutive relations for the Zaki and Moumni (2007a) model.

Stress–strain relation

$\boldsymbol{\sigma} = [(1-\xi)\boldsymbol{K}_{\mathrm{A}}^{-1} + \xi\boldsymbol{K}_{\mathrm{M}}^{-1}]^{-1} : (\boldsymbol{\varepsilon} - \xi\bar{\boldsymbol{\varepsilon}}^{\mathrm{tr}})$.

Loading functions

$$\mathcal{F}_{\xi}^{\mathrm{F}} = \frac{G_{\mathrm{ma}}}{3}\sigma_{\mathrm{vm}}^2 + \frac{H_{\mathrm{ma}}}{2}(\mathrm{Tr}\,(\boldsymbol{\sigma}))^2 - C(T) + \boldsymbol{\sigma} : \bar{\boldsymbol{\varepsilon}}^{\mathrm{tr}} - (G+a_2)\xi - a_1(1-\xi) - \left[(b_1-b_2)\xi + \frac{b_2}{2}\right]\|\bar{\boldsymbol{\varepsilon}}^{\mathrm{tr}}\|^2,$$

$$\mathcal{F}_{\xi}^{\mathrm{R}} = -\frac{G_{\mathrm{ma}}}{3}\sigma_{\mathrm{vm}}^2 - \frac{H_{\mathrm{ma}}}{2}(\mathrm{Tr}\,(\boldsymbol{\sigma}))^2 + C(T) - \boldsymbol{\sigma} : \bar{\boldsymbol{\varepsilon}}^{\mathrm{tr}} + (G-a_2)\xi - a_1(1-\xi) + \left[(b_1-b_2)\xi + \frac{b_2}{2}\right]\|\bar{\boldsymbol{\varepsilon}}^{\mathrm{tr}}\|^2,$$

$$\mathcal{F}_{\mathrm{ori}} = \left\|\boldsymbol{\sigma}^{\mathrm{d}} - \frac{2}{3}[b_1\xi + b_2(1-\xi)]\bar{\boldsymbol{\varepsilon}}^{\mathrm{tr}} - \frac{2\lambda_3}{3\xi}\frac{\bar{\boldsymbol{\varepsilon}}^{\mathrm{tr}}}{\|\bar{\boldsymbol{\varepsilon}}^{\mathrm{tr}}\|}\right\| - \xi Y = \|\boldsymbol{X}\| - \xi Y, \quad \text{for } \xi > 0.$$

Consistency conditions and flow rules

$\dot{\xi}\dot{\mathcal{F}}_{\xi}^{\mathrm{F}} = 0, \dot{\xi} \geq 0, \dot{\mathcal{F}}_{\xi}^{\mathrm{F}} \leq 0$, and $\dot{\boldsymbol{\varepsilon}}^{\mathrm{tr}} = \eta\frac{\partial\mathcal{F}_{\xi}^{\mathrm{F}}}{\partial\boldsymbol{\sigma}}, \eta \geq 0, \mathcal{F}_{\xi}^{\mathrm{F}} \leq 0, \eta\mathcal{F}_{\xi}^{\mathrm{F}} = 0,$

$-\dot{\xi}\dot{\mathcal{F}}_{\xi}^{\mathrm{R}} = 0, -\dot{\xi} \geq 0, \dot{\mathcal{F}}_{\xi}^{\mathrm{R}} \leq 0$, and $\dot{\boldsymbol{\varepsilon}}^{\mathrm{tr}} = \eta\frac{\partial\mathcal{F}_{\xi}^{\mathrm{R}}}{\partial\boldsymbol{\sigma}}, \eta \geq 0, \mathcal{F}_{\xi}^{\mathrm{R}} \leq 0, \eta\mathcal{F}_{\xi}^{\mathrm{R}} = 0,$

$\dot{\xi}\dot{\mathcal{F}}_{\mathrm{ori}} = 0, \dot{\xi} \geq 0, \dot{\mathcal{F}}_{\mathrm{ori}} \leq 0$, and $\dot{\boldsymbol{\varepsilon}}^{\mathrm{tr}} = \eta\frac{\partial\mathcal{F}_{\mathrm{ori}}}{\partial\boldsymbol{X}}, \eta \geq 0, \mathcal{F}_{\mathrm{ori}} \leq 0, \eta\mathcal{F}_{\mathrm{ori}} = 0.$

Additional constraints

$0 \leq \xi \leq 1$, and $\|\boldsymbol{\varepsilon}^{\mathrm{tr}}\| < = \varepsilon_{\mathrm{L}}$.

$$\boldsymbol{\varepsilon} = \boldsymbol{\varepsilon}^{\mathrm{el}} + \boldsymbol{\varepsilon}^{\mathrm{tr}}. \tag{67}$$

The authors considered $\boldsymbol{\varepsilon}^{\mathrm{tr}}$ as the product of the scalar martensite volume fraction ξ and an average transformation/reorientation deviatoric strain tensor $\bar{\boldsymbol{\varepsilon}}^{\mathrm{tr}}$ with the physical restrictions

$$\begin{aligned} &0 \leq \xi \leq 1, \\ &\sqrt{\frac{2}{3}\boldsymbol{\varepsilon}^{\mathrm{tr}} : \boldsymbol{\varepsilon}^{\mathrm{tr}}} \leq \varepsilon_{\mathrm{max}}^{\mathrm{tr}}, \end{aligned} \tag{68}$$

where $\varepsilon_{\mathrm{max}}^{\mathrm{tr}}$ is the magnitude of the transformation strain at saturation. The Gibbs free energy of an isolated representative volume element was constructed as the summation of four energy contributions as follows:

$$\Psi = \Psi_{\mathrm{pot}} - \Psi_{\mathrm{el}} - \Psi_{\mathrm{chem}} - \Psi_{\mathrm{int}}, \tag{69}$$

where Ψ_{pot} is the potential energy of the SMA, Ψ_{el} is the elastic energy, Ψ_{chem} is the chemical energy and Ψ_{int} is the energy of austenite–martensite interfaces that was neglected. The potential energy Ψ_{pot} is given in terms of the stress and strain tensors by

$$\Psi_{\mathrm{pot}} = \boldsymbol{\sigma} : \boldsymbol{\varepsilon}. \tag{70}$$

The elastic energy Ψ_{elastic} was then split into three parts as follows:

$$\Psi_{\mathrm{el}} = \Psi_{\mathrm{macroscopic}} + \Psi_{\mathrm{intergranular}} + \Psi_{\mathrm{intervariant}}, \tag{71}$$

where the macroscopic elastic energy $\Psi_{\mathrm{macroscopic}}$, intergranular interaction $\Psi_{\mathrm{intergranular}}$ and the intervariant interaction $\Psi_{\mathrm{intervariant}}$ are given by

$$\begin{aligned} \Psi_{\mathrm{macroscopic}} &= \frac{1}{2}\boldsymbol{\sigma} : \boldsymbol{\varepsilon} - \frac{1}{2V}\int_{\mathrm{V}} \boldsymbol{\sigma}^{I}(r) : \boldsymbol{\varepsilon}^{\mathrm{tr}}(r)dV = \frac{1}{2}\boldsymbol{\sigma} : \boldsymbol{\varepsilon}^{\mathrm{el}}, \\ \Psi_{\mathrm{intergranular}} &= -\frac{1}{2V}\int_{\mathrm{V}} \left(\boldsymbol{\sigma}^{II}(r) : \boldsymbol{\varepsilon}^{\mathrm{tr}}\right)(r)dV = \frac{1}{2}H_{\mathrm{grn}}\xi^2\bar{\boldsymbol{\varepsilon}}^{\mathrm{tr}} : \bar{\boldsymbol{\varepsilon}}^{\mathrm{tr}}, \\ \Psi_{\mathrm{intervariant}} &= -\frac{1}{2V_N}\int_{\mathrm{V}} \boldsymbol{\sigma}^{III}(r) : \boldsymbol{\varepsilon}^{\mathrm{tr}}(r)dV = \frac{1}{2}H_{\mathrm{var}}\xi^2. \end{aligned} \tag{72}$$

In the above equations, $\boldsymbol{\sigma}^{I}$ is the macroscopic stress in the representative volume element (RVE), $\boldsymbol{\sigma}^{II}(r)$ is the stress fluctuation between the average stress in the grain and $\boldsymbol{\sigma}^{I}$, and $\boldsymbol{\sigma}^{III}(r)$ is the stress fluctuation due to incompatibilities between different martensite variants. In (72), H_{grn} and H_{var} are two parameters governing the intergranular and intervariant interactions. Using (71) and (72), the elastic energy was then expressed as

$$\Psi_{\text{el}} = \frac{1}{2}\left(\boldsymbol{\sigma} : \boldsymbol{\varepsilon}^{\text{el}}\right) + \frac{1}{2}H_{\text{grn}}\left(\bar{\boldsymbol{\varepsilon}}^{\text{tr}} : \bar{\boldsymbol{\varepsilon}}^{\text{tr}}\right)\xi^2 + \frac{1}{2}H_{\text{var}}\xi^2. \tag{73}$$

The chemical energy Ψ_{chem} is related to the heat density of phase change and is given by

$$\Psi_{\text{chem}} = B(T - T_0)\xi, \tag{74}$$

where T_0 is the thermodynamic equilibrium temperature and B is a material parameter. Assuming the martensite transformation in SMAs to occur without volume change, the Gibbs free energy of the material is defined as follows:

$$\Psi\left(\boldsymbol{\sigma}, \xi, \bar{\boldsymbol{\varepsilon}}^{\text{tr}}, T\right) = \frac{1}{2}(\boldsymbol{\sigma} : \boldsymbol{S} : \boldsymbol{\sigma}) + \left(\boldsymbol{\sigma}^{\text{dv}} : \bar{\boldsymbol{\varepsilon}}^{\text{tr}}\right)\xi - B(T - T_0)\xi - \frac{1}{2}H_{\text{grn}}\left(\bar{\boldsymbol{\varepsilon}}^{\text{tr}} : \bar{\boldsymbol{\varepsilon}}^{\text{tr}}\right)\xi^2 - \frac{1}{2}H_{\text{var}}\xi^2, \tag{75}$$

where $\boldsymbol{\sigma}^{\text{dv}}$ is the deviatoric stress and $\boldsymbol{S}$ is the elastic compliance tensor. Phase transformation and martensite orientation criteria were then established in terms of the thermodynamic forces conjugate to the state variables ξ and $\bar{\boldsymbol{\varepsilon}}^{\text{tr}}$, the evolution of which is governed by considerations of consistency with the relevant loading conditions. Using the material parameters identified from the experimental data in (Entemeyer, 1996), the authors successfully simulated the SME and PE behavior of Cu87.9Al11.6Be0.5 (at%) as shown in Fig. 20.

This model was later extended by Peultier et al. (2008) to account for tension-compression asymmetry. Following the work of Peultier et al. (2006) and Niclaeys et al. (2002), Jemal et al. (2009) proposed a constitutive model for iron based SMAs (Fe-SMAs) that accounts for plastic deformation of austenite. This work was extended by Khalil et al. (2012) to account for nonlinear plastic and transformation hardening. Using the initial model of Peultier et al. (2006), Duval et al. (2011) and Armattoe et al. (2014) developed nonlocal phenomenological models that can simulate the localization and propagation of oriented martensite transformation in SMA wires and thin films under non-proportional loading. The models differ in that Duval et al. (2011) assumed the local volume fraction of martensite to be oriented by the deviatoric stress tensor, while in (Armattoe et al., 2014) the direction was given by the mean transformation strain. Chemisky et al. (2011) used the work of Peultier et al. (2006, 2008) to develop a 3D model using different internal variables for the description of phase transformation, martensite reorientation and accommodation of martensite twins in NiTi. For this purpose, they introduced additional internal variables corresponding to the volume fraction ξ^{twin} and the inelastic deformation $\bar{\boldsymbol{\varepsilon}}^{\text{twin}}$ of accommodated martensite twins. In a subsequent work, Piotrowski et al. (2012) studied the influence of niobium precipitates on the thermomechanical behavior of Ni47Ti44Nb9 (at%) SMA. The authors used the work of Chemisky et al. (2011) to assess the behavior of the NiTi matrix and the elastoplastic constitutive model of Wilkins (1964) to describe the niobium inclusions. The Mori–Tanaka transition technique was then utilized to obtain the averaged behavior of the SMA. The results of this work showed an increase of the hysteresis size due to plastic deformation of niobium inclusions. More recently, Thiébaud and Ben Zineb (2014) extended the work of Peultier et al. (2006), Duval et al. (2010) and Chemisky et al. (2011) to carry out finite element analysis of a SMA passive damper. In addition, the authors carried out experimental work and validated their model for the simulation of the nonlinear dynamic behavior of a helical NiTi spring considering force vs. displacement, equivalent complex stiffness and Bode diagrams. Models similar to that of Peultier et al. (2006) were developed by Zhou et al. (2009,

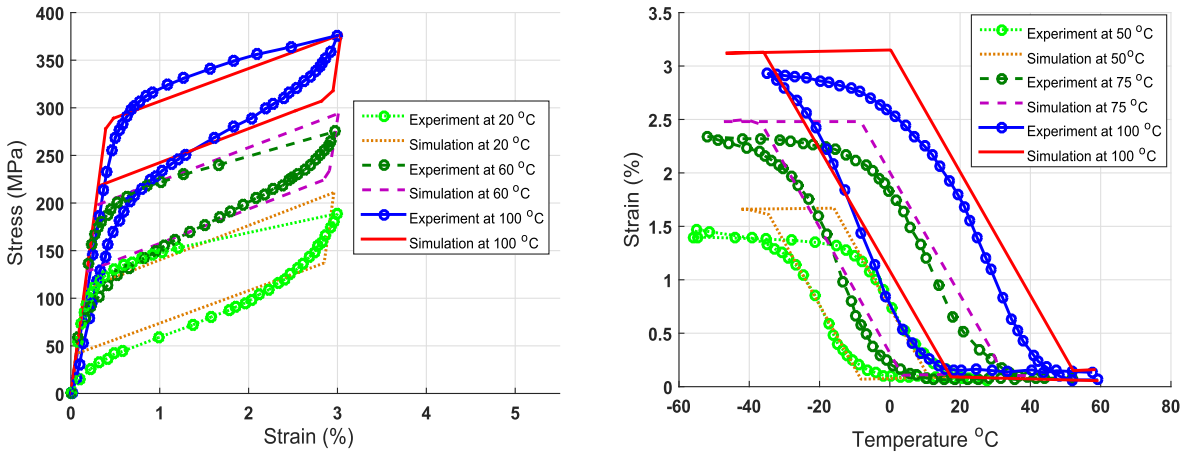

(a) pseudoelastic tensile behavior. (b) shape memory effect under constant stress.

Fig. 20. Numerical results of the PE and SME using the macroscopic model of Peultier et al. (2006).

2010) and Zhou (2012). The 3D model of Zhou et al. (2010) simulates plastic deformation with linear hardening and was extended by Zhou (2012) to account for 24 martensite variants. The authors considered thermal expansion and resolved the transformation strain into stress-induced and temperature-induced parts, following Brinson (1993). A summary of the constitutive equations of the model of Peultier et al. (2006) is given in Table 9.

4.2.3. The model of Leclercq and Lexcellent (1996)

Leclercq and Lexcellent (1996) generalized the R_L model proposed by Raniecki et al. (1992) to develop the first general macroscopic model that explicitly takes into account the reorientation of martensite variants. To this end, they considered a separation of the volume fraction of martensite into oriented and self-accommodating parts, like in (Brinson, 1993). The constitutive relations were derived from a Helmholtz free energy Φ of the material taken as

$$\Phi = (1-\xi)\Phi_{\mathrm{A}} + \xi_T \Phi_{\mathrm{tr}} + \xi_\sigma \Phi_\sigma + \Delta\Phi, \tag{76}$$

where ξ_T is the volume fraction of twinned martensite and ξ_σ is the volume fraction of detwinned martensite, such that the total martensite volume fraction is $\xi = \xi_T + \xi_\sigma$. In the expression of Φ, Φ_{A} is the free energy of austenite, Φ_{tr} is the free energy of twinned martensite, Φ_σ is the free energy of oriented martensite and $\Delta\Phi$ is referred to as the configurational energy. The free energy Φ_φ of each phase $\varphi \in \{\mathrm{A},\mathrm{M}\}$ is given by

$$\Phi_\varphi = u_0^\varphi - T s_0^\varphi + \frac{1}{2\rho}\boldsymbol{\varepsilon}_\varphi^{\mathrm{el}} : \boldsymbol{K} : \boldsymbol{\varepsilon}_\varphi^{\mathrm{el}} + C_{\mathrm{V}}\left[(T-T_0) - T\ln\left(\frac{T_0}{T}\right)\right]. \tag{77}$$

In this equation, u_0^φ is the specific energy, s_0^φ is the specific entropy, and $\boldsymbol{\varepsilon}_\varphi^{\mathrm{el}}$ is the elastic strain tensor for phase φ, $\boldsymbol{K}$ is the elastic stiffness tensor assumed to be identical for all phases, ρ is the mass density, T_0 is the equilibrium temperature and C_{V} is the specific heat at constant volume. Since the two martensite phases are crystallographically equivalent, they were considered to have the same free energy and interaction energy with the austenite, i.e. $\Phi_{\mathrm{AT}} = \Phi_{A\sigma} = \Phi_{\mathrm{it}}$. Denoting $\Phi_{\mathrm{it}}^{\mathrm{m}}$ the interaction energy between the two martensites, the configurational energy was taken as

$$\Delta\Phi = \xi(1-\xi)\Phi_{\mathrm{it}} + \xi_\sigma \xi_T \Phi_{\mathrm{it}}^{\mathrm{m}}. \tag{78}$$

The authors constructed the following closed-form expressions of $\Phi_{\mathrm{it}}^{\mathrm{m}}$ and Φ_{it} based on experimental data:

$$\begin{aligned} \Phi_{\mathrm{it}}^{\mathrm{m}} &= \frac{\varepsilon_{\mathrm{L}}\sigma^{T\sigma}}{\rho}, \\ \Phi_{\mathrm{it}} &= \frac{\rho\sigma^{\mathrm{AM}}}{2\varepsilon_{\mathrm{L}}}\left(\frac{M_{\mathrm{s}}^0 - A_{\mathrm{s}}^0}{M_{\mathrm{s}}^0 - T_{\mathrm{pe}}}\right), \end{aligned} \tag{79}$$

where T_{pe} is the pseudoelastic test temperature, and σ^{AM} and $\sigma^{T\sigma}$ are the stress onsets for direct transformation and martensite reorientation respectively. Considering that only oriented martensite induces macroscopic transformation strain, the authors established the following flow rule based on the work of Vacher (1991):

$$\dot{\boldsymbol{\varepsilon}}^{\mathrm{tr}} = \frac{3}{2}\boldsymbol{\varepsilon}_{\mathrm{sat}}\dot{\xi}_\sigma \frac{\mathrm{dev}\,(\boldsymbol{\sigma})}{\sigma_{\mathrm{vm}}}, \tag{80}$$

where $\varepsilon_{\mathrm{sat}}$ is the maximum uniaxial transformation strain. The thermodynamic forces governing the evolution of ξ_T, ξ_σ were then derived in accordance with the laws of thermodynamics as

Table 9
Summary of constitutive relations for the Peultier et al. (2006) model.

Stress–strain relation
$\boldsymbol{\sigma} = \boldsymbol{S}^{-1} : (\boldsymbol{e} - \xi\bar{\boldsymbol{\varepsilon}}^{\mathrm{tr}})$.
Loading functions
$\mathcal{F}_{\mathrm{tr}} = \boldsymbol{\sigma} : \bar{\boldsymbol{\varepsilon}}^{\mathrm{tr}} - B(T-T_0) - H_{\mathrm{grn}}\xi\bar{\boldsymbol{\varepsilon}}^{\mathrm{tr}} : \bar{\boldsymbol{\varepsilon}}^{\mathrm{tr}} - H_{\mathrm{var}}\xi - F_\xi^{\mathrm{crit}}$,
$\mathcal{F}_{\mathrm{ori}} = \sigma_{\mathrm{vm}}\xi - H_{\mathrm{grn}}\bar{\varepsilon}_{\mathrm{vm}}^{\mathrm{tr}}\xi^2 - \lambda_3$.
Consistency conditions and flow rules
$\dot{\xi}\dot{\mathcal{F}}_{\mathrm{tr}} = 0, \dot{\xi} \geq 0, \dot{\mathcal{F}}_{\mathrm{tr}} \leq 0; \dot{\mathcal{F}}_{\mathrm{tr}} = 0$ giving $\dot{\xi}$,
$\dot{\xi}\dot{\mathcal{F}}_{\mathrm{ori}} = 0, \dot{\xi} \geq 0, \dot{\mathcal{F}}_{\mathrm{ori}} \leq 0; \dot{\mathcal{F}}_{\mathrm{ori}} = 0$ giving $\bar{\boldsymbol{\varepsilon}}^{\mathrm{tr}}$.
Additional constraints
$0 \leq \xi \leq 1$, and $\|\boldsymbol{\varepsilon}^{\mathrm{tr}}\| <= \varepsilon_{\mathrm{L}}$.

$$\pi_T = \frac{\varepsilon_L \sigma_{vm}}{\rho} - (1-2\xi)\Phi_{it} - \xi_T \Phi_{it}^m + \pi_0(T),$$
$$\pi_\sigma = -(1-2\xi)\Phi_{it} - \xi_\sigma \Phi_{it}^m + \pi_0(T), \tag{81}$$

where $\pi_0(T)$ is the chemical potential associated with phase transformation. The following loading functions were then defined: $F_\sigma^F = \pi_\sigma - k_\sigma^F$ and $F_\sigma^R = -\pi_\sigma + k_\sigma^R$ for forward and reverse stress-induced transformations, $F_T^F = \pi_T - k_T^F$ and $F_T^R = -\pi_T + k_T^R$ for forward and reverse temperature-induced transformations, and $F_{\sigma T} = \pi_{\sigma T} - k_{\sigma T}$ for the orientation of twinned martensite. The phase transformation thresholds k_σ^F, k_σ^R, k_T^F, k_T^R and $k_{\sigma T}$ were obtained from the kinetic relations proposed by Koistinen and Marburger (1959). The model of Leclercq and Lexcellent (1996) was validated against experimental data taken from Vacher (1991) for CuZnAl and NiTi. It was shown to properly simulate the isothermal and non-isothermal behaviors of these SMAs but was not validated for non-proportional loading cases. Lexcellent et al. (2000) successfully modified (76) to simulate the two-way shape memory effect in CuZnAl SMA using the experimental data of Bourbon et al. (1995). Juhasz et al. (2000) used the transformation surfaces proposed by Brinson (1993) in the model of Leclercq and Lexcellent (1996) to predict the effects of thermomechanical coupling in viscoplastic SMAs. Later, Lexcellent et al. (2006) extended the 1996 model to account for the anisothermal behavior of SMAs under proportional loading. The authors considered the thermal expansion effects and used the following temperature-dependent interaction energies:

$$\Phi_{it} = \bar{u}_0 - T\bar{s}_0 \quad \text{and} \quad \Phi_{it}^m = \bar{u}_0^m - T\bar{s}_0^m, \tag{82}$$

where $\bar{u}_0$, $\bar{s}_0$, $\bar{u}_0^m$ and $\bar{u}_0^m$ are related to the internal energy and entropy of the phases. A non-associative evolution law for $\boldsymbol{\varepsilon}^{tr}$ was also introduced to account for the non-convexity of the elastic domain during reverse phase change and was given by

$$\dot{\boldsymbol{\varepsilon}}^{tr} = \frac{\varepsilon_L \dot{\xi}_\sigma}{\left(\frac{2}{3}\boldsymbol{\varepsilon}^{tr} : \boldsymbol{\varepsilon}^{tr}\right)^{\frac{1}{2}}} \boldsymbol{\varepsilon}^{tr}. \tag{83}$$

However, this analytical model was neither used for simulations nor validated experimentally. The formulation of Leclercq and Lexcellent (1996) was further developed by Thiebaud et al. (2007) to account for tension-compression asymmetry in pseudoelastic SMAs. From Koistinen and Marburger (1959), they defined the following transformation kinetics:

$$\dot{\xi} = \begin{cases} \dfrac{\varepsilon_L \dot{\sigma}_{eq} - \rho \Delta s_0 \dot{T}}{A_1 - 2(1-\xi)\Phi_{it}} \dfrac{(1-\xi)}{\rho} & \text{for } \dot{\xi} > 0, \\ \dfrac{\varepsilon_L \dot{\sigma}_{eq} - \rho \Delta s_0 \dot{T}}{A_2 - 2\xi\Phi_{it}} \dfrac{\xi}{\rho} & \text{for } \dot{\xi} < 0, \end{cases} \tag{84}$$

where $\dot{\sigma}_{eq}$ is the rate of equivalent stress defined by Bouvet et al. (2002), A_1 and A_2 are two parameters depending on the entropy of austenite and martensite and Δs_0 is the entropy gap between the two phases. Simulation results are shown in Fig. 21 based on which the authors concluded that the behavior approaches isothermal for low loading rates and adiabatic for

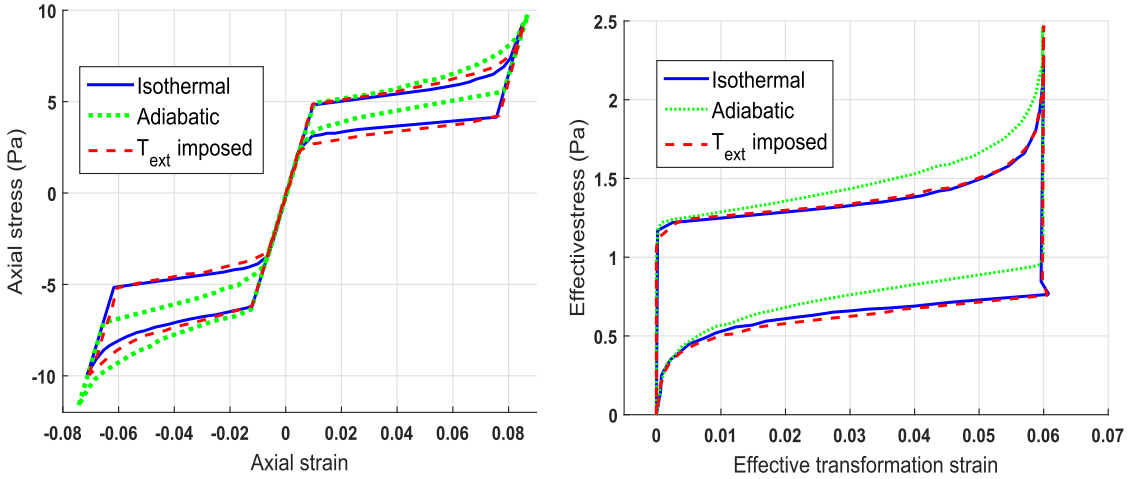

(a) uniaxial stress-strain response. (b) equivalent stress-strain response.

Fig. 21. Pseudoelastic behavior for isothermal, adiabatic and imposed external temperature cases (Thiebaud et al., 2007).

high loading rate. Based on (Leclercq and Lexcellent, 1996), Panico and Brinson (2007) developed the first 3D phenomenological model in which martensite transformation and reorientation under multiaxial non-proportional loading are decoupled. In this model, the configurational energy is defined as a simple quadratic function of ξ_σ given by

$$\Delta\Phi = \frac{1}{2}H_\sigma \xi_\sigma^2, \tag{85}$$

where H_σ is a transformation hardening parameter. The expression used for ξ_σ is taken from Andra et al. (2001) and given by

$$\xi_\sigma = \frac{||\boldsymbol{\varepsilon}^{\text{inel}}||}{\sqrt{(3/2)}\varepsilon_{\text{L}}}. \tag{86}$$

The work of Panico and Brinson (2007) was later improved and utilized by Stebner and Brinson (2013) to carry out 3D finite element analysis of SMAs. Lexcellent et al. (2008) used the 1996 model to discuss the validity of the four criteria proposed by James and Zhang (2005) for hysteresis minimization in alloys exhibiting first order transition. The work of Raniecki et al. (1992) was also extend by Hirsinger and Lexcellent (2003) and Hirsinger et al. (2004) to study the thermo-magneto-mechanical behavior of ferromagnetic Ni–Mn–Ga SMAs by incorporating a magnetic energy density

$$\Phi_{\text{magnet}} = \frac{1}{\rho}\mu_0 \boldsymbol{H}.\boldsymbol{M}, \tag{87}$$

where μ_0 is the magnetic permeability of vacuum, $\boldsymbol{H}$ is the magnetic field and $\boldsymbol{M}$ is the magnetization. The constitutive equations of the model of Leclercq and Lexcellent (1996) are summarized in Table 10.

In the current state of science, the macroscopic models remain the most commonly used in structural analysis and design because of their overall simplicity and smaller number of parameters, which make them easier to integrate and less-expensive to run compared to other types of models.

4.3. Equivalence of the basic formulations of different macroscopic models

Under the assumption of identical elastic stiffness for austenite and martensite, and disregarding tension-compression asymmetry and thermal expansion, the stress–strain relation for all the macroscopic models reviewed here becomes

$$\boldsymbol{\sigma} = \boldsymbol{K} : \left(\boldsymbol{\varepsilon} - \boldsymbol{\varepsilon}^{\text{tr}}\right) \tag{88}$$

Considering a single martensite variant and simple uniaxial tensile loading in the pseudoelastic range, the expressions of the phase transformation function for the different models can be written as follows:

- For the model of Auricchio and Petrini (2004),

$$\mathcal{F}_\xi^{\text{tr}} = \sigma - \beta\langle T - M_{\text{f}}\rangle + h\xi\varepsilon_{\text{L}} - \sigma_{\text{tr}}^{\text{crit}}, \tag{89}$$

- For the model of Boyd and Lagoudas (1996),

Table 10
Summary of constitutive relations for the Leclercq and Lexcellent (1996) model.

Stress–strain relation
$\boldsymbol{\sigma} = \boldsymbol{K} : (\boldsymbol{\varepsilon} - \boldsymbol{\varepsilon}^{\text{tr}})$.
Loading functions
$\mathcal{F}_\sigma^{\text{F}} = \left[\frac{\varepsilon_{\text{L}}\sigma_{\text{vm}}}{\rho} - (1-2\xi)\Phi_{\text{it}} - \xi_T\Phi_{\text{it}}^{\text{m}} + \pi_0(T) - k_T^{\text{F}}\right]\text{sgn}(\dot{\xi}), \quad \text{for } \dot{\xi} > 0,$
$\mathcal{F}_T^{\text{F}} = -[(1-2\xi)\Phi_{\text{it}} + \xi_\sigma\Phi_{\text{it}}^{\text{m}} - \pi_0(T) + k_\sigma^{\text{F}}]\text{sgn}(\dot{\xi}), \quad \text{for } \dot{\xi} > 0.$
Consistency conditions and flow rule
$\dot{\xi}_\sigma\dot{\mathcal{F}}_\sigma^{\text{F}} = 0, \dot{\xi}_\sigma \geq 0, \mathcal{F}_\sigma^{\text{F}} \leq 0,$
$\dot{\xi}_T\dot{\mathcal{F}}_T^{\text{F}} = 0, \dot{\xi}_T \geq 0, \dot{\mathcal{F}}_T^{\text{F}} \leq 0,$
$\dot{\boldsymbol{\varepsilon}}^{\text{tr}} = \frac{3}{2}\varepsilon_{\text{L}}\dot{\xi}_\sigma\frac{\text{dev}(\boldsymbol{\sigma})}{\sigma_{\text{vm}}}.$
Additional constraints
$0 \leq \xi \leq 1$ and $\|\boldsymbol{\varepsilon}^{\text{tr}}\| <= \varepsilon_{\text{L}}.$

$$\mathcal{F}_{\xi}^{\mathrm{tr}}=\begin{cases}\sigma\varepsilon_{\mathrm{L}}-\rho^{2}b^{\mathrm{M}}\,\xi-\left(\mu_{1}^{\mathrm{p}}+\mu_{2}^{\mathrm{p}}\right)-\widehat{Y}, & \dot{\xi}>0,\\ -\sigma\varepsilon_{\mathrm{L}}+\rho^{2}b^{\mathrm{A}}\xi+\left(\mu_{1}^{\mathrm{p}}-\mu_{2}^{\mathrm{p}}\right)-\widehat{Y}, & \dot{\xi}<0,\end{cases} \tag{90}$$

- For the ZM model (Zaki and Moumni, 2007a),

$$\mathcal{F}_{\xi}^{\mathrm{tr}}=\begin{cases}\sigma\varepsilon_{\mathrm{L}}-\zeta\left(T-A_{\mathrm{f}}^{0}\right)-\left[G-a_{1}+a_{2}+(b_{1}-b_{2})\varepsilon_{\mathrm{L}}^{2}\right]\xi-\left(a_{1}+\dfrac{b_{2}}{2}\varepsilon_{\mathrm{L}}^{2}+C_{0}\right), & \dot{\xi}>0,\\ -\sigma\varepsilon_{\mathrm{L}}+\zeta\left(T-A_{\mathrm{f}}^{0}\right)+\left[G+a_{1}-a_{2}+(b_{1}-b_{2})\varepsilon_{\mathrm{L}}^{2}\right]\xi-\left(a_{1}-\dfrac{b_{2}}{2}\varepsilon_{\mathrm{L}}^{2}-C_{0}\right), & \dot{\xi}<,\end{cases} \tag{91}$$

- For the model of Peultier et al. (2006).

$$\mathcal{F}_{\mathrm{tr}}=\sigma\varepsilon_{\mathrm{L}}-B(T-T_{0})-H_{\mathrm{grn}}\varepsilon_{\mathrm{L}}\xi-H_{\mathrm{var}}\xi-F_{\xi}^{\mathrm{crit}}, \tag{92}$$

- For the model of Leclercq and Lexcellent (1996).

$$\mathcal{F}_{\xi}^{\mathrm{tr}}=\left[\frac{\varepsilon_{\mathrm{L}}\sigma}{\rho}+2\Phi_{\mathrm{it}}\xi-\Phi_{\mathrm{it}}+\pi_{0}(T)-k_{T}^{\mathrm{F}}\right]\mathrm{sgn}\,(\dot{\xi}),\quad \text{for } \dot{\xi}>0. \tag{93}$$

All the above functions can be written in the form

$$\sigma\varepsilon_{\mathrm{L}}-H_{1}\xi-H_{2}(T-T_{0})-H_{3}=\sigma_{\xi}^{\mathrm{crit}}\varepsilon_{\mathrm{L}}. \tag{94}$$

where H_1, H_2 and H_3 are constant material parameters, such that for forward transformation:

$$H_{1}=-h\varepsilon_{\mathrm{L}}^{2}=\rho^{2}b^{\mathrm{M}}=\left[G-a_{1}+a_{2}+(b_{1}-b_{2})\varepsilon_{\mathrm{L}}^{2}\right]=H_{\mathrm{grn}}\varepsilon_{\mathrm{L}}+H_{\mathrm{var}}=-2\rho\Phi_{\mathrm{it}} \tag{95}$$

$$H_{2}=\beta\varepsilon_{\mathrm{L}}=\zeta=B=-\rho\Delta s \tag{96}$$

$$H_{3}=\beta\varepsilon_{\mathrm{L}}<T_{0}-M_{\mathrm{f}}>=\mu_{1}^{\mathrm{p}}+\mu_{2}^{\mathrm{p}}=\zeta\left(T_{0}-A_{\mathrm{f}}^{0}\right)+C_{0}+\frac{b_{2}}{2}\varepsilon_{\mathrm{L}}^{2}=\Phi_{\mathrm{it}}+\rho(T_{0}\Delta s-\Delta u) \tag{97}$$

$$\sigma_{\xi}^{\mathrm{crit}}=\sigma_{\mathrm{tr}}^{\mathrm{crit}}=\frac{\widehat{Y}}{\varepsilon_{\mathrm{L}}}=\frac{a_{1}}{\varepsilon_{\mathrm{L}}}=\frac{\rho k_{T}^{\mathrm{F}}}{\varepsilon_{\mathrm{L}}}=\frac{F_{\xi}^{\mathrm{crit}}}{\varepsilon_{\mathrm{L}}} \tag{98}$$

The identical stress–strain relations and loading functions make the different models equivalent under the assumptions made here. The same conclusion cannot be made in the more general case of multiaxial loading, mainly because of the different expressions used for the inelastic strain component as well as different evolution kinetics.

4.4. Finite deformation and geometric non-linearity

Constitutive models for SMAs with finite strain formulation (FSF) are needed to accurately simulate large structural rotations (Reese and Christ, 2008) and distortions (Ziolkowski, 2007). Following the pioneering work of Lubliner and Auricchio (1996), Auricchio and Taylor (1997) and Masud et al. (1997), many finite strain models (FSM) were developed by generalizing small strain formulations (SSF). FSM uses either additive or multiplicative decomposition of the deformation gradient $\boldsymbol{F}$ into elastic and inelastic parts. One of the rare FSM using additive decomposition was proposed by Müller and Bruhns (2006) who extended the work of Raniecki and Lexcellent (1998) to simulate minor hysteresis loops and cycling effects in NiTi. Anand and Gurtin (2003) used multiplicative decomposition to develop a FSM that successfully describes isothermal pseudoelasticity of an initially textured NiTi SMA. Helm and Haupt (2003) and Helm (2007) also used multiplicative decomposition in their thermo-viscoplastic SMA models. Stupkiewicz and Petryk (2006) extended the SSF of Stupkiewicz and Petryk (2002) to develop a micromechanical FSM for SMAs with elastic anisotropy. Pan et al. (2007) modeled the multiaxial finite deformation response of SMAs by separating the reorientation and detwinning processes of martensite. Extending the R_L model,

Ziolkowski (2007) also developed a FSM for isothermal proportional loading. Later, Thamburaja (2010) generalized the work of Sun and Hwang (1993) to propose a FSM considering both plasticity and tension-compression asymmetry. For computation efficiency, Arghavani et al. (2011a) proposed a FSF with a robust integration scheme based on the work of Souza et al. (1998). More recently, Zaki (2012a) proposed an efficient implementation for the finite deformation extension of the work of Zaki (2011) considering a hypoelastic framework.

In FSM, the right and left Cauchy Green deformation tensors, $\boldsymbol{C}$ and $\boldsymbol{b}$, are derived from the deformation gradient as follows (Anand and Gurtin, 2003; Jung et al., 2004; Pan et al., 2007; Christ and Reese, 2009; Arghavani et al., 2011b; Stupkiewicz and Petryk, 2013):

$$\boldsymbol{C} = \boldsymbol{F}^{\mathrm{T}}\boldsymbol{F} \ \text{ and } \ \boldsymbol{b} = \boldsymbol{F}\boldsymbol{F}^{\mathrm{T}}. \tag{99}$$

By analogy with the theory of plasticity, Pethő (2000) decomposed the deformation gradient as follows:

$$\boldsymbol{F} = \boldsymbol{F}^{\mathrm{el}}\boldsymbol{F}^{\mathrm{tr}}\boldsymbol{F}^{\mathrm{pl}}, \tag{100}$$

where the elastic, transformation and plastic deformation gradients, $\boldsymbol{F}^{\mathrm{el}}$, $\boldsymbol{F}^{\mathrm{tr}}$ and $\boldsymbol{F}^{\mathrm{pl}}$ are given by

$$\boldsymbol{F}^{\mathrm{el}} = \boldsymbol{V}^{\mathrm{el}}\boldsymbol{R}^{\mathrm{el}}, \boldsymbol{F}^{\mathrm{pl}} = \boldsymbol{R}^{\mathrm{pl}}\boldsymbol{U}^{\mathrm{pl}} \ \text{ and } \ \boldsymbol{F}^{\mathrm{tr}} = \boldsymbol{R}^{\mathrm{tr}}\boldsymbol{B}^{\mathrm{tr}}\boldsymbol{S}^{\mathrm{tr}}. \tag{101}$$

In the above equations, $\boldsymbol{V}^{\mathrm{el}}$ is the elastic left stretch tensor, $\boldsymbol{U}^{\mathrm{pl}}$ is the elastic right stretch tensor, $\boldsymbol{R}^{\mathrm{el}}$ and $\boldsymbol{R}^{\mathrm{pl}}$ are the elastic and plastic rotation tensors, $\boldsymbol{R}^{\mathrm{tr}}$ is the lattice rotation, $\boldsymbol{B}^{\mathrm{tr}}$ is the Bain distortion, and $\boldsymbol{S}^{\mathrm{tr}}$ is the lattice invariant shear. The Green–Lagrange strain tensor $\boldsymbol{E}$ and its rate $\dot{\boldsymbol{E}}$ are then given by

$$\boldsymbol{E} = \frac{1}{2}\boldsymbol{C} - \mathbb{1} \ \text{ and } \ \dot{\boldsymbol{E}} = \boldsymbol{F}^{\mathrm{T}}\boldsymbol{d}\boldsymbol{F}, \tag{102}$$

where the strain rate tensor $\boldsymbol{d}$ corresponds to the symmetric part of the velocity gradient tensor $\boldsymbol{l}$ such that

$$\boldsymbol{d} = \frac{\boldsymbol{l} + \boldsymbol{l}^{\mathrm{T}}}{2} \ \text{ and } \ \boldsymbol{l} = \dot{\boldsymbol{F}}\boldsymbol{F}^{-1}. \tag{103}$$

From these considerations, Helm and Haupt (2003) and Christ and Reese (2009) proposed the following Helmholtz free energy for SMAs:

$$\Psi = \Psi^{\mathrm{tr}}(\boldsymbol{C}^{\mathrm{tr}}) + \Psi^{\mathrm{el}}\left(\boldsymbol{C}^{\mathrm{el}}, \xi, T\right). \tag{104}$$

The transformation part Ψ_{tr} is given by

$$\Psi^{\mathrm{tr}} = \frac{\mu_{\mathrm{tr}}}{2}\left(\mathrm{Tr}\,(\boldsymbol{C}^{\mathrm{tr}}) - 3\right), \tag{105}$$

where μ_{tr} is a material parameter. The elastic part Ψ^{el} is obtained by means of a Voigt mixture rule from the energies of the individual phases as follows:

$$\begin{aligned}\Psi_{\alpha}^{\mathrm{el}}\left(\boldsymbol{C}^{\mathrm{el}}, T\right) = {} & \frac{\mu^{\alpha}}{2}\left(\mathrm{Tr}\left(\boldsymbol{C}^{\mathrm{el}}\right) - 3 - 2\ln\left(J_{\mathrm{el}}\right)\right) + \frac{\lambda^{\alpha}}{4}\left(J_{\mathrm{el}}^{2} - 1 - 2\ln\left(J_{\mathrm{el}}\right)\right) + u_{0}^{\alpha} - Ts_{0}^{\alpha} + c^{\alpha}\left(T\left(1 - \ln\frac{T}{T_{0}}\right)\right) \\ & - 3\alpha_{T}^{\alpha}(T - T_{0})\left(\lambda^{\alpha} + \frac{2}{3}\mu^{\alpha}\right)\frac{\ln\left(J_{\mathrm{el}}\right)}{J_{\mathrm{el}}},\end{aligned} \tag{106}$$

where μ^{α} and λ^{α} are the Lamé coefficients of phase $\alpha \in \{\mathrm{A},\mathrm{M}\}$, $J_{\mathrm{el}} = \det(\boldsymbol{F}_{\mathrm{el}})$ represents volume change, c^{α} is the heat capacity, α_{T}^{α} is the thermal expansion coefficient of phase α, and T_0 is the initial temperature at which the specific internal energy and entropy of the phases take the respective values u_0^{α} and s_0^{α}. To penalize the presence of austenite–martensite interfaces, Thamburaja (2010) added to (104) the gradient energy defined by Fried and Gurtin (1994) as

$$\Psi^{\mathrm{g}} = \frac{K_{\xi}}{2}|\nabla\xi|, \tag{107}$$

where K_{ξ} is a material constant. Arghavani et al. (2010a) proposed an additive split of the deviatoric inelastic strain rate tensor $\boldsymbol{d}^{\mathrm{ine}}$ into a transformation part $\boldsymbol{d}^{\mathrm{tr}}$ and a reorientation $\boldsymbol{d}^{\mathrm{re}}$ part. Their results in Fig. 22 show under small shear deformation γ_{sh} that the Cauchy stress components σ_{11}, σ_{12} and σ_{22} are similar for both small and large strain formulations. However, the two formulations give very different results when γ_{sh} becomes large. The use of FSM can be substituted in certain cases with incremental objective methods in SSF to eliminate errors due e.g. to large rotation (Jaber et al., 2008).

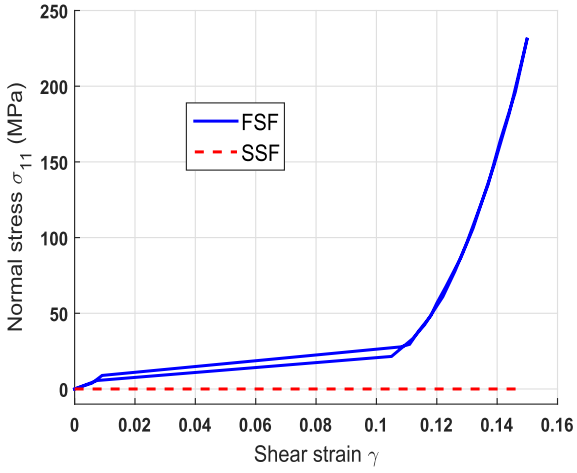

(a) σ_{11} vs. γ.

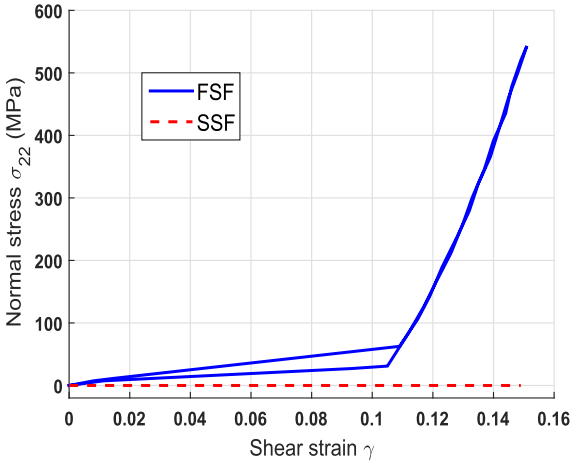

(b) σ_{22} vs. γ.

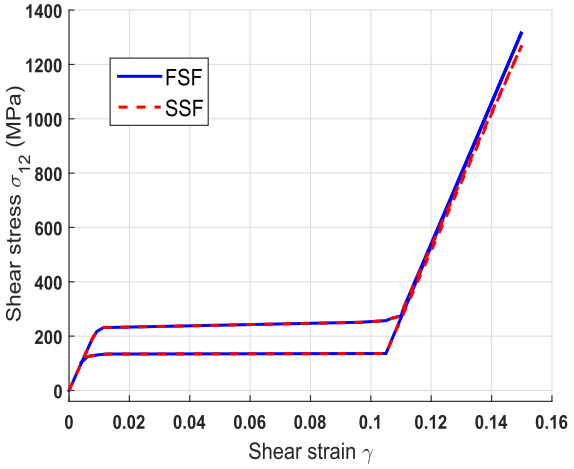

(c) σ_{12} vs. γ.

Fig. 22. Comparison of small (SSF) and finite (FSF) strain formulations for the case of simple shear (Arghavani et al., 2010a).

4.5. Models based on statistical physics

Statistical physics models are established based on local equilibrium considerations for single crystal SMAs. Bhattacharya and Lagoudas (1997) combined the work of Boyd and Lagoudas (1996) with statistical physics to simulate strain recovery in temperature-induced transformation. The homogenized behavior of the polycrystal was obtained from the responses of clusters of grains that were assumed to transform at constant temperatures, i.e. $M_s = M_f$ and $A_s = A_f$. For thermal loading under zero stress, the total volume fraction was given by

$$\dot{\xi} = \begin{cases} \int_{-\infty}^{+\infty} \xi_c p(M_0) dM_0 & \text{for forward transformation,} \\ \int_{-\infty}^{+\infty} \xi_c g(A_0) dA_0 & \text{for reverse transformation,} \end{cases} \tag{108}$$

where ξ_c is the volume fraction of clusters having a forward transformation temperature less than M_0 or a reverse transformation temperature not higher than A_0. The authors selected a normal distribution for $p(M_0)$ and $g(A_0)$. For instance,

$$p(M_0) = \frac{1}{s\sqrt{2\pi}} \exp\left[-\frac{1}{2}\left(\frac{M_0 - \overline{M}_0}{s}\right)\right], \quad s > 0, -\infty \leq M_0 \leq +\infty, \tag{109}$$

where s is the standard deviation and $\overline{M}_0$ is the mean of the distribution. The flow rule was then obtained from (44). Under non-zero external stress, M_0 is replaced by $M_\sigma - \sigma/C_M$ and A_0 by $A_\sigma - \sigma/C_A$, where C_M and C_A are the slopes of the stress-temperature boundaries for direct and reverse transformations respectively. The authors suggested the introduction of an additional parameter that accounts for material degradation to improve accuracy.

Later, Fischlschweiger and Oberaigner (2012) developed a statistical physics model by analogy with phase transformation in magnets that features an order parameter. They assumed the thermodynamic equilibrium to be satisfied in the RVE for a short time increment Δt under constant stress and temperature. The entropy of the RVE was assumed extremal under the following canonical constraints (Le Bellac et al., 2004):

$$\begin{aligned} &\sum_i w_i = 1, \\ &\sum_i w_i E_i = E, \end{aligned} \tag{110}$$

where E is the average total energy of the RVE in which a state i, representing austenite or martensite with discrete energy E_i, can exist with the probability w_i. From entropy extremization, the authors defined the canonical Gibbs free energy like in (Stanley, 1987; Schwabl, 2006):

$$G(T, \sigma) = -k_B T \ln Z(T, \sigma), \tag{111}$$

where k_B is the effective Boltzmann constant and Z is the partition function given by

$$Z = \mathrm{Tr}\left(e^{-\beta H}\right) = \sum_i e^{-\beta E_i}. \tag{112}$$

In (112), β is a Lagrange multiplier inversely proportional to temperature. For a single crystal of pure austenite or pure martensite, the Hamiltonians H_A for austenite and H_M for martensite were directly related to the free energy per mole F of the corresponding phase via the relations

$$\begin{aligned} H_A(T, \boldsymbol{\sigma}) &= F_A(T) - \frac{1}{2}\frac{\boldsymbol{\sigma} : \boldsymbol{S}_A : \boldsymbol{\sigma}}{\eta_A} = G_A(T, \boldsymbol{\sigma}), \\ H_M(T, \boldsymbol{\sigma}) &= F_M(T) - \frac{1}{\eta_M}\boldsymbol{\sigma} : \boldsymbol{\varepsilon}^{tr}_{cryst} - \frac{1}{2}\frac{\boldsymbol{\sigma} : \boldsymbol{S}_M : \boldsymbol{\sigma}}{\eta_M} = G_M(T, \boldsymbol{\sigma}). \end{aligned} \tag{113}$$

In the above equations, $\boldsymbol{S}_\alpha$ is the elastic compliance tensor and η_α is the specific molar density of phase $\alpha \in \{A,M\}$. The transformation strain $\boldsymbol{\varepsilon}^{tr}_{cryst}$ is constant for pure martensite. An interface Hamiltonian H^{AM} was defined to account for the interactions between austenite and martensite. From the above equation, the order parameter taken as the total strain was derived at constant temperature as follows:

$$\boldsymbol{\varepsilon} = -\left(\frac{\partial G}{\partial \boldsymbol{\sigma}}\right)_T, \tag{114}$$

and the volume fraction of martensite was defined in the interval [0,1] by the relation

$$\xi_M = \frac{\eta_A - \eta_T}{\eta_A - \eta_M}. \tag{115}$$

The total molar density η_T was determined by averaging as follows:

$$\langle \eta_T \rangle = \sum_i w_i \eta_{T_i} \sum_i \eta_{T_i} \frac{e^{-\beta E_i}}{Z}, \tag{116}$$

where η_{Ti} is the molar density of state i. This model was implemented for a linear chain of Nitinol quasi-particles using the parameters identified using data from Sun et al. (1995). The numerical results show sigmoidal curves for the evolution of ξ and $\boldsymbol{\varepsilon}$ during temperature-driven transformations for various stress levels (see Fig. 23(a) and (b)), with stress-dependent slopes for the obtained $\varepsilon - T$ curves and stress-independent slopes for the $\sigma - T$ curves. The dependence on stress was explained by the elastic energy (Hamilton et al., 2004). A statistical physics model was also developed by Müller and Seelecke (2001) and Müller (2012) and was shown to successfully simulate the pseudoelastic behavior in shape memory alloys.

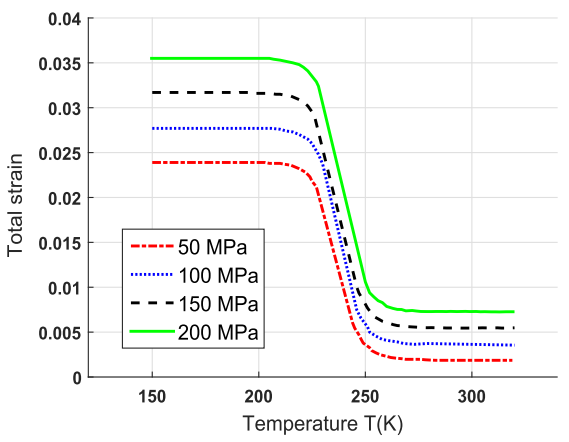

(a) evolution of ε with T.

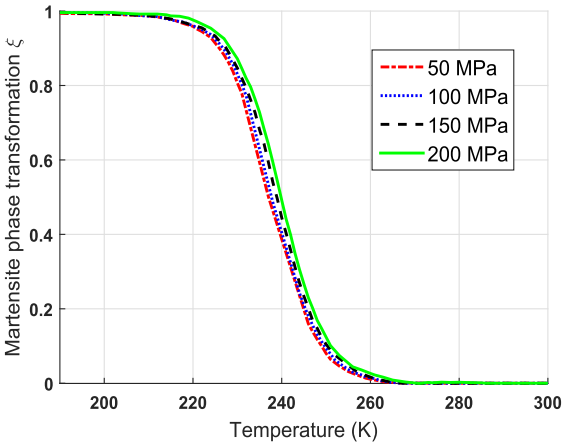

(b) evolution of ξ with T.

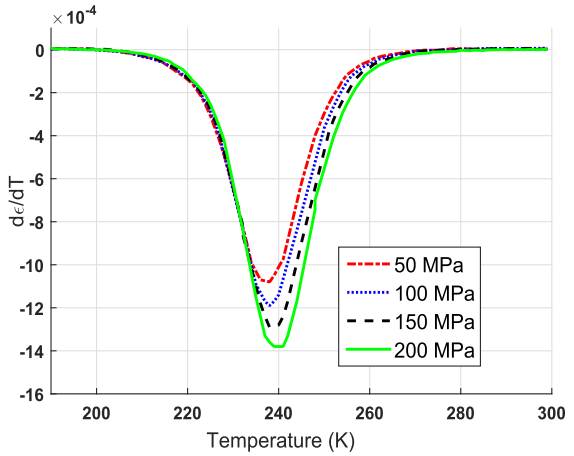

(c) evolution of $\mathrm{d}\varepsilon/\mathrm{d}T$ with T.

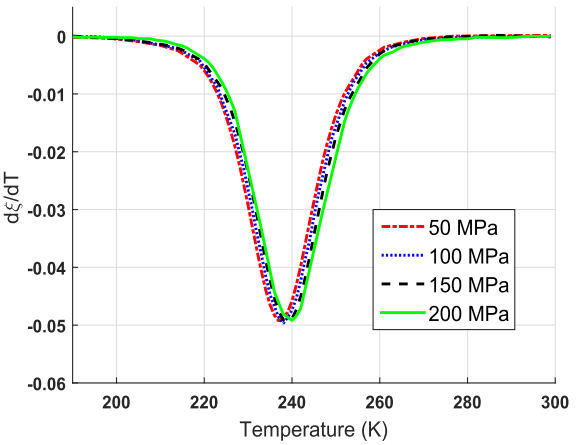

(d) evolution of $\mathrm{d}\xi/\mathrm{d}T$ with T.

Fig. 23. Simulation of temperature-induced transformation using statistical physics (Fischlschweiger and Oberaigner, 2012).

5. Conclusion

An overview of constitutive models for shape memory alloys was presented in this paper. The models were classified in terms of their modeling scale and level of detail in describing key aspects of SMA behavior. An attempt was made to track the historic progression of key models starting with early work on uniaxial SMA behavior and leading to the most recent developments. On top of this work, it would be interesting to review the modeling techniques used to describe complex processes such as martensite reorientation under non-proportional multiaxial loading, coupling between transformation-induced plasticity and its influence on the overall material behavior in a 3D setting, simulation of training and two-way shape memory, the role of thermomechanical coupling and tensile-compressive asymmetry, the evolution of the elastic stiffness with phase transformation, the analysis and prediction of functional and structural fatigue and the investigation of static and propagating cracks and fracture, as well as developments in finite element analysis of SMA structures.

References

Abeyaratne, R., Knowles, J.K., 1990. On the driving traction acting on a surface of strain discontinuity in a continuum. J. Mech. Phys. Solids 38 (3), 345–360.
Ackland, G.J., Jones, A., Noble-Eddy, R., 2008. Molecular dynamics simulations of the martensitic phase transition process. Mater. Sci. Eng. A 481, 11–17.
Airoldi, G., Riva, G., Vanelli, M., 1995. Superelasticity and shape memory effect in NiTi orthodontic wires. J. Phys. IV 5 (8), C8–C1205.
Alder, B.J., Wainwright, T., 1959. Studies in molecular dynamics. I. General method. J. Chem. Phys. 31 (2), 459–466.

Amengual, A., Cesari, E., Pons, J., 1995. Characteristics of the two-way memory effect induced by thermomechanical cycling in Cu-Zn-Al single crystals. J. Phys. IV 5 (8), 871–876.
Anand, L., Gurtin, M.E., 2003. Thermal effects in the superelasticity of crystalline shape-memory materials. J. Mech. Phys. Solids 51 (6), 1015–1058.
Andra, H., Hesebeck, O., Juhasz, L., Schnack, E., 2001. Simulation of thermomechanical behavior of shape-memory alloys under multiaxial non-proportional stress. Z. Angew. Math. Mech. 81, S329–S330.
Araki, Y., Endo, T., Omori, T., Sutou, Y., Koetaka, Y., Kainuma, R., Ishida, K., 2011. Potential of superelastic Cu–Al–Mn alloy bars for seismic applications. Earthq. Eng. Struct. Dyn. 40 (1), 107–115.
Araki, Y., Maekawa, N., Omori, T., Sutou, Y., Kainuma, R., Ishida, K., 2012. Rate-dependent response of superelastic Cu–Al–Mn alloy rods to tensile cyclic loads. Smart Mater. Struct. 21 (3), 032002.
Araya, R., Marivil, M., Mir, C., Moroni, O., Sepúlveda, A., 2008. Temperature and grain size effects on the behavior of CuAlBe SMA wires under cyclic loading. Mater. Sci. Eng. A 496 (1), 209–213.
Arghavani, J., Auricchio, F., Naghdabadi, R., Reali, A., Sohrabpour, S., 2010a. A 3D finite strain phenomenological constitutive model for shape memory alloys considering martensite reorientation. Contin. Mech. Thermodyn. 22 (5), 345–362.
Arghavani, J., Auricchio, F., Naghdabadi, R., Reali, A., Sohrabpour, S., 2010b. A 3-D phenomenological constitutive model for shape memory alloys under multiaxial loadings. Int. J. Plast. 26 (7), 976–991.
Arghavani, J., Auricchio, F., Naghdabadi, R., Reali, A., 2011a. On the robustness and efficiency of integration algorithms for a 3D finite strain phenomenological SMA constitutive model. Int. J. Numer. Methods Eng. 85 (1), 107–134.
Arghavani, J., Auricchio, F., Naghdabadi, R., Reali, A., 2011b. An improved, fully symmetric, finite-strain phenomenological constitutive model for shape memory alloys. Finite Elem. Anal. Des. 47 (2), 166–174.
Armattoe, K., Haboussi, M., Ben Zineb, T., 2014. A 2D finite element based on a nonlocal constitutive model describing localization and propagation of phase transformation in shape memory alloy thin structures. Int. J. Solids Struct. 51 (6), 1208–1220.
Ashrafi, M., Arghavani, J., Naghdabadi, R., Auricchio, F., 2015a. A three-dimensional phenomenological constitutive model for porous shape memory alloys including plasticity effects. J. Intell. Material Syst. Struct. 42, 1–317.
Ashrafi, M., Arghavani, J., Naghdabadi, R., Sohrabpour, S., 2015b. A 3-D constitutive model for pressure-dependent phase transformation of porous shape memory alloys. J. Mech. Behav. Biomed. Mater. 42, 292–310.
Auricchio, F., Bonetti, E., 2013. A new flexible 3D macroscopic model for shape memory alloys. Discret. Contin. Dyn. Syst. 6, 277–291.
Auricchio, F., Petrini, L., 2002. Improvements and algorithmical considerations on a recent three-dimensional model describing stress-induced solid phase transformations. Int. J. Numer. Methods Eng. 55 (11), 1255–1284.
Auricchio, F., Petrini, L., 2004. A three-dimensional model describing stress-temperature induced solid phase transformations: solution algorithm and boundary value problems. Int. J. Numer. Methods Eng. 61 (6), 807–836.
Auricchio, F., Reali, A., 2007. A phenomenological one-dimensional model describing stress-induced solid phase transformation with permanent inelasticity. Mech. Adv. Mater. Struct. 14 (1), 43–55.
Auricchio, F., Taylor, R.L., 1997. Shape-memory alloys: modelling and numerical simulations of the finite-strain superelastic behavior. Comput. Methods Appl. Mech. Eng. 143 (1), 175–194.
Auricchio, F., Taylor, R.L., Lubliner, J., 1997. Shape-memory alloys: macromodelling and numerical simulations of the superelastic behavior. Comput. Methods Appl. Mech. Eng. 146 (3), 281–312.
Auricchio, F., Marfia, S., Sacco, E., 2003. Modeling of SMA materials: training and two way memory effects. Comput. Struct. 81 (24), 2301–2317.
Auricchio, F., Reali, A., Stefanelli, U., 2007. A three-dimensional model describing stress-induced solid phase transformation with permanent inelasticity. Int. J. Plast. 23 (2), 207–226.
Auricchio, F., Reali, A., Stefanelli, U., 2009. A macroscopic 1D model for shape memory alloys including asymmetric behaviors and transformation-dependent elastic properties. Comput. Methods Appl. Mech. Eng. 198 (17), 1631–1637.
Auricchio, F., Bessoud, A.-L., Reali, A., Stefanelli, U., 2011. A three-dimensional phenomenological model for magnetic shape memory alloys. GAMM-Mitt. 34 (1), 90–96.
Auricchio, F., Bonetti, E., Scalet, G., Uberitini, F., 2014. Theoretical and numerical modeling of shape memory alloys accounting for multiple phase transformations and martensite reorientation. Int. J. Plast. 59, 30–54.
Auricchio, F., Bessoud, A.-L., Reali, A., Stefanelli, U., July -August 2015. A phenomenological model for the magneto-mechanical response of single-crystal magnetic shape memory alloys. Eur. J. Mech. A Solids 52, 1–11.
Ball, J.M., James, R.D., 1989. Fine phase mixtures as minimizers of energy. In: Analysis and Continuum Mechanics. Springer, pp. 647–686.
Bansiddhi, A., Sargeant, T., Stupp, S., Dunand, D., 2008. Porous NiTi for bone implants: a review. Acta Biomater. 4 (4), 773–782.
Barsch, G., Krumhansl, J., 1988. Nonlinear and nonlocal continuum model of transformation precursors in martensites. Metall. Trans. A 19 (4), 761–775.
Batdorf, S.B., Budiansky, B., 1949. A Mathematical Theory of Plasticity Based on the Concept of Slip. National Advisory Committee for Aeronautics.
Bažant, P., Oh, B., 1986. Efficient numerical integration on the surface of a sphere. ZAMM J. Appl. Math. Mech. Z. Angew. Math. Mech. 66 (1), 37–49.
Bažant, Z., 1984. chapter 3. In: Desai, C.S., Gallagher, R.H. (Eds.), Microplane Model for Strain Controlled Inelastic Behaviour.
Bažant, Z., Oh, B., 1985. Microplane model for progressive fracture of concrete and rock. J. Eng. Mech. 111 (4), 559–582.
Bažant, Z.P., Caner, F.C., Carol, I., Adley, M.D., Akers, S.A., 2000. Microplane model M4 for concrete. I: formulation with work-conjugate deviatoric stress. J. Eng. Mech. 126 (9), 944–953.
Bekker, A., Brinson, L., 1998. Phase diagram based description of the hysteresis behavior of shape memory alloys. Acta Mater. 46 (10), 3649–3665.
Bel Haj Khalifa, S., Engels-Deutsch, M., Thiébaud, F., Mordeniz, J., Ben Zineb, T., 2013. Finite element analysis of superelastic behaviour of endodontic file in Cu-based single crystal SMA. In: The International Conference on Shape Memory and Superelastic Technologies (SMST). ASME.
Bertram, A., 1983. Thermo-mechanical constitutive equations for the description of shape memory effects in alloys. Nucl. Eng. Des. 74 (2), 173–182.
Bhattacharya, A., Lagoudas, D., 1997. A stochastic thermodynamic model for the gradual thermal transformation of SMA polycrystals. Smart Mater. Struct. 6 (3), 235.
Blanc, P., Lexcellent, C., 2004. Micromechanical modelling of a CuAlNi shape memory alloy behaviour. Mater. Sci. Eng. A 378 (1), 465–469.
Bo, Z., Lagoudas, D.C., 1999. Thermomechanical modeling of polycrystalline SMAs under cyclic loading, part III: evolution of plastic strains and two-way shape memory effect. Int. J. Eng. Sci. 37 (9), 1175–1203.
Bourbon, G., Lexcellent, C., Leclercq, S., 1995. Modelling of the non isothermal cyclic behaviour of a polycrystalline CuZnAl shape memory alloy. J. Phys. IV 5 (C8), 221–226.
Bouvet, C., Calloch, S., Lexcellent, C., 2002. Mechanical behavior of a Cu-Al-Be shape memory alloy under multiaxial proportional and nonproportional loadings. J. Eng. Mater. Technol. 124 (2), 112–124.
Bouvet, C., Calloch, S., Lexcellent, C., 2004. A phenomenological model for pseudoelasticity of shape memory alloys under multiaxial proportional and nonproportional loadings. Eur. J. Mech. A Solids 23 (1), 37–61.
Bowles, J., Mackenzie, J., 1954. The crystallography of martensitic transformations. Acta Metall. 2, 129–147.
Boyd, J.G., Lagoudas, D.C., 1996. A thermodynamical constitutive model for shape memory materials. Part I. The monolithic shape memory alloy. Int. J. Plast. 12 (6), 805–842.
Brinson, L., 1993. One-dimensional constitutive behavior of shape memory alloys: thermomechanical derivation with non-constant material functions and redefined martensite internal variable. J. Intell. Material Syst. Struct. 4 (2), 229–242.
Brinson, L., Huang, M., 1996. Simplifications and comparisons of shape memory alloy constitutive models. J. Intell. Material Syst. Struct. 7, 108–114.
Brinson, L., Lammering, R., 1993. Finite element analysis of the behavior of shape memory alloys and their applications. Int. J. Solids Struct. 30 (23), 3261–3280.

Brocca, M., Brinson, L., Bažant, Z., 2002. Three-dimensional constitutive model for shape memory alloys based on microplane model. J. Mech. Phys. Solids 50 (5), 1051–1077.
Buehler, W.J., Cross, W.B., 1969. 55-Nitinol-unique wire alloy with a memory. WIRE J. 2 (6), 41–49.
Buehler, W.J., Gilfrich, J., Wiley, R., 1963. Effect of low-temperature phase changes on the mechanical properties of alloys near composition TiNi. J. Appl. Phys. 34 (5), 1475–1477.
Carol, I., Bazant, Z.P., 1997. Damage and plasticity in microplane theory. Int. J. Solids Struct. 34 (29), 3807–3835.
Carol, I., Prat, P., 1990. A statically constrained microplane model for the smeared analysis of concrete cracking. Comput. Aided Anal. Des. Concr. Struct. 2, 919–930.
Carol, I., Jirásek, M., Bažant, Z., 2001. A thermodynamically consistent approach to microplane theory. Part I. Free energy and consistent microplane stresses. Int. J. Solids Struct. 38 (17), 2921–2931.
Casciati, F., Casciati, S., Faravelli, L., 2007. Fatigue characterization of a Cu-based shape memory alloy, 1999. In: Proceedings of the Estonian Academy of Sciences. Physics, Mathmatics, vol. 56. Estonian Academy Publishers, pp. 207–217.
Chang, L., Read, T., 1951. Plastic deformation and diffusionless phase changes in metals-the gold-cadmium beta-phase. Trans. Am. Inst. Min. Metall. Eng. 191 (1), 47–52.
Chemisky, Y., Duval, A., Patoor, E., Ben Zineb, T., 2011. Constitutive model for shape memory alloys including phase transformation, martensitic reorientation and twins accommodation. Mech. Mater. 43 (7), 361–376.
Chemisky, Y., Chatzigeorgiou, G., Kumar, P., Lagoudas, D.C., 2014. A constitutive model for cyclic actuation of high-temperature shape memory alloys. Mech. Mater. 68, 120–136.
Chen, S., Srolovitz, D., Voter, A., 1989. Computer simulation on surfaces and [001] symmetric tilt grain boundaries in Ni, Al, and Ni3Al. J. Mater. Res. 4 (01), 62–77.
Cho, J.-Y., Idesman, A., Levitas, V., Park, T., 2012. Finite element simulations of dynamics of multivariant martensitic phase transitions based on Ginzburg–Landau theory. Int. J. Solids Struct. 49 (14), 1973–1992.
Christ, D., Reese, S., 2009. A finite element model for shape memory alloys considering thermomechanical couplings at large strains. Int. J. Solids Struct. 46 (20), 3694–3709.
Cingolani, E., Yawny, A., Ahlers, M., 1995. The two way shape memory effect in stabilized and pseudoelastically trained Cu-Zn-Al single crystals. J. Phys. IV 5 (8).
Clementi, E., Roetti, C., 1974. Roothaan-Hartree-Fock atomic wavefunctions: basis functions and their coefficients for ground and certain excited states of neutral and ionized atoms, $z \leq 54$. Atomic Data Nucl. Data Tables 14 (3), 177–478.
Collard, C., Ben Zineb, T., 2012. Simulation of the effect of elastic precipitates in SMA materials based on a micromechanical model. Compos. B Eng. 43 (6), 2560–2576.
Contardo, L., 1988. Etude des traitements d'education, de la stabilite et de l'origine de l'effet memoire de forme double sens dans un alliage Cu-Zn-Al (PhD thesis). INSA, Villeurbanne.
Daw, M.S., Baskes, M.I., 1984. Embedded-atom method: derivation and application to impurities, surfaces, and other defects in metals. Phys. Rev. B 29 (12), 6443.
De Araujo, C.J., 1999. Comportement cyclique de fils en alliage à mémoire de forme Ti-Ni-Cu: analyse électro-thermomécanique, dégradation et fatigue par cyclage thermique sous contrainte (PhD thesis). INSA-Lyon.
De Vos, J., Aernoudt, E., Delaey, L., 1978. The crystallography of the martensitic transformation of BCC into 9R: a generalized mathematical model. Z. Met. 69 (7), 438–444.
Delaey, L., Krishnan, R., Tas, H., Warlimont, H., 1974. Thermoelasticity, pseudoelasticity and the memory effects associated with martensitic transformations. J. Mater. Sci. 9 (9), 1521–1535.
Delaey, L., Ortin, J., Van Humbeeck, J., 1987. Hysteresis effects in martensitic non-ferrous alloys. Phase Transform. 87, 60–66.
Deng, J., Ding, X., Lookman, T., Suzuki, T., Saxena, A., Otsuka, K., Sun, J., Ren, X., 2010. Origin of ultrafast annihilation effect of martensite aging: atomistic simulations. Phys. Rev. B 82 (18), 184101.
Dhote, R., Melnik, R., Zu, J., 2014. Dynamic multi-axial behavior of shape memory alloy nanowires with coupled thermo-mechanical phase-field models. Meccanica 1–15.
Duval, A., Haboussi, M., Zineb, T.B., 2010. Modeling of sma superelastic behavior with nonlocal approach. Phys. Procedia 10, 33–38.
Duval, A., Haboussi, M., Ben Zineb, T., 2011. Modelling of localization and propagation of phase transformation in superelastic SMA by a gradient nonlocal approach. Int. J. Solids Struct. 48 (13), 1879–1893.
Entemeyer, D., 1996. Etude micromécanique du comportement thermomécanique des alliages à mémoire de forme (PhD thesis). Université de Metz.
Es-Souni, M., Es-Souni, M., Fischer-Brandies, H., 2005. Assessing the biocompatibility of NiTi shape memory alloys used for medical applications. Anal. Bioanal. Chem. 381 (3), 557–567.
Evangelista, V., Marfia, S., Sacco, E., 2009. Phenomenological 3D and 1D consistent models for shape-memory alloy materials. Comput. Mech. 44 (3), 405–421.
Falk, F., 1980. Model free energy, mechanics, and thermodynamics of shape memory alloys. Acta Metall. 28 (12), 1773–1780.
Falk, F., 1983. Ginzburg-Landau theory of static domain walls in shape-memory alloys. Z. Phys. B Condens. Matter 51 (2), 177–185.
Farkas, D., Mutasa, B., Vailhe, C., Ternes, K., 1995. Interatomic potentials for B2 NiAl and martensitic phases. Model. Simul. Mater. Sci. Eng. 3 (2), 201.
Federzoni, L., Guenin, G., Mantel, M., 1993. Improvement of the shape memory effect of a Fe-Mn-Cr-Si-Ni by original thermomechanical treatments. J. Phys. IV 3 (C7), C7–C557.
Finnis, M., Sinclair, J., 1984. A simple empirical N-body potential for transition metals. Philos. Mag. A 50 (1), 45–55.
Fischer, F., Tanaka, K., 1992. A micromechanical model for the kinetics of martensitic transformation. Int. J. Solids Struct. 29 (14), 1723–1728.
Fischlschweiger, M., Oberaigner, E.R., 2012. Kinetics and rates of martensitic phase transformation based on statistical physics. Comput. Mater. Sci. 52 (1), 189–192.
Foiles, S., Daw, M., 1987. Application of the embedded atom method to Ni_3 Al. J. Mater. Res. 2 (01), 5–15.
Frémond, M., 1987. Matériaux à mémoire de forme. Comptes rendus Acad. Sci. Série 2 Méc. Phys. Chim. Sci. univers Sci. Terre 304 (7), 239–244.
Frémond, M., 2002. Non-smooth Thermomechanics. Springer.
Fried, E., Gurtin, M.E., 1994. Dynamic solid-solid transitions with phase characterized by an order parameter. Phys. D. Nonlinear Phenom. 72 (4), 287–308.
Gall, K., Sehitoglu, H., 1999. The role of texture in tension–compression asymmetry in polycrystalline NiTi. Int. J. Plast. 15 (1), 69–92.
Gall, K., Lim, T.J., McDowell, D.L., Sehitoglu, H., Chumlyakov, Y.I., 2000. The role of intergranular constraint on the stress-induced martensitic transformation in textured polycrystalline NiTi. Int. J. Plast. 16 (10), 1189–1214.
Gao, X., Huang, M., Brinson, L.C., 2000. A multivariant micromechanical model for SMAs. Part 1. Crystallographic issues for single crystal model. Int. J. Plast. 16 (10), 1345–1369.
Goo, B., Lexcellent, C., 1997. Micromechanics-based modeling of two-way memory effect of a single crystalline shape-memory alloy. Acta Mater. 45 (2), 727–737.
Govindjee, S., Hall, G.J., 2000. A computational model for shape memory alloys. Int. J. Solids Struct. 37 (5), 735–760.
Govindjee, S., Miehe, C., 2001. A multi-variant martensitic phase transformation model: formulation and numerical implementation. Comput. Methods Appl. Mech. Eng. 191 (3), 215–238.
Grandi, D., Stefanelli, U., 2015. The souza-auricchio model for shape memory alloys. Discrete Contin. Dyn. Syst. Series S 8 (4).
Gu, X., Zaki, W., Morin, C., Moumni, Z., Zhang, W., 2015. Time integration and assessment of a model for shape memory alloys considering multiaxial nonproportional loading cases. Int. J. Solids Struct. 54, 82–99.
Guilemany, J., Fernández, J., 1995. Mechanism of two way shape memory effect obtained by stabilised stress induced martensite. J. Phys. IV 05 (C2).

Guo, Y.-F., Wang, Y.-S., Wu, W.-P., Zhao, D.-L., 2007. Atomistic simulation of martensitic phase transformation at the crack tip in B2 NiAl. Acta Mater. 55 (11), 3891–3897.
Guthikonda, V.S., Elliott, R.S., 2013. Modeling martensitic phase transformations in shape memory alloys with the self-consistent lattice dynamics approach. J. Mech. Phys. Solids 61 (4), 1010–1026.
Hackl, K., Heinen, R., 2008. A micromechanical model for pretextured polycrystalline shape-memory alloys including elastic anisotropy. Contin. Mech. Thermodyn. 19 (8), 499–510.
Halphen, B., Nguyen, Q., 1974. Plastic and visco-plastic materials with generalized potential. Mech. Res. Commun. 1 (1), 43–47.
Hamilton, R., Sehitoglu, H., Chumlyakov, Y., Maier, H., 2004. Stress dependence of the hysteresis in single crystal NiTi alloys. Acta Mater. 52 (11), 3383–3402.
Hane, K.F., Shield, T., 1999a. Microstructure in the cubic to monoclinic transition in titanium–nickel shape memory alloys. Acta Mater. 47 (9), 2603–2617.
Hane, K.F., Shield, T.W., 1999b. Microstructure in a copperaluminiumnickel shape–memory alloy. In: Proceedings of the Royal Society of London a: Mathematical, Physical and Engineering Sciences, vol. 455, pp. 3901–3915.
Hartl, D., Lagoudas, D., 2009. Constitutive modeling and structural analysis considering simultaneous phase transformation and plastic yield in shape memory alloys. Smart Mater. Struct. 18 (10), 104017.
Hartl, D.J., Chatzigeorgiou, G., Lagoudas, D.C., 2010. Three-dimensional modeling and numerical analysis of rate-dependent irrecoverable deformation in shape memory alloys. Int. J. Plast. 26 (10), 1485–1507.
Hazar, S., Zaki, W., Moumni, Z., Anlas, G., 2013. Steady state crack growth in shape memory alloys. In: ASME 2013 Conference on Smart Materials, Adaptive Structures and Intelligent Systems. American Society of Mechanical Engineers. V001T03A018–V001T03A018.
Hazar, S., Zaki, W., Moumni, Z., Anlas, G., 2015. Modeling of steady-state crack growth in shape memory alloys using a stationary method. Int. J. Plast. 67, 26–38.
Hebda, D.A., White, S.R., 1995. Effect of training conditions and extended thermal cycling on nitinol two-way shape memory behavior. Smart Mater. Struct. 4 (4), 298.
Helm, D., 2007. Thermomechanics of martensitic phase transitions in shape memory alloys, I: constitutive theories for small and large deformations. J. Mech. Mater. Struct. 2 (1), 87–112.
Helm, D., Haupt, P., 2001. Thermomechanical behavior of shape memory alloys. In: SPIE's 8th Annual International Symposium on Smart Structures and Materials. International Society for Optics and Photonics, pp. 302–313.
Helm, D., Haupt, P., 2003. Shape memory behaviour: modelling within continuum thermomechanics. Int. J. Solids Struct. 40 (4), 827–849.
Hirsinger, L., Lexcellent, C., 2003. Modelling detwinning of martensite platelets under magnetic and (or) stress actions on Ni–Mn–Ga alloys. J. Magn. Magn. Mater. 254, 275–277.
Hirsinger, L., Creton, N., Lexcellent, C., 2004. Stress-induced phase transformations in Ni–Mn–Ga alloys: experiments and modelling. Mater. Sci. Eng. A 378 (1), 365–369.
Huang, M., Brinson, L., 1998. A multivariant model for single crystal shape memory alloy behavior. J. Mech. Phys. Solids 46 (8), 1379–1409.
Huang, M., Gao, X., Brinson, L.C., 2000. A multivariant micromechanical model for SMAs Part 2. polycrystal model. Int. J. Plast. 16 (10), 1371–1390.
Idesman, A.V., Cho, J.-Y., Levitas, V.I., 2008. Finite element modeling of dynamics of martensitic phase transitions. Appl. Phys. Lett. 93 (4), 043102.
Ishida, H., Hiwatari, Y., 2007. MD simulation of martensitic transformations in NiTi alloys with MEAM. Mol. Simul. 33 (4–5), 459–461.
Jaber, M.B., SMAoui, H., Terriault, P., 2008. Finite element analysis of a shape memory alloy three-dimensional beam based on a finite strain description. Smart Mater. Struct. 17 (4), 045005.
James, R., Zhang, Z., 2005. A way to search for multiferroic materials with unlikely combinations of physical properties. In: Magnetism and Structure in Functional Materials. Springer, pp. 159–175.
James, R.D., Hane, K.F., 2000. Martensitic transformations and shape-memory materials. Acta Mater. 48 (1), 197–222.
Jemal, F., Bouraoui, T., Ben Zineb, T., Patoor, E., Bradaï, C., 2009. Modelling of martensitic transformation and plastic slip effects on the thermo-mechanical behaviour of Fe-based shape memory alloys. Mech. Mater. 41 (7), 849–856.
Jin, Y., Artemev, A., Khachaturyan, A., 2001. Three-dimensional phase field model of low-symmetry martensitic transformation in polycrystal: simulation of ζ_2 martensite in AuCd alloys. Acta Mater. 49 (12), 2309–2320.
A. D. Johnson. Biocompatible copper-based single-crystal shape memory alloys, Oct. 15 2013. US Patent 8,556,969.
Juhasz, L., Andrä, H., Hesebeck, O., 2000. A constitutive model of shape memory alloys based on viscoplastic like evolution equations. Mech. Eng. 44 (1), 59–69.
Jung, Y., Papadopoulos, P., Ritchie, R., 2004. Constitutive modelling and numerical simulation of multivariant phase transformation in superelastic shape-memory alloys. Int. J. Numer. Methods Eng. 60 (2), 429–460.
Junker, P., Hackl, K., 2011. Finite element simulations of poly-crystalline shape memory alloys based on a micromechanical model. Comput. Mech. 47 (5), 505–517.
Kadkhodaei, M., Salimi, M., Rajapakse, R., Mahzoon, M., 2008. Modeling of shape memory alloys based on microplane theory. J. Intell. Material Syst. Struct. 19 (5), 541–550.
Kastner, O., 2006. Molecular-dynamics of a 2D model of the shape memory effect. Contin. Mech. Thermodyn. 18 (1–2), 63–81.
Kastner, O., Eggeler, G., Weiss, W., Ackland, G.J., 2011. Molecular dynamics simulation study of microstructure evolution during cyclic martensitic transformations. J. Mech. Phys. Solids 59 (9), 1888–1908.
Khalil, W., Mikolajczak, A., Bouby, C., Zineb, T.B., 2012. A constitutive model for Fe-based shape memory alloy considering martensitic transformation and plastic sliding coupling: application to a finite element structural analysis. J. Intell. Material Syst. Struct. 23, 1143–1160.
Kim, H.W., 2004. A study of the two-way shape memory effect in Cu–Zn–Al alloys by the thermomechanical cycling method. J. Mater. Process. Technol. 146 (3), 326–329.
Kim, H.W., 2005. Investigation of a Cu-Zn-Al alloy with two-way shape memory effect by the cycled constrained heating/cooling technique. J. Mater. Sci. 40 (1), 211–212.
Koistinen, D., Marburger, R., 1959. A general equation prescribing the extent of the austenite-martensite transformation in pure iron-carbon alloys and plain carbon steels. Acta Metall. 7 (1), 59–60.
Kudoh, Y., Tokonami, M., Miyazaki, S., Otsuka, K., 1985. Crystal structure of the martensite in Ti-49.2at%Ni alloy analyzed by the single crystal X-ray diffraction method. Acta Metall. 33 (11), 2049–2056.
Kuhl, E., Steinmann, P., Carol, I., 2001. A thermodynamically consistent approach to microplane theory. Part II. Dissipation and inelastic constitutive modeling. Int. J. Solids Struct. 38 (17), 2933–2952.
Lagoudas, D., Hartl, D., Chemisky, Y., Machado, L., Popov, P., 2012. Constitutive model for the numerical analysis of phase transformation in polycrystalline shape memory alloys. Int. J. Plast. 32, 155–183.
Lagoudas, D.C., Entchev, P.B., 2004. Modeling of transformation-induced plasticity and its effect on the behavior of porous shape memory alloys. Part I: constitutive model for fully dense SMAs. Mech. Mater. 36 (9), 865–892.
Lagoudas, D.C., Bo, Z., Qidwai, M.A., 1996. A unified thermodynamic constitutive model for SMA and finite element analysis of active metal matrix composites. Mech. Compos. Mater. Struct. 3 (2), 153–179.
Lagoudas, D.C., Entchev, P.B., Popov, P., Patoor, E., Brinson, L.C., Gao, X., 2006. Shape memory alloys, part II: modeling of polycrystals. Mech. Mater. 38 (5), 430–462.
Lai, W., Liu, B., 2000. Lattice stability of some Ni-Ti alloy phases versus their chemical composition and disordering. J. Phys. Condens. Matter 12 (5), L53.
Le Bellac, M., Mortessagne, F., Batrouni, G.G., 2004. Equilibrium and Non-equilibrium Statistical Thermodynamics. Cambridge University Press.
Leclercq, S., Lexcellent, C., 1996. A general macroscopic description of the thermomechanical behavior of shape memory alloys. J. Mech. Phys. Solids 44 (6), 953–980.

Leukart, M., 2005. Kombinierte anisotrope Schädigung und Plastizität bei kohäsiven Reibungsmaterialien (PhD thesis). Univ. Stuttgart, Institut fr Baustatik.
Leukart, M., Ramm, E., 2003. A comparison of damage models formulated on different material scales. Comput. Mater. Sci. 28 (3), 749–762.
Levitas, V.I., 2013. Thermodynamically consistent phase field approach to phase transformations with interface stresses. Acta Mater. 61 (12), 4305–4319.
Levitas, V.I., Ozsoy, I.B., 2009. Micromechanical modeling of stress-induced phase transformations. Part 1. thermodynamics and kinetics of coupled interface propagation and reorientation. Int. J. Plast. 25 (2), 239–280.
Levitas, V.I., Preston, D.L., 2002a. Three-dimensional Landau theory for multivariant stress-induced martensitic phase transformations. I. Austenite ↔ martensite. Phys. Rev. B 66 (13), 134206.
Levitas, V.I., Preston, D.L., 2002b. Three-dimensional Landau theory for multivariant stress-induced martensitic phase transformations. II. Multivariant phase transformations and stress space analysis. Phys. Rev. B 66 (13), 134207.
Levitas, V.I., Preston, D.L., Lee, D.-W., 2003. Three-dimensional Landau theory for multivariant stress-induced martensitic phase transformations. III. Alternative potentials, critical nuclei, kink solutions, and dislocation theory. Phys. Rev. B 68 (13), 134201.
Lexcellent, C., 2013. Handbook of Shape Memory Alloys. Wiley-ISTE.
Lexcellent, C., Leclercq, S., Gabry, B., Bourbon, G., 2000. The two way shape memory effect of shape memory alloys: an experimental study and a phenomenological model. Int. J. Plast. 16 (10), 1155–1168.
Lexcellent, C., Boubakar, M., Bouvet, C., Calloch, S., 2006. About modelling the shape memory alloy behaviour based on the phase transformation surface identification under proportional loading and anisothermal conditions. Int. J. Solids Struct. 43 (3), 613–626.
Lexcellent, C., Blanc, P., Creton, N., 2008. Two ways for predicting the hysteresis minimisation for shape memory alloys. Mater. Sci. Eng. A 481, 334–338.
Liang, C., Rogers, C., 1990. One-dimensional thermomechanical constitutive relations for shape memory materials. J. Intell. Material Syst. Struct. 1 (2), 207–234.
Lim, T., McDowell, D., 2002. Cyclic thermomechanical behavior of a polycrystalline pseudoelastic shape memory alloy. J. Mech. Phys. Solids 50 (3), 651–676.
Lin, K.-M., Chen, J.-H., Lin, C.-C., Liu, C.-H., Lin, H.-C., 2014. Optimization of shape-memory effect in Fe-Mn-Si-Cr-Re shape-memory alloys. J. Mater. Eng. Perform. 23, 12327–12332.
Liu, Y., McCormick, P., 1990. Factors influencing the development of two-way shape memory in NiTi. Acta Metall. Mater. 38 (7), 1321–1326.
Lovey, F., Rodriguez, P., Malarria, J., Sade, M., Torra, V., 1995. On the origin of the two way shape memory effect in Cu-Zn-Al alloys. J. Phys. IV 5 (C2), 287–292.
Lu, Z., Weng, G., 1997. Martensitic transformation and stress-strain relations of shape-memory alloys. J. Mech. Phys. Solids 45 (11), 1905–1928.
Lu, Z., Weng, G., 1998. A self-consistent model for the stress–strain behavior of shape-memory alloy polycrystals. Acta Mater. 46 (15), 5423–5433.
Lubliner, J., Auricchio, F., 1996. Generalized plasticity and shape memory alloys. Int. J. Solids Struct. 33 (7), 991–1003.
Mahapatra, D.R., Melnik, R., 2006. Finite element analysis of phase transformation dynamics in shape memory alloys with a consistent Landau-Ginzburg free energy model. Mech. Adv. Mater. Struct. 13 (6), 443–455.
Mahnken, R., Wilmanns, S., 2008. Simulation of asymmetric effects for shape memory alloys by decomposition of transformation strains. Comput. Mater. Sci. 42 (2), 295–305.
Maranganti, R., Sharma, P., 2010. Revisiting quantum notions of stress. In: Proceedings of the Royal Society of London a: Mathematical, Physical and Engineering Sciences, vol. 466. The Royal Society, pp. 2097–2116.
Masud, A., Panahandeh, M., Aurrichio, F., 1997. A finite-strain finite element model for the pseudoelastic behavior of shape memory alloys. Comput. Methods Appl. Mech. Eng. 148 (1), 23–37.
McNaney, J.M., Imbeni, V., Jung, Y., Papadopoulos, P., Ritchie, R., 2003. An experimental study of the superelastic effect in a shape-memory nitinol alloy under biaxial loading. Mech. Mater. 35 (10), 969–986.
Mehrabi, R., Kadkhodaei, M., 2013. 3D phenomenological constitutive modeling of shape memory alloys based on microplane theory. Smart Mater. Struct. 22 (2), 025017.
Mehrabi, R., Kadkhodaei, M., Ghaei, A., 2012. Numerical implementation of a thermomechanical constitutive model for shape memory alloys using return mapping algorithm and microplane theory. Adv. Mater. Res. 516, 351–354.
Mehrabi, R., Kadkhodaei, M., Elahinia, M., 2014. A thermodynamically-consistent microplane model for shape memory alloys. Int. J. Solids Struct. 51 (14), 2666–2675.
Mirzaeifar, R., Shakeri, M., DesRoches, R., Yavari, A., 2011. A semi-analytic analysis of shape memory alloy thick-walled cylinders under internal pressure. Arch. Appl. Mech. 81 (8), 1093–1116.
Mirzaeifar, R., Gall, K., Zhu, T., Yavari, A., DesRoches, R., 2014. Structural transformations in NiTi shape memory alloy nanowires. J. Appl. Phys. 115 (19), 194307.
Miyazaki, S., Otsuka, K., Suzuki, Y., 1981. Transformation pseudoelasticity and deformation behavior in a Ti-50.6at%Ni alloy. Scr. Metall. 15 (3), 287–292.
Mollica, F., Rajagopal, K., Srinivasa, A., 2001. The inelastic behavior of metals subject to loading reversal. Int. J. Plast. 17 (8), 1119–1146.
Mori, T., Tanaka, K., 1973. Average stress in matrix and average elastic energy of materials with misfitting inclusions. Acta Metall. 21 (5), 571–574.
Morin, C., 2011. A Comprehensive Approach for Fatigue Analysis of Shape Memory Alloys (PhD thesis). Ecole Polytechnique, Palaiseau.
Morin, C., Moumni, Z., Zaki, W., 2011a. A constitutive model for shape memory alloys accounting for thermomechanical coupling. Int. J. Plast. 27 (5), 748–767.
Morin, C., Moumni, Z., Zaki, W., 2011b. Thermomechanical coupling in shape memory alloys under cyclic loadings: experimental analysis and constitutive modeling. Int. J. Plast. 27 (12), 1959–1980.
Morin, C., Moumni, Z., Zaki, W., 2011c. Direct numerical determination of the asymptotic cyclic behavior of pseudoelastic shape memory structures. J. Eng. Mech. 137 (7), 497–503.
Morin, C., Moumni, Z., Zaki, W., 2011d. Influence of heat transfer on the thermomechanical behavior of shape memory alloys. Int. Rev. Mech. Eng. 5 (2), 329–339.
Moumni, Z., Zaki, W., Maitournam, H., 2008a. Cyclic and fatigue behavior of niti shape memory alloys. In: SMST-2007-Proceedings of the International Conference on Shape Memory and Superelastic Technologies, pp. 193–200.
Moumni, Z., Zaki, W., Nguyen, Q.S., 2008b. Theoretical and numerical modeling of solid–solid phase change: application to the description of the thermomechanical behavior of shape memory alloys. Int. J. Plast. 24 (4), 614–645.
Moumni, Z., Zaki, W., Maitournam, H., 2009. Cyclic behavior and energy approach to the fatigue of shape memory alloys. J. Mech. Mater. Struct. 4 (2), 395–411.
Moumni, Z., Zaki, W., Nguyen, Q.S., Zhang, W., 2015. Modeling of materials capable of solid-solid phase transformation. application to the analytical solution of the semi-infinite mode iii crack problem in a phase-changing solid. Int. J. Non-Linear Mech. 69, 146–156.
Müller, C., Bruhns, O., 2006. A thermodynamic finite-strain model for pseudoelastic shape memory alloys. Int. J. Plast. 22 (9), 1658–1682.
Müller, I., 2012. Pseudo-elastic hysteresis in shape memory alloys. Phys. B Condens. Matter 407 (9), 1314–1315.
Müller, I., Seelecke, S., 2001. Thermodynamic aspects of shape memory alloys. Math. Comput. Model. 34 (12), 1307–1355.
Murakami, M., Otsuka, H., Suzuki, H., Matsuda, S., 1986. Complete shape memory effect in polycrystalline Fe-Mn-Si alloys. In: Proceedings of the International Conference on Martensitic Transformations. ICOMAT-86, pp. 985–990.
Mutter, D., Nielaba, P., 2013. Simulation of the shape memory effect in a NiTi nano model system. J. Alloys Compd. 577, S83–S87.
Niclaeys, C., Ben Zineb, T., Arbab-Chirani, S., Patoor, E., 2002. Determination of the interaction energy in the martensitic state. Int. J. Plast. 18 (11), 1619–1647.
Niitsu, K., Omori, T., Kainuma, R., 2011. Superelasticity at low temperatures in Cu-17Al-15Mn (at%) shape memory alloy. Mater Trans. 52 (8), 1713–1715.
Novák, V., Šittner, P., 2004. Micromechanics modelling of NiTi polycrystalline aggregates transforming under tension and compression stress. Mater. Sci. Eng. A 378 (1), 490–498.
Olson, G., Cohen, M., 1982. Stress-assisted isothermal martensitic transformation: application to trip steels. Metall. Trans. A 13 (11), 1907–1914.

Oshima, R., Naya, E., 1978. Reversible shape memory effect in a β_1 Cu–Zn alloy containing α precipitates. J. Jpn. Inst. Met. 42 (5), 463–469.
Ostwald, R., Bartel, T., Menzel, A., 2010a. A micro-sphere approach applied to the modelling of phase-transformations. PAMM 10 (1), 315–316.
Ostwald, R., Bartel, T., Menzel, A., 2010b. A computational micro-sphere model applied to the simulation of phase-transformations. ZAMM J. Appl. Math. Mech. Z. Angew. Math. Mech. 90 (7–8), 605–622.
Ostwald, R., Bartel, T., Menzel, A., 2011. Interaction of phase-transformations and plasticity–a multi-phase micro-sphere approach. PAMM 11 (1), 417–418.
Ostwald, R., Bartel, T., Menzel, A., 2014. A gibbs-energy-barrier-based computational micro-sphere model for the simulation of martensitic phase-transformations. Int. J. Numer. Methods Eng. 97, 851–877.
Ostwald, R., Bartel, T., Menzel, A., 2015. An energy-barrier-based computational micro-sphere model for phase-transformations interacting with plasticity. Comput. Methods Appl. Mech. Eng. 293, 232–265.
Otsuka, K., Wayman, C.M., 1999. Shape Memory Materials. Cambridge University Press.
Ozgen, S., Adiguzel, O., 2004. Investigation of the thermoelastic phase transformation in a NiAl alloy by molecular dynamics simulation. J. Phys. Chem. Solids 65 (5), 861–865.
Pan, H., Thamburaja, P., Chau, F., 2007. Multi-axial behavior of shape-memory alloys undergoing martensitic reorientation and detwinning. Int. J. Plast. 23 (4), 711–732.
Panico, M., Brinson, L., 2007. A three-dimensional phenomenological model for martensite reorientation in shape memory alloys. J. Mech. Phys. Solids 55 (11), 2491–2511.
Parrinello, M., Rahman, A., 1981. Polymorphic transitions in single crystals: a new molecular dynamics method. J. Appl. Phys. 52 (12), 7182–7190.
Patoor, E., Eberhardt, A., Berveiller, M., 1988. Thermomechanical behaviour of shape memory alloy. Arch. Mech. 40 (5–6), 775–794.
Patoor, E., Eberhardt, A., Berveiller, M., 1994. Micromechanical modelling of the shape behavior. In: Proceedings of ASME International Congress and Exposition, vol. 189. AMD, Chicago, pp. 23–37.
Patoor, E., Lagoudas, D.C., Entchev, P.B., Brinson, L.C., Gao, X., 2006. Shape memory alloys, part i: general properties and modeling of single crystals. Mech. Mater. 38 (5), 391–429.
Perkins, J., 1974. Residual stresses and the origin of reversible (two-way) shape memory effects. Scr. Metall. 8 (12), 1469–1476.
Perkins, J., Sponholz, R., 1984. Stress-induced martensitic transformation cycling and two-way shape memory training in Cu-Zn-Al alloys. Metall. Trans. A 15 (2), 313–321.
Pethő, Á., 2000. Constitutive modelling of shape memory alloys based on a finite strain description. Mech. Eng. 44 (1), 115–126.
Peultier, B., Ben Zineb, T., Patoor, E., 2006. Macroscopic constitutive law of shape memory alloy thermomechanical behaviour. application to structure computation by FEM. Mech. Mater. 38 (5), 510–524.
Peultier, B., Ben Zineb, T., Patoor, E., 2008. A simplified micromechanical constitutive law adapted to the design of shape memory applications by finite element methods. Mater. Sci. Eng. A 481, 384–388.
Piotrowski, B., Ben Zineb, T., Patoor, E., Eberhardt, A., 2012. Modeling of niobium precipitates effect on the Ni_{47} Ti_{44} Nb_9 shape memory alloy behavior. Int. J. Plast. 36, 130–147.
Pons, J., Masse, M., Portier, R., 1999. Thermomechanical cycling and two-way memory effect induced in Cu-Zn-Al. Mater. Sci. Eng. A 273, 610–615.
Popov, P., Lagoudas, D.C., 2007. A 3-D constitutive model for shape memory alloys incorporating pseudoelasticity and detwinning of self-accommodated martensite. Int. J. Plast. 23 (10), 1679–1720.
Qidwai, M., Lagoudas, D., 2000a. Numerical implementation of a shape memory alloy thermomechanical constitutive model using return mapping algorithms. Int. J. Numer. Methods Eng. 47 (6), 1123–1168.
Qidwai, M., Lagoudas, D., 2000b. On thermomechanics and transformation surfaces of polycrystalline NiTi shape memory alloy material. Int. J. Plast. 16 (10), 1309–1343.
Rahman, A., 1964. Correlations in the motion of atoms in liquid argon. Phys. Rev. 136 (2A), 405–411.
Rajagopalan, S., Little, A.L., Bourke, M.A.M., Vaidyanathan, R., 2005. Elastic modulus of shape-memory NiTi from in situ neutron diffraction during macroscopic loading, instrumented indentation, and extensometry. Appl. Phys. Lett. 86 (8), 081901.
Raniecki, B., Lexcellent, C., 1994. RL-models of pseudoelasticity and their specification for some shape memory solids. Eur. J. Mech. A. Solids 13 (1), 21–50.
Raniecki, B., Lexcellent, C., 1998. Thermodynamics of isotropic pseudoelasticity in shape memory alloys. Eur. J. Mech. A Solids 17 (2), 185–205.
Raniecki, B., Lexcellent, C., Tanaka, K., 1992. Thermodynamic models of pseudoelastic behaviour of shape memory alloys. Arch. Mech. Arch. Mech. Stosow. 44, 261–284.
Reese, S., Christ, D., 2008. Finite deformation pseudo-elasticity of shape memory alloys–constitutive modelling and finite element implementation. Int. J. Plast. 24 (3), 455–482.
Rogueda, C., Vacher, P., Lexvellent, C., Contardo, L., Guenin, G., 1991. Pseudoelastic behavior and two way memory effect in Cu-Zn-Al alloys. J. Phys. IV Fr. 1 (C4), 409–414.
Rong, L., Ping, D., Li, Y., Shi, C., 1995. Improvement of shape memory effect in Fe-Mn-Si alloy by Cr and Ni addition. Scr. Metall. Mater. 32 (12), 1905–1909.
Rose, J.H., Smith, J.R., Guinea, F., Ferrante, J., 1984. Universal features of the equation of state of metals. Phys. Rev. B 29 (6), 2963.
Rubini, S., Ballone, P., 1993. Quasiharmonic and molecular-dynamics study of the martensitic transformation in Ni-Al alloys. Phys. Rev. B 48 (1), 99–111.
Sadjadpour, A., Bhattacharya, K., 2007. A micromechanics inspired constitutive model for shape-memory alloys: the one-dimensional case. Smart Mater. Struct. 16 (1), S51–S62.
Saitoh, K.-i., Liu, W.K., 2009. Molecular dynamics study of surface effect on martensitic cubic-to-tetragonal transformation in Ni–Al alloy. Comput. Mater. Sci. 46 (2), 531–544.
Sato, A., Chishima, E., Soma, K., Mori, T., 1982. Shape memory effect in $\lambda \rightleftarrows \varepsilon$ transformation in Fe-30Mn-1Si alloy single crystals. Acta Metall. 30 (6), 1177–1183.
Sato, T., Saito, K., Uehara, T., Shinke, N., 2004. Molecular dynamics study on nano structure and shape-memory property of Ni-Ti alloy. Trans. Mat. Res. Soc. Jpn. 29, 3615–3618.
Sato, T., Saitoh, K., Shinke, N., 2008. Atomistic modelling of reversible phase transformations in Ni–Ti alloys: a molecular dynamics study. Mater. Sci. Eng. A 481, 250–253.
Schroeder, T., Wayman, C., 1977. The two-way shape memory effect and other training phenomena in CuZn single crystals. Scr. Metall. 11 (3), 225–230.
Schwabl, F., 2006. Statistische Mechanik, vol. 3. Springer.
Sengupta, A., Papadopoulos, P., Taylor, R.L., 2009. Multiscale finite element modeling of superelasticity in Nitinol polycrystals. Comput. Mech. 43 (5), 573–584.
Shabalovskaya, S.A., 1996. On the nature of the biocompatibility and on medical applications of NiTi shape memory and superelastic alloys. Bio-med. Mater. Eng. 6 (4), 267–289.
Shaw, J.A., Kyriakides, S., 1995. Thermomechanical aspects of NiTi. J. Mech. Phys. Solids 43 (8), 1243–1281.
She, H., Liu, Y., Wang, B., Ma, D., 2013. Finite element simulation of phase field model for nanoscale martensitic transformation. Comput. Mech. 52 (4), 949–958.
Shield, T., 1995. Orientation dependence of the pseudoelastic behavior of single crystals of Cu-Al-Ni in tension. J. Mech. Phys. Solids 43 (6), 869–895.
Siredey, N., Patoor, E., Berveiller, M., Eberhardt, A., 1999. Constitutive equations for polycrystalline thermoelastic shape memory alloys: part I. Intragranular interactions and behavior of the grain. Int. J. Solids Struct. 36 (28), 4289–4315.
Šittner, P., Novák, V., 2000. Anisotropy of martensitic transformations in modeling of shape memory alloy polycrystals. Int. J. Plast. 16 (10), 1243–1268.
Sittner, P., Hara, Y., Tokuda, M., 1995. Experimental study on the thermoelastic martensitic transformation in shape memory alloy polycrystal induced by combined external forces. Metall. Mater. Trans. A 26 (11), 2923–2935.

Souza, A.C., Mamiya, E.N., Zouain, N., 1998. Three-dimensional model for solids undergoing stress-induced phase transformations. Eur. J. Mech. A Solids 17 (5), 789–806.
Stalmans, R., Van Humbeeck, J., Delaey, L., 1992. The two way memory effect in copper-based shape memory alloys – thermodynamics and mechanisms. Acta Metall. Mater. 40 (11), 2921–2931.
Stanley, H.E., Jul 1987. Introduction to Phase Transitions and Critical Phenomena. Introduction to Phase Transitions and Critical Phenomena, by H Eugene Stanley. Foreword by H Eugene Stanley. Oxford University Press, p. 336. ISBN-10: 0195053168. ISBN-13: 9780195053166, 1, 1987.
Stebner, A., Brinson, L., 2013. Explicit finite element implementation of an improved three dimensional constitutive model for shape memory alloys. Comput. Methods Appl. Mech. Eng. 257, 17–35.
Stein, E., Sagar, G., 2008. Theory and finite element computation of cyclic martensitic phase transformation at finite strain. Int. J. Numer. Methods Eng. 74 (1), 1–31.
Stupkiewicz, S., Górzyńska-Lengiewicz, A., 2012. Almost compatible X-microstructures in CuAlNi shape memory alloy. Contin. Mech. Thermodyn. 24 (2), 149–164.
Stupkiewicz, S., Petryk, H., 2002. Modelling of laminated microstructures in stress-induced martensitic transformations. J. Mech. Phys. Solids 50 (11), 2303–2331.
Stupkiewicz, S., Petryk, H., 2006. Finite-strain micromechanical model of stress-induced martensitic transformations in shape memory alloys. Mater. Sci. Eng. A 438, 126–130.
Stupkiewicz, S., Petryk, H., 2010a. Grain-size effect in micromechanical modelling of hysteresis in shape memory alloys. ZAMM J. Appl. Math. Mech. Z. Angew. Math. Mech. 90 (10–11), 783–795.
Stupkiewicz, S., Petryk, H., 2010b. A bi-crystal aggregate model of pseudoelastic behaviour of shape-memory alloy polycrystals. Int. J. Mech. Sci. 52 (2), 219–228.
Stupkiewicz, S., Petryk, H., 2013. A robust model of pseudoelasticity in shape memory alloys. Int. J. Numer. Methods Eng. 93 (7), 747–769.
Sun, G.-Y., Tan, Z.-C., Yang, G.-J., Hao, S.-M., et al., 1995. Adiabatic calorimetric study on shape memory alloys: heat capacities and martensitic phase transformation of Ni_{47} Ti_{44} Nb_9 and Nb_{80} Ti_{14} Ni_6 alloys. Thermochim. Acta 266, 231–238.
Sun, Q., Hwang, K.C., Yu, S., 1991. A micromechanics constitutive model of transformation plasticity with shear and dilatation effect. J. Mech. Phys. Solids 39 (4), 507–524.
Sun, Q.P., Hwang, K.C., 1993. Micromechanics modelling for the constitutive behavior of polycrystalline shape memory alloys I. derivation of general relations. J. Mech. Phys. Solids 41 (1), 1–17.
Sun, Q.-P., Hwang, K.-C., 1994. Micromechanics constitutive description of thermoelastic martensitic transformations. Adv. Appl. Mech. 31, 249–298.
Sutou, Y., Koeda, N., Omori, T., Kainuma, R., Ishida, K., 2009. Effects of ageing on bainitic and thermally induced martensitic transformations in ductile Cu–Al–Mn-based shape memory alloys. Acta Mater. 57 (19), 5748–5758.
Sutou, Y., Omori, T., Kainuma, R., Ishida, K., 2013. Grain size dependence of pseudoelasticity in polycrystalline Cu–Al–Mn-based shape memory sheets. Acta Mater. 61 (10), 3842–3850.
Suzuki, T., Shimono, M., 2003. A simple model for martensitic transformation. In: Journal de Physique IV (Proceedings), vol. 112. EDP Sciences, pp. 129–132.
Suzuki, T., Shimono, M., Ren, X., Otsuka, K., Onodera, H., 2006. Study of martensitic transformation by use of monte-carlo method and molecular dynamics. Mater. Sci. Eng. A 438, 95–98.
Tadaki, T., Otsuka, K., Shimizu, K., 1988. Shape memory alloys. Annu. Rev. Mater. Sci. 18 (1), 25–45.
Tanaka, K., 1986. A thermomechanical sketch of shape memory effect: one-dimensional tensile behavior. Res. Mech. 18, 251–263.
Tanaka, K., Nagaki, S., 1982. A thermomechanical description of materials with internal variables in the process of phase transitions. Ing. Archiv 51 (5), 287–299.
Taylor, G., 1938. Plastic strain in metals. J. Inst. Met. 63, 307–324.
Thamburaja, P., 2010. A finite-deformation-based phenomenological theory for shape-memory alloys. Int. J. Plast. 26 (8), 1195–1219.
Thamburaja, P., Anand, L., 2001. Polycrystalline shape-memory materials: effect of crystallographic texture. J. Mech. Phys. Solids 49 (4), 709–737.
Thiébaud, F., Ben Zineb, T., 2014. Experimental and finite element analysis of superelastic behaviour of shape memory alloy for damping applications. Mech. Ind. 15 (5), 371–376.
Thiebaud, F., Lexcellent, C., Collet, M., Foltete, E., 2007. Implementation of a model taking into account the asymmetry between tension and compression, the temperature effects in a finite element code for shape memory alloys structures calculations. Comput. Mater. Sci. 41 (2), 208–221.
Uehara, T., Tamai, T., 2006. An atomistic study on shape-memory effect by shear deformation and phase transformation. Mech. Adv. Mater. Struct. 13 (2), 197–204.
Uehara, T., Tamai, T., Ohno, N., 2006. Molecular dynamics simulations of shape-memory behavior based on martensite transformation and shear deformation. JSME Int. J. Ser. A 49 (3), 300–306.
Uehara, T., Asai, C., Ohno, N., 2009. Molecular dynamics simulation of shape memory behaviour using a multi-grain model. Model. Simul. Mater. Sci. Eng. 17 (3), 035011.
Ueland, S.M., Schuh, C.A., 2012. Superelasticity and fatigue in oligocrystalline shape memory alloy microwires. Acta Mater. 60 (1), 282–292.
Vacher, P., 1991. Etude du comportement pseudoélastique d'alliages à mémoire de forme Cu-Zn-Al polycristallins (PhD thesis). Université de Besanon.
Wang, L.X., Melnik, R.V., 2007. Thermo-mechanical wave propagations in shape memory alloy rod with phase transformations. Mech. Adv. Mater. Struct. 14 (8), 665–676.
Wang, X., Yue, Z., 2006. Three-dimensional thermomechanical modeling of pseudoelasticity in shape memory alloys with different elastic properties between austenite and martensite. Mater. Sci. Eng. A 425 (1), 83–93.
Wang, X., Xu, B., Yue, Z., 2008. Micromechanical modelling of the effect of plastic deformation on the mechanical behaviour in pseudoelastic shape memory alloys. Int. J. Plast. 24 (8), 1307–1332.
Wang, Y., Khachaturyan, A., 1997. Three-dimensional field model and computer modeling of martensitic transformations. Acta Mater. 45 (2), 759–773.
Wayman, C., Bhadeshia, H., 1983. Phase transformations, nondiffusive. Phys. Metall. 2, 1507–1554.
Wechsler, M., Lieberman, D., Read, T., 1953. On the theory of the formation of martensite. Trans. AIME J. Metals 197, 1503–1515.
Wen, Y., Xiong, L., Li, N., Zhang, W., 2008. Remarkable improvement of shape memory effect in an Fe–Mn–Si–Cr–Ni–C alloy through controlling precipitation direction of Cr_{23} C_6. Mater. Sci. Eng. A 474 (1), 60–63.
Wilkins, M., 1964. Calculations of elasto-plastic flow. In: Balder, et al. (Eds.).
Wu, X., Sun, G., Wu, J., 2003. The nonlinear relationship between transformation strain and applied stress for nitinol. Mater. Lett. 57 (7), 1334–1338.
Yu, C., Kang, G., Song, D., Kan, Q., 2012. Micromechanical constitutive model considering plasticity for super-elastic NiTi shape memory alloy. Comput. Mater. Sci. 56, 1–5.
Yu, C., Kang, G., Kan, Q., Song, D., 2013. A micromechanical constitutive model based on crystal plasticity for thermo-mechanical cyclic deformation of NiTi shape memory alloys. Int. J. Plast. 44, 161–191.
Yu, C., Kang, G., Kan, Q., 2014. Study on the rate-dependent cyclic deformation of super-elastic NiTi shape memory alloy based on a new crystal plasticity constitutive model. Int. J. Solids Struct. 51 (25), 4386–4405.
Yu, C., Kang, G., Song, D., Kan, Q., 2015. Effect of martensite reorientation and reorientation-induced plasticity on multiaxial transformation ratchetting of super-elastic NiTi shape memory alloy: new consideration in constitutive model. Int. J. Plast. 67, 69–101.
Zaki, W., 2010. An approach to modeling tensile–compressive asymmetry for martensitic shape memory alloys. Smart Mater. Struct. 19 (2), 025009.
Zaki, W., 2011. Modeling and simulation of the mechanical response of martensitic shape memory alloys. In: ASME 2011 Conference on Smart Materials, Adaptive Structures and Intelligent Systems, SMASIS 2011, vol. 1, pp. 189–193 cited By 2.

Zaki, W., 2012a. An efficient implementation for a model of martensite reorientation in martensitic shape memory alloys under multiaxial nonproportional loading. Int. J. Plast. 37, 72–94.
Zaki, W., 2012b. Implicit integration for a model of martensite reorientation in shape memory alloys. In: ECCOMAS 2012-European Congress on Computational Methods in Applied Sciences and Engineering, e-Book Full Papers, pp. 8250–8259.
Zaki, W., 2012c. Time integration of a model for martensite detwinning and reorientation under nonproportional loading using Lagrange multipliers. Int. J. Solids Struct. 49 (21), 2951–2961.
Zaki, W., Moumni, Z., 2007a. A three-dimensional model of the thermomechanical behavior of shape memory alloys. J. Mech. Phys. Solids 55 (11), 2455–2490.
Zaki, W., Moumni, Z., 2007b. A 3D model of the cyclic thermomechanical behavior of shape memory alloys. J. Mech. Phys. Solids 55 (11), 2427–2454.
Zaki, W., Morin, C., Moumni, Z., 2010a. A simple 1d model with thermomechanical coupling for superelastic smas. In: IOP Conference Series: Materials Science and Engineering, vol. 10, p. 012149.
Zaki, W., Zamfir, S., Moumni, Z., 2010b. An extension of the ZM model for shape memory alloys accounting for plastic deformation. Mech. Mater. 42 (3), 266–274.
Zaki, W., Moumni, Z., Morin, C., 2011. Modeling tensile-compressive asymmetry for superelastic shape memory alloys. Mech. Adv. Mater. Struct. 18 (7), 559–564.
Zaki, W., Gu, X., Morin, C., Moumni, Z., Zhang, W., 2014. Time integration and assessment of a model for shape memory alloys considering multiaxial nonproportional loading cases. V001T03A024–V001T03A024. In: ASME 2014 Conference on Smart Materials, Adaptive Structures and Intelligent Systems. American Society of Mechanical Engineers.
Zhao, C., 1999. Improvement of shape memory effect in Fe-Mn-Si-Cr-Ni alloys. Metall. Mater. Trans. A 30 (10), 2599–2604.
Zhao, Y., Taya, M., Kang, Y., Kawasaki, A., 2005. Compression behavior of porous NiTi shape memory alloy. Acta Mater. 53 (2), 337–343.
Zhong, Y., Zhu, T., 2012. Patterning of martensitic nanotwins. Scr. Mater. 67 (11), 883–886.
Zhong, Y., Zhu, T., 2014. Phase-field modeling of martensitic microstructure in NiTi shape memory alloys. Acta Mater. 75, 337–347.
Zhou, B., 2012. A macroscopic constitutive model of shape memory alloy considering plasticity. Mech. Mater. 48, 71–81.
Zhou, B., Yoon, S.-H., Leng, J.-S., 2009. A three-dimensional constitutive model for shape memory alloy. Smart Mater. Struct. 18 (9), 095016.
Zhou, B., Liu, Y., Leng, J., 2010. A macro-mechanical constitutive model for shape memory polymer. Sci. China Phys. Mech. Astron. 53 (12), 2266–2273.
Zhu, Y., Zhang, Y., Zhao, D., 2014. Softening micromechanical constitutive model of stress induced martensite transformation for NiTi single crystal shape memory alloy. Sci. China Phys. Mech. Astron. 57 (10), 1946–1958.
Ziolkowski, A., 2007. Three-dimensional phenomenological thermodynamic model of pseudoelasticity of shape memory alloys at finite strains. Contin. Mech. Thermodyn. 19 (6), 379–398.